Dissertation zur Erlangung des Doktorgrades

der Fakultät für Chemie und Pharmazie
der Ludwig-Maximilians-Universität München

Retrograde trafficking to the trans-Golgi network and its effect on β1 integrin function

Alexandros Anastasakis
aus
Köln, Deutschland

2025

Erklärung

Diese Dissertation wurde im Sinne von § 7 der Promotionsordnung vom 28. November 2011 von Herrn Prof. Dr. Veit Hornung und von Herrn Dr. Ralph Böttcher betreut.

Eidesstattliche Versicherung

Diese Dissertation wurde eigenständig und ohne unerlaubte Hilfe erarbeitet.

München, 2 3 . 0 9 . 2 0 2 5

_____
Alexandros Anastasakis

Dissertation eingereicht am 23.09.2025

1. Gutachter: Prof. Dr. Veit Hornung

2. Gutachter: Prof. Dr. Julian Stingele

Mündliche Prüfung am: 18.12.2025

Table of Contents

Summary

Virtually all morphogenetic events in multicellular organisms, including tissue homeostasis, wound healing, and tumorigenesis, rely on dynamic cell–cell and cell–matrix adhesion. Central to these processes are integrins, a family of heterodimeric transmembrane receptors, that mediate adhesion to extracellular matrix (ECM) proteins and cell-surface counter-receptors, thereby linking the extracellular environment to the intracellular actin cytoskeleton. Integrins are therefore indispensable regulators of cell adhesion and migration, processes critical for development, physiology, and pathology.

Integrin function is tightly regulated at multiple levels, including an activation step involving conformational changes that promote ligand binding, clustering that increases adhesion stability, the formation of signaling hubs that integrate biochemical, biophysical cues, and trafficking through the endosomal system. The cytoplasmic tails of integrins, along with their associated binding partners, play a central role in these processes by linking integrins to the actin cytoskeleton, initiating downstream signaling, and interfacing with the endocytic machinery.

Although integrins primarily function at the plasma membrane by recruiting adaptor and signaling proteins upon ligand binding, they continuously cycle between the cell surface and intracellular compartments. With a typical residence time of 15–20 minutes at the membrane, integrins are internalized via clathrin-dependent and -independent pathways and routed through the endosomal network. They are then either recycled back to the plasma membrane for reuse or targeted for degradation in late endosomes and lysosomes.

This intracellular trafficking of integrins is crucial for maintaining their stability and surface distribution, which in turn determines the speed and persistence of directional cell migration. Beyond membrane dynamics, integrin trafficking also supports endosomal signaling, modulates the activity of growth factor receptors, and regulates ECM turnover. Collectively, these functions have profound implications for integrin-mediated cellular behaviors, including spreading, polarity, migration, and proliferation.

In this thesis, I identified the FAM91A1–WDR11–C17orf75 (FWC) complex as a key regulator of integrin retrograde trafficking. I determined the preferred integrin isoform

trafficked by the complex and uncovered the physiological consequences of aberrant integrin trafficking in cells lacking the FWC complex. Loss of the complex led to severe defects in cell polarization, impaired cell spreading, and compromised cellular motility.

Furthermore, I identified the binding motif within the integrin cytoplasmic tail that is essential for interaction with WDR11. Using AlphaFold2 modeling, I generated a high-confidence structural model that illustrates the interface between WDR11 and integrins. Finally, I successfully purified the FWC complex and obtained initial structural insights into the FAM91A1–C17orf75 dimer using cryo-electron microscopy.

1. Introduction

1.1 Integrins as mediators of cellular adhesion and signaling

Integrins constitute a family of heterodimeric cell surface receptors that mechanically link the extracellular matrix (ECM) to the intracellular actomyosin cytoskeleton, thereby establishing bidirectional signaling across the plasma membrane (1, 2). The term “integrins” derives from their function as the integrators of the ECM with the intracellular actomyosin cytoskeleton, thereby establishing a direct link between the exterior and interior of the cell (3).

Integrins are found in metazoan organisms and have expanded into a larger and more diverse family, vertebrates and humans, through evolutionary processes (4). In mammals, stable interactions are formed between 18 α- and 8 β-subunits, creating 24 heterodimers with distinct functions depending on their extracellular binding partner (4). The most prevalent integrins are those containing β1-subunits. β1-subunits can dimerize with 12 α-subunits to form 12 integrin isoforms (5). β1-containing integrins recognize various ECM ligands, including fibronectin, collagen, and laminin, through specific binding motifs (6). Through bidirectional signaling, integrins act as conduits that modulate their own expression and activity at the plasma membrane, thereby directly influencing cellular migration, proliferation, and survival (6, 7).

1.2 Integrin domain architecture and ligand recognition

All integrin heterodimers share a conserved domain architecture: both α- and β-subunits are composed of an ectodomain that binds the ECM, a single transmembrane domain, and a short cytoplasmic domain that mediates downstream signaling cascades (2, 8).

The α-subunit ectodomain contains a headpiece formed by a β-propeller domain composed of seven blades arranged in a circular structure, followed by a stalk that connects the headpiece to the transmembrane domain (9). The β-propeller constitutes the N-terminus of the integrin, and in certain isoforms (e.g., α1, α2), contains an α-I (α-inserted) domain, the primary binding site for collagen-binding integrins (10, 11). The α-I domain spans approximately 200 amino acids and inserts between the second and third blades of the β-

propeller (9). Consequently, the α-I domain can directly engage ECM ligands independently of the β-subunit ectodomain. The α-I domain harbors a metal-ion-dependent adhesion site (MIDAS) that coordinates divalent cations such as Mg^{2+} or Mn^{2+} (10, 12, 13). These cations are required for interactions between integrins and ECM ligands such as collagen or intercellular adhesion molecules (ICAMs).

Compared to the rather simplistic architecture of the α-subunits head domain, the β-subunit head domain displays a complex domain architecture. It contains a β-I domain, structurally related to the α-I domain. Both β-I and α-I domains bear a MIDAS site that facilitates binding of integrins to their ECM ligand (10, 14). The β-I domain possesses the specificity-determining loop (SDL) that specifically binds ECM ligands. Based on the recognition sequence identified by the β-subunit, integrins can be categorized by the binding motif present in the ECM ligands. The RGD (Arg-Gly-Asp) motif represents the most prevalent binding sequence, recognized by multiple integrin heterodimers that bind fibronectin, fibrinogen and vitronectin (10, 14-16).

Laminin-binding integrins bind to various laminin-specific domains, there is no conserved peptide motif present (17). Laminin is a highly specialized extracellular matrix component of the basement membrane critical for providing a functional and structural robust interface between epithelial, endothelial, or muscle cells and the underlying connective tissue (18, 19). It is predominantly found in the lamina lucida, the upper layer of the basement membrane adjacent to the cell membrane (20). Conversely, the lamina densa, the lower layer of the basement membrane, is comprised primarily of type IV collagen, perlecan, and nidogen (20). These interactions stabilize various cell layers, ensuring tissue integrity and cohesion (17).

Collagen is the most prevalent protein in the ECM (21). Structurally, collagens are a family marked by a unique triple helical structure. The best studied recognition motif is GFOGER (Gly-Phe-Hyp-Gly-Glu-Arg), present in fibrillar collagens like types I, II, and III (20-23). Collagen-integrin interactions provide mechanical stability and anchorage for the cell (21).

Leukocyte-specific integrins are specifically found in the immune system (24). They are expressed on leukocytes and mediate cell adhesion to ligands expressed on endothelial cells and ECM proteins (4). These integrins mediate immune responses by facilitating

leukocyte adhesion, migration, and trafficking during inflammation, tissue repair, and immune surveillance (24, 25). ICAMs and vascular cell adhesion molecule-1 (VCAM-1) are single transmembrane glycoproteins expressed on multiple cell types in response to pathogen entry or inflammation and are the primary binding partners of leukocyte-specific integrins (26, 27). Leukocyte-specific integrins recognize the Leu-Asp-Val (LDV) motif, found on ECM proteins such as fibronectin, VCAM-1, mucosal addressin cell adhesion molecule-1 (MAdCAM-1), and tenascin-C (28).

Additionally, certain integrins bind to the RGD motif present in latent transforming growth factor β (TGF-β), facilitating conversion of TGF-β from its inactive to its active form (29, 30). In its active form, TGF-β acts as a potent immunosuppressive cytokine (29). It promotes T-cell differentiation and suppresses pro-inflammatory responses.

Table 1. Simplified depictions of integrin classification based on the ECM recognition motif.

Binding motif	ECM Ligand	Integrins	Function
RGD (Arg-Gly-Asp)	Fibronectin, vitronectin, fibrinogen	αvβ3, αvβ5, α5β1, αIIbβ3	Cell adhesion, migration, angiogenesis
Laminin-specific	Laminin	α3β1, α6β1, α6β4, α7β1	Basement membrane adhesion, hemidesmosomes
GFOGER (collagen)	Collagen	α1β1, α2β1, α10β1, α11β1	ECM remodeling, adhesion to collagen
ICAM/VCAM	IXAM-1, VCAM-1	αLβ2, αMβ2, αXβ2, α4β1, α4β7	Immune cell trafficking, adhesion
LDV (Leu-Asp-Val)	Fibronectin	α4β1, α9β1	Specialized ECM interactions
Latent TGF-β RGD	Latent TGF-β complex	αvβ6, αvβ8	TGF-β activation, immune regulation

1.3 Integrin structure - transmembrane and cytoplasmic domains

The integrin transmembrane domain (TMD) comprises 25 to 29 hydrophobic amino acid residues that span the plasma membrane (31). The TMD is conserved among different species and mediates integrin activation (32, 33). Besides anchoring integrins at the plasma membrane, the TMD enables bidirectional signaling (inside-out and outside-in) (34).

Both α-subunit and β-subunit have distinct transmembrane helices, which interact to stabilize the integrin in its inactive conformational state. The GxxxG motif present in the β-subunit TMD mediates helix-helix interactions with the α-subunit (35). During integrin

activation, the α-subunit TMD and β-subunit TMD interactions are destabilized, leading to separation of the TMDs (36). This separation initiates a cascade of conformational changes that extend the ectodomain, enabling integrins to bind ECM ligands.

The integrin cytoplasmic tail is highly conserved across different species and mediates regulation of integrin activation, signal transmission bidirectionally, and linking the ECM to the cytoskeleton (37). The intracellular tails of the α-subunits and β-subunits have distinct functions that act synergistically.

The β-subunit tail, spanning 20-70 amino acids, acts as a control center by binding multiple effector proteins that initiate intracellular signaling cascades (38, 39). The exception is the β4-subunit with its extended 1000 amino acids tail (40). The intracellular tail, which contains high levels of polar and charged residues (e.g., Arg, Glu, and Lys), mediates interactions with cytoplasmic proteins (38). Two NPXY motifs within the β-subunit intracellular tail serve as the primary binding sites for integrin binding partners (2).

The intracellular tail of the α-subunit is shorter than the β-subunit cytoplasmic tail (9-20 amino acids) and is less conserved. The α-subunit cytoplasmic tail significantly contributes to integrin function by stabilizing interactions with the β-subunit cytoplasmic tail (37, 38). The variability in the α-subunit cytoplasmic tail reflects the diverse functional roles of various α-subunits.

In the inactive state, the α-subunit cytoplasmic tail interacts with the β-subunit cytoplasmic tail via a conserved Gly-Phe-Phe-Lys-Arg (GFFKR) motif near the juxtamembrane region, thereby maintaining the inactive conformational state of integrin by stabilizing interactions between both cytoplasmic tails (41). Certain α-subunits (e.g., α4 and α6) contain phosphorylation sites or additional binding sites for adaptor proteins that regulate integrin-specific functions such as cell migration and survival (42, 43). For example, filamin links integrins to the actin cytoskeleton, thereby contributing to structural stability while permitting transmission of mechanical forces between the ECM and the cytoskeleton (44).

The cytosolic tail also regulates intracellular trafficking after endocytosis. The clathrin adaptor disabled homologue 2 (DAB2) and NUMB, which facilitate clathrin-dependent

endocytosis, bind to the NPXY motifs in the β-tails (45). Similarly, the α-subunit tail binds Rab GTPases, which mediate integrin recycling from early endosomes (46).

1.4 Integrin conformational states and activation mechanisms

Integrins exist in multiple conformational states that alternate between an inactive state, characterized by low binding affinity for ECM ligands, and an active form with high binding affinity (Fig. 1) (31, 32).

In the inactive conformation, the integrin's TMDs are tightly associated, and the ligand binding pocket is masked. This conformation is termed "bent-closed" (BC). During activation, integrins adopt an intermediate state where the ectodomain extends while maintaining the ligand-binding pocket inaccessible. This conformation is therefore referred to as "extended closed" (EC) (47, 48). The fully activated conformational state requires complete separation of the cytoplasmic tails of the α- and β-subunits. This separation, combined with headpiece opening, results in the "extended open" (EO) conformation (Fig.1) (47, 48).

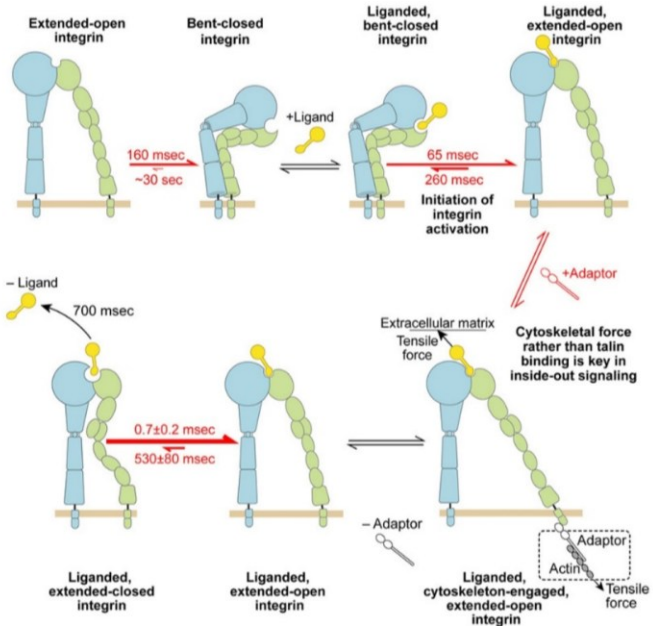

Figure 1. **Mechanism of integrin activation.** Illustration of integrin specific conformational states and the time required for the transition between the various conformations. Adapted from Li et. al. (49).

Li et al. recently elucidated the time required for transitions between conformational states. Unliganded integrins require approximately 30 seconds to transition from BC to EO, whereas in the presence of ligand, the transition occurs within milliseconds (Fig. 1) (49). Furthermore, the force required for conformational transitions reveals that high mechanical energy is required to shift from BC to EC. However, the subsequent transition from EC to EO requires only a fraction of the initial force. These energetic barriers explain the low abundance of EC and EO integrins on the plasma surface (49). EO integrins, however, are stabilized due to the presence of a ligand and the intracellular binding of Talin and Kindlin. The use of mechanical forces for integrin activation is referred to “outside-in” signaling, as the activation of the integrin resulted through environmental forces.

1.5 Integrin activation: inside-out signaling through Talin and Kindlin

Inside-out signaling refers to the transition of integrins from their low affinity state to their high affinity state in response to intracellular signals (50). These signals originate from other receptors embedded in the cell surface, most commonly including growth factor receptors, receptor tyrosine kinase (RTKs), and G-protein coupled receptors (GPCRs). Upon ligand binding, a signaling cascade is initiated that eventually targets integrins. Two primary intracellular signaling pathways mediating integrin activation are: (1) the phosphoinositide 3-kinase (PI3K)/Akt pathway and (2) the Rap1 GTPase pathway (51).

The PI3K/Akt pathway is activated by growth factor receptors or GPCRs. Activation leads to the production of phosphatidylinositol (3,4,5)-trisphosphate (PIP3), which recruits Akt and Talin to the plasma membrane, leading to integrin activation (52, 53).

The Rap1 GTPase pathway relies on guanine nucleotide exchange factors (GEFs) to promote the exchange of guanosine diphosphate (GDP) for guanosine triphosphate (GTP) on Rap1, activating Rap1 (53). Activated Rap1 recruits Rap1-GTP-interacting adaptor molecule (RIAM) which acts as a scaffold linking Rap1 and Talin.

Talin and Kindlin are two key intracellular proteins that initiate and stabilize integrin activation by binding to the intracellular tail of the β1-subunit (54, 55). Talin is a large cytoplasmic protein consisting of two key regions: its N-terminal head domain and C-terminal rod domain. Talin's head domain contains a 4.1, Ezrin, Radixin, Moesin (FERM)

domain that directly binds to the β-subunit cytoplasmic tail (55). Talin exists in an autoinhibitory state where the head is masked by its rod domain, preventing premature integrin activation (56). The autoinhibitory state of Talin is relieved in response to Rap1 and lipid signaling through phosphatidylinositol 4,5-bisphosphate (PIP2)/PIP3. RIAM binding to Talin's rod domain disrupts the interaction between the head and rod domain of Talin. Upon binding, RIAM induces a conformational change in Talin, causing the rod domain to dissociate from the head domain. This conformational change relieves the autoinhibition of Talin and exposes the FERM domain, allowing binding to the β integrin tail (57).

The autoinhibitory state of Talin can also be relieved by PIP2 binding. Talin possesses a PIP2 binding site in its head domain, and upon recruitment to the plasma membrane, Talin binds to PIP2 present in the inner leaflet of the plasma membrane. Binding of PIP2, like RIAM binding, induces a conformational change in Talin that weakens the interaction between the rod and head domain. The interaction with PIP2 not only activates Talin but also brings Talin into proximity with integrins (58). Additionally, formation of PIP3 through the PI3K pathway further facilitates Talin recruitment and contributes to its activation. Despite multiple integrin isoforms, the activation mechanism is conserved (59). I focus here on β1 integrin activation given its biological relevance for this thesis.

The β1 intracellular tail possesses two Asn-Pro-X-Tyr (NPXY) motifs termed proximal and distal based on their proximity to the plasma membrane (60, 61). These motifs are highly conserved among isoforms and are critical for integrin regulation, especially during activation and intracellular signal transduction (61). Talin binds to the membrane-proximal NPXY motif through its F3 domain in the Talin head region (54). Upon Talin binding, a series of conformational changes are initiated that disrupt the interaction between the integrin α- and β- subunit cytoplasmic tails. These changes cause breakage of the salt bridges in the transmembrane domain (TMD) between the subunits, permitting their dissociation. The separation of the TMD stabilizes the extended conformation of the extracellular domain. Salt bridge breakage and subsequent TMD dissociation are prerequisites for the transition of integrins to their extended conformation. The TMD dissociation exerts a mechanical force on the integrins that extends the extracellular domain, unfolding the integrin from its bent conformation, revealing the ligand binding site.

The conformational changes are further stabilized by Talin's interaction with the cytoskeleton (54).

Talin's rod domain, in its activated form, binds to actomyosin filaments, resulting in the transduction of actomyosin-mediated pulling forces along the TMD to the integrin-ligand bond, enhancing the ligand integrin bond (62, 63). In the final step, the hybrid domain embedded in the β-subunit extracellular domain swings outward to render the ligand binding domain accessible to the ECM.

Kindlin binds to the membrane distal NPXY motif and works synergistically with Talin to facilitate and maintain integrin activation. Like Talin, Kindlin possesses a FERM domain that binds to the NPXY motif on the β cytoplasmic tail (56, 64). Within the FERM domain, specifically in the F2 subdomain, Kindlin possesses a PH domain, which facilitates Kindlin recruitment to the plasma membrane by binding to PIP2. Furthermore, the C-terminus of Kindlin possesses multiple protein binding sites for cytoskeletal proteins that regulate integrin clustering and signaling.

While Talin is the primary linker of integrins to the cytoskeleton, Kindlin enhances this connection by acting as a scaffold, recruiting additional proteins involved in cytoskeletal organization (64). These proteins include Parvin, Paxillin, and integrin-linked kinase (ILK), key components of mature adhesomes (65).

It remained unclear how Kindlin and Talin bind to the β cytoplasmic tail since the two binding sites partly overlap. Moreover, previous results did not explain how Talin’s relatively low affinity for the β cytoplasmic tail could transmit forces up to 10 to 40 pN. Recent work from our laboratory revealed, using single molecule force spectroscopy by optical tweezers, that Kindlin and Talin individually form weak and highly dynamic slip bonds with the β cytoplasmic tail. However, together, Kindlin stabilizes the Talin-integrin bond. The authors provide compelling evidence that this cooperative behavior results in an "ideal bond". The ideal bond relies on the proximity of both Kindlin and Talin on the β cytoplasmic tail, resulting in the transmission of large mechanical forces across the cytoskeleton required for stabilization of cell adhesions (66).

1.6 Outside-in signaling and focal adhesion formation

Outside-in signaling involves binding of ECM ligands (e.g., fibronectin or collagen) to the extracellular domain of integrins. This ligand-integrin interaction induces intracellular signaling cascades, regulating essential cellular functions, including migration, adhesion, survival, and proliferation. Like inside-out signaling, outside-in signaling involves major conformational changes in the integrin structure and requires recruitment of various cytoplasmic adaptor proteins and signaling proteins (51).

Upon ECM ligand binding to the headpiece of integrins, mechanical tension propagates through the integrin molecule, leading to partial unbending of the integrin (51). Subsequently, the mechanical tension separates the legs of the α-subunit and β-subunit, breaking the cytoplasmic salt bridges that maintain the inactive state. The breakage of salt bridges results in the fully extended, high-affinity conformational state, permitting efficient ligand binding (67, 68). The separation of the α-subunit and β-subunit cytoplasmic tails reveals docking sites for adaptor proteins, triggering recruitment of proteins involved in focal adhesion assembly and signal transduction (68).

1.7 Focal adhesions and adhesome formation

Integrin activation initiates focal adhesions formation. Focal adhesions are highly dynamic, multi-protein complexes at sites of active integrins that create an interconnected network between integrins, cytoskeletal proteins, and signaling molecules (69, 70). They regulate adhesive interactions with the ECM or neighboring cells. By connecting the cell's cytoskeleton to the ECM through integrins, these structures mediate mechano-transduction and signal transduction, allowing cells to sense and respond to mechanical and biochemical cues from their environment (69, 70). A fully matured adhesome consists of more than 200 proteins that dynamically assemble and disassemble at focal adhesion sites (71). Key proteins include Vinculin, an actin filament binding protein that links Talin to the actin cytoskeleton, thereby stabilizing focal adhesions; Paxillin, a regulator of adhesome formation; and focal adhesion kinase (FAK), responsible for downstream signaling (72).

Paxillin functions as an adaptor protein, interacting with Vinculin, ILK, and FAK (73, 74). Through these interactions, Paxillin facilitates assembly of the adhesome complex, linking integrins to the cytoskeleton and downstream signaling pathways (73).

FAK, upon recruitment to integrins, is activated by autophosphorylation. Once activated, FAK serves as a docking site for Src family kinases and additional signaling proteins (75-77). FAK activates the MAPK/ERK pathway, which regulates cell proliferation and differentiation; the PI3K/Akt pathway, promoting cell survival and growth; and the Rho GTPase pathway, responsible for cytoskeletal rearrangement and cell migration (78-80).

1.8 Biological implications of integrin function and turnover

Following signal transduction, the adhesome is disassembled. Regulated disassembly of focal adhesion sites prevents constant signal transduction (81, 82). Decreased tension at the adhesion site or intracellular signaling events trigger breakdown of focal adhesion components (82). Focal adhesion disassembly primarily occurs at the trailing edge of migrating cells, enabling detachment from the ECM. This highly coordinated process involves multiple enzymes, post-translational modifications, and changes in mechanical forces (83). During disassembly, key phosphorylation sites on FAK undergo dephosphorylation (e.g., Tyr397) by tyrosine phosphatases, causing focal adhesions to lose their signaling capacity (84). Subsequently, Paxillin undergoes phosphorylation (e.g., Tyr31, Tyr118), which disrupts its interaction with other focal adhesion proteins and the actin cytoskeleton (85).

Focal adhesion dynamics broadly impact cellular processes. Cellular movement and maintenance of tissue integrity is regulated by the formation and turnover of focal adhesions that enable cells to migrate across the ECM and to form structurally cohesive structures by linking the ECM to the intracellular cytoskeleton (2, 21). This is crucial for wound healing, immune responses, and cancer metastasis (82, 86). Furthermore, cell fate is actively modulated by responding to the environment's mechanical properties, such as stiffness. Thus, mechano-transduction of forces detected by integrin-based adhesions influences cell differentiation, proliferation, and survival (87).

1.9 Endocytosis of integrins

Despite their half-life of approximately 24 hours, integrins are retained on the plasma membrane for only 15-20 minutes before being internalized and recycled (88, 89). Integrins are constitutively internalized through clathrin-dependent and independent mechanisms and routed into the endosomal network. Endocytosis begins with membrane invagination followed by vesicle formation and pinching off from the plasma membrane (90).

Vesicle formation at the cell membrane requires assembly of a clathrin coat (90, 91). Initially, cargo is recognized by adaptor proteins. The primary adaptor complex in clathrin-dependent endocytosis (CDE) of integrins is the adaptor protein complex 2 (AP-2) (91). AP-2 binds to the YxxΦ motif in the α-chain intracellular tail and to phosphatidylinositol 4,5-bisphosphate ($PI(4,5)P_2$) on the inner leaflet of the plasma membrane, recruiting clathrin triskelions to the site of vesicle formation (90, 92, 93). Clathrin triskelions comprise three heavy and three light chains (94). Multiple triskelion structures polymerize to form a lattice on the cytoplasmic side of the membrane that promotes membrane curvature, forming a clathrin-coated pit (CCP) (90).

As the CCP grows, the forming vesicle is invaginated, incorporating cargo and lipid components. Finally, Dynamin, a large GTPase, oligomerizes around the neck of the invaginated CCP and facilitates scission of the vesicle from the plasma membrane (90). Upon scission, the vesicle sheds its clathrin coat to fuse with early endosomes. The uncoating process is mediated by auxilin and Hsc70 (95, 96).

1.10 The essential role of integrin trafficking

Integrin functions rely not only on appropriate plasma membrane expression but also on dynamic trafficking between the cell surface, endosomes and recycling pathways (74, 88). This trafficking enables cells to dynamically modulate adhesion strength, regulate migration and maintain tissue integrity (34, 85). Dysregulation of integrin trafficking is implicated in cancer, immune disorders and developmental defects. After internalization from the plasma membrane via endocytosis, integrins follow one of three primary pathways:

1. Recycling back to the plasma membrane (via early or recycling endosomes). This trafficking route is primarily facilitated by the Retriever complex and its accessory proteins (89-91). It rescues integrins from degradation early to maintain integrin levels on the cell surface.
2. Degradation in lysosomes (to regulate receptor turnover) (92, 93). During this trafficking route, the endosomal sorting complex required for transport (ESCRT) directs integrins towards the lysosome for degradation.
3. Transport to other cellular compartments (e.g., the Golgi for post-translational modifications). Transport to the trans-Golgi network (TGN) is facilitated by the Retromer complex (94, 95). The retrograde route is associated with polarized re-expression of endocytosed integrins at the leading edge of cells to sustain migration (96).

The spatiotemporal regulation of integrin trafficking, by employing fast (Rab4) or slow (Rab11, Rab6) recycling routes, enables cells to dynamically control integrin surface levels and adhesion strength during migration (88, 97). These trafficking mechanisms are essential for embryogenesis, wound healing, and immune responses (88).

1.11 Endosomes as central trafficking hubs

Endosomes sort proteins and lipids to either the anterograde route or the trans-Golgi network (TGN) (88). Endosomal sorting is essential for maintaining cellular homeostasis and development.

The endosomal system is classified based on the maturation process of the organelle. During endosomal maturation, endosomes undergo morphological, biochemical, and functional changes that define their role in protein sorting and trafficking (89, 90).

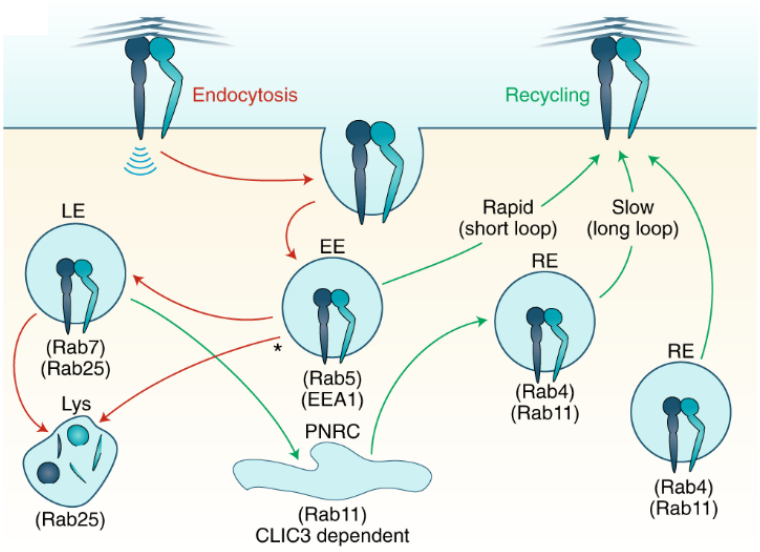

Figure 2. Integrin internalization and recycling. Illustration of the various pathways integrins can employ to be recycled back to the plasma membrane. Small Rab GTPases govern these pathways and facilitate integrin recycling from various endosomal species. Adapted from Paulina Moreno-Layseca et.al. (91).

Early endosomes (EEs) act as the primary sorting station for proteins following internalization. At this stage, decisions are made regarding whether cargo should be recycled to the plasma membrane, trafficked to the TGN via the retrograde route, or targeted for degradation (92, 93). Morphologically, EEs display a tubular-vesicular shape and are located in proximity to the plasma membrane (94).

EEs are distinguished by four key features: 1) the small GTPase Rab5, which mediates EE formation and function by recruiting effector proteins that regulate vesicle fusion and cargo sorting (95, 96); 2) PI3P in the endosomal membrane (97) that recruits PX domain-containing proteins (e.g., sorting nexins) and FYVE domain-containing proteins (e.g., EEA1) (118, 119) ; 3) early endosome antigen 1 (EEA1), a tethering factor that facilitates vesicle fusion by bridging Rab5-positive vesicles with EEs (97, 98); and 4) specific soluble N-ethylmaleimide-sensitive factor attachment protein receptors (SNAREs) that mediate fusion of endocytic vesicles with EE membranes. Within the early endosome network, sorting endosomes (SEs) exist (99). The transition from EEs to SEs is poorly understood, however, it occurs when EEs stop accepting endocytic vesicles (100).

Endosomal maturation diverges at this point as sorting endosomes compartmentalize cargo into specific domains destined for recycling (recycling endosomes) or degradation (late endosomes) (92, 101). Key proteins on SE membranes include the Retromer complex, which retrieves cargo from endosomes and reroutes it towards the Golgi, and the ESCRT complex, which facilitates intralumenal vesicle (ILVs) formation, for packaging ubiquitinated cargo into multivesicular bodies (MVBs) for degradation (102, 103).

EEs undergo complex maturation, including multiple fusion fission events, to become late endosomes (LEs) (99, 104). Maturation is required to prepare for endosome-lysosome fusion. These processes occur at ER-endosome contact sites, where proteins such as protruding and PDZD8 facilitate lipid and protein exchanges on the endosomal membrane (104). The most significant changes in the endosomal membrane are the exchange of Rab5 for Rab7 and altered phosphoinositides (104, 105).

Late endosomes (LEs) resemble multivesicular bodies. They receive cargo from early endosomes and facilitate transport to other cellular compartments. LEs primarily fuse with lysosomes, thus facilitating the degradation of ubiquitinated cargo (104, 105). However, LEs also mediate retrograde transport of proteins by bypassing lysosomal degradation. The LE-TGN connection thereby prevents degradation of proteins and facilitates their reintegration into the secretory system (106).

In summary, EEs serve as initial sorting stations, guiding cargo to subsequent cellular destinations, whereas LEs act as central hubs connecting multiple intracellular pathways.

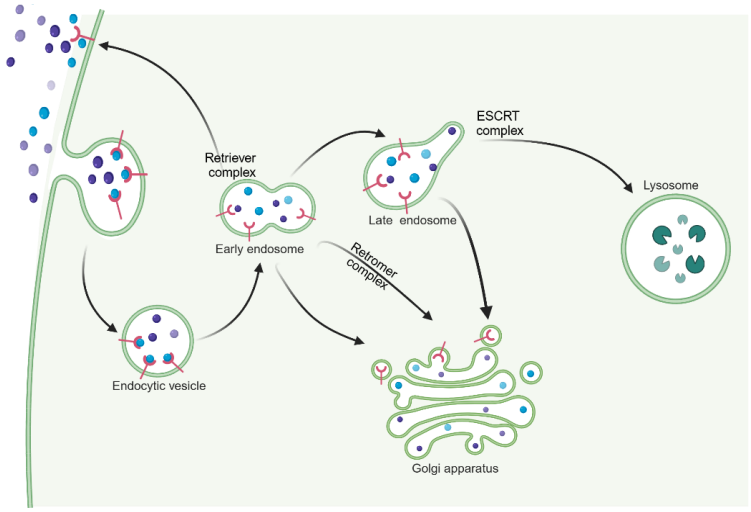

Figure 3. Endosomal sorting. Depiction of protein trafficking after endocytosis. At the endosomes, the trafficking hub of the cells, proteins can be rerouted into various paths that would determine their fate. Figure was generated using Biorender.

1.12 The Retromer complex

The Retromer complex mediates retrograde transport of cargo proteins through recycling transmembrane receptors from early/recycling endosomes to the TGN (Table 2) (107). First discovered in yeast in 1998, the Retromer is highly conserved in all eukaryotic cells (108-110). The Retromer is a hetero-pentamer. The core comprises vacuolar protein sorting 35 (VPS35), VPS29, and VPS26 that mediate recognition and binding of cargo proteins (102, 110, 111).

VPS35, the largest core member (92 kDa), serves as a structural backbone providing a scaffold for VPS29, VPS26, and other accessory proteins, thus providing the necessary platform for interactions with cargo proteins. VPS35 binds many cytoplasmic motifs of cargo proteins, in contrast to VPS29 (111, 112). VPS29 directly binds VPS35 but does not interact with cargo proteins. VPS29 primarily stabilizes the Retromer complex by mediating interactions between VPS35 and accessory proteins such as the Wiskott-Aldrich syndrome protein and SCAR homologue (WASH) complex (111). Although VPS29 displays a phosphatase-like domain architecture resembling metallophosphatases (112-114), its catalytic activity remains inconclusive (113, 114).

VPS26's primary function is recognizing specific cargo proteins and interacting with sorting nexin (SNXs) proteins (111). It binds specific sorting motifs on cytosolic tails of transmembrane cargo proteins, thereby assisting VPS35 in identifying cargo. Structurally, VPS26 has a HEAT-like repeat structure with an arrestin-like fold, which is ideal for interacting with other proteins such as VPS35 and with membranes (115).

In addition to the core complex, SNX proteins are essential for membrane association and forming transport vesicles or tubules. Several SNX family members participate, including SNX1, SNX2, SNX5, and SNX6 (116-119). SNXs are defined by their Phox homology (PX) domain, a lipid-binding domain that specifically binds phosphoinositides such as PI3P, which is enriched in endosomal membranes (120). The PX domain, thus, tethers the Retromer complex to endosomal membranes. Many SNXs contain additional domains, including the Bin-Amphiphysin-RVs (BAR) domain, which senses membrane curvature, and thus promotes membrane tubulation (119, 121).

SNX1, SNX2, SNX5, and SNX6 belong to the BAR-containing SNX sub-group. The BAR domain promotes tubule formation by serving as a scaffold for membrane curvature. SNXs with BAR domains bind to endosomal membranes via their PX domains, and facilitate tubulation and vesicle formation to transport cargo back to the TGN or plasma membrane (122, 123).

Multiple accessory proteins assist the Retromer complex in retrograde trafficking of cargo proteins from endosomes to the TGN. The WASH complex regulates actin dynamics on endosomal membranes and, together with the Retromer complex, facilitates retrograde trafficking (124). Structurally, the WASH complex is a multi-protein assembly comprising WASH1 (Wiskott-Aldrich syndrome protein homologue), FAM21 (Family with sequence similarity 21), Strumpellin, SWIP (Strumpellin and WASH interacting protein), and CCDC53 (Coiled-coil domain-containing protein 53) (124-129).

The function of the WASH complex is to drive actin polymerization at endosomal surfaces. The resulting actin networks stabilize membrane domains where vesicles or tubules form (130). These actin filaments also provide force for scission and budding of vesicles from endosomes that transport cargo proteins to their target destinations (131). Additionally, the WASH complex assists in clustering specific cargo proteins recycled by the Retromer

complex. This coordination ensures that cargo sorting and vesicle formation occur in a controlled manner, allowing efficient recycling of proteins like the mannose-6-phosphate receptor (M6PR), which directs lysosomal enzymes back to the TGN, or various signaling receptors that are returned to the plasma membrane (124). The WASH complex functions by activating the Arp2/3 complex, which nucleates new actin filaments that branch from pre-existing filaments (132, 133). These branched actin networks provide structural support during vesicle formation and scission of transport vesicles from the endosomal membrane.

WASH1 is the primary actin nucleation-promoting factor, while FAM21 bridges the WASH complex to the Retromer complex and recruits it to the endosomal surface (124, 134). The remaining components, Strumpellin, SWIP, and CCDC53, provide structural integrity to the WASH complex and regulate its activity (124, 128, 129). Dysregulation of the Retromer complex resulted by WASH associated mutations causes intracellular accumulation of protein aggregates, increasing toxicity in neuronal cells. This has been linked to Alzheimer's disease (135).

1.13 The Endosomal Sorting Complex Required for Transport (ESCRT)

The ESCRT is a multi-protein machinery essential for several processes of membrane remodeling, especially those involving membrane scission and budding events (Table 2) (103). It is involved in protein trafficking, membrane repair, vesicle formation, and cytokinesis. The ESCRT machinery is best known for its role in sorting and trafficking proteins from late endosomes into intraluminal vesicles (ILVs) that form multivesicular bodies (MVBs), a key step in sending cargo to lysosomes for degradation (136). Additionally, it participates in other membrane remodeling events such as the final abscission in cytokinesis, virus budding, and membrane repair (137, 138).

The ESCRT machinery consists of five core sub-complexes that work in a sequential and coordinated manner to recognize, sort, and package cargo proteins into vesicles. These sub-complexes are ESCRT-0, ESCRT-I, ESCRT-II, ESCRT-III, and associated factors like VPS4. Each complex plays a specific role in the process of cargo selection, vesicle formation, and membrane remodeling (103, 139-141).

Aberrant trafficking caused by loss of function of the ESCRT complex has been linked to the intracellular accumulation of ubiquitinated proteins. This insufficient clearance by lysosomal degradation has far reaching effects, ranging from ER stress to induction of necroptosis (142, 143). Similarly, to disrupted Retromer trafficking, perturbed ESCRT trafficking has been linked to neurodegenerative disorders, including frontotemporal dementia (FTD), amyotrophic lateral sclerosis (ALS), and hereditary spastic paraplegia (HSP) (143).

1.14 The Retriever complex

The Retriever complex is located on early and recycling endosomes and ensures recycling of membrane proteins from endosomes back to the plasma membrane, thereby circumventing lysosomal degradation (Table 2) (144). The Retriever complex is a multi-subunit protein complex consisting of three core subunits:

1. VPS35L (Vacuolar Protein Sorting 35-like, also known as VPS35F or VPS35b)
2. VPS26C (VPS26-related protein C, also called DSCR3)
3. VPS29 (Vacuolar Protein Sorting 29)

VPS35L is a homolog of Retromer's VPS35 and acts as the scaffolding protein ensuring structural integrity of the Retriever complex.

VPS26C is a paralog of Retromer´s VPS26 but specific to the Retriever complex. VPS26C regulates function by interacting with various recycling machineries and with further endosomal compartments (e.g., CCC complex, SNX proteins, Retromer complex). VPS29 is shared between the Retromer and Retriever complexes. It stabilizes the Retriever complex and facilitates recruitment of sorting adaptors (e.g., SNX proteins) (144).

Unlike the Retromer complex, which primarily sorts cargo via WASH-mediated actin assembly, Retriever works with the COMMD/CCDC22/CCDC93 (CCC) complex and SNX proteins to guide recycling (144). The CCC complex facilitates Retriever recruitment and stabilization to early endosomes. The CCC complex also functions through SNX17, a sorting nexin protein that binds cargo proteins like integrins, LDLR, and other transmembrane receptors (145).

SNX17 and its role in integrin trafficking have been one of the major research focuses of our department. Boettcher et al. demonstrated that SNX17 directly binds the Kindlin-associated NPxY motif on β1 integrin tails, which are critical for endosomal sorting. In the absence of SNX17, integrins are rapidly degraded, disrupting cell adhesion (146).

Aberrant trafficking due to loss of Retriever function causes downregulation of cell surface receptors, including α5β1 integrins, that can be rescued by inhibiting lysosomal degradation. This indicates that in the absence of the Retriever complex, integrins are rerouted to lysosomes (147). A similar phenotype was also observed in the absence of SNX17 (146).

Table 2. Integrin trafficking complexes. Summary of trafficking complexes involved in integrin recycling to the plasma membrane, Golgi, and the lysosome.

Trafficking complex	Core components	Destination	Endosomal species	Accessory proteins	Function
Retromer complex	1. VPS35 2. VPS29 3. VPS26	TGN	Early endosomes/ Recycling endosomes	1. SNX proteins 2. WASH complex	Retrograde trafficking
ESCRT complex	1. ESCRT-0 2. ESCRT-I 3. ESCRT-II 4. ESCRT-III 5. VPS4	Lysosomes	Late endosomes	-	Lysosomal degradation
Retriever complex	1. VPS35L 2. VPS26C 3. VPS29	Plasma membrane	Early endosomes	1. CCC complex 2. SNX17	Avoiding degradation

1.15 Small GTPases governing integrin trafficking

The progression of endocytosed cargo through the endolysosomal system, from EE to LE and lysosomes or back to the plasma membrane via recycling endosomes, is tightly regulated by Rab GTPases, membrane tethering factors, and SNAREs (Fig. 4).

Rab GTPases belong to the Ras superfamily. These small GTPases act as molecular switches regulating intracellular trafficking of membrane proteins. The formation of vesicles, their transport, tethering, and fusion of endosomal-derived vesicles to their final destination

is orchestrated by various Rab GTPases. GTPases cycle between their active (GTP-bound) and inactive (GDP-bound) states. In their active GTP-bound state, they interact with multiple effector proteins to facilitate trafficking (148).

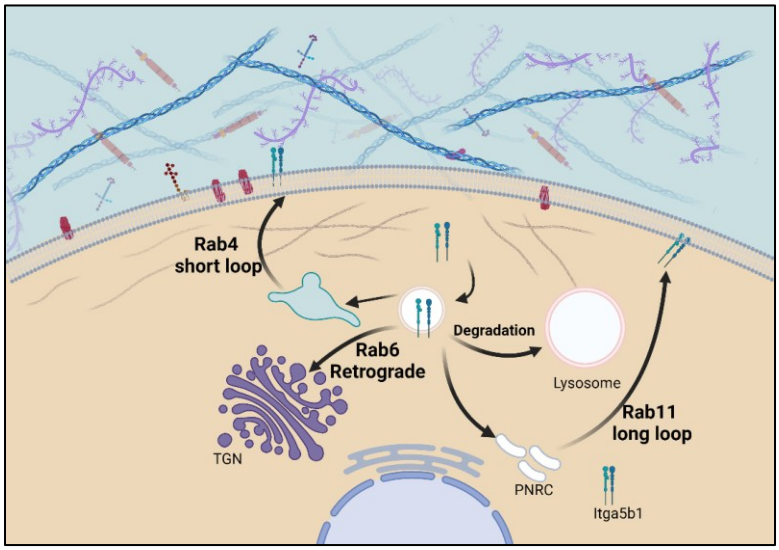

Figure 4. Visualization of various intracellular trafficking pathways employed to re-express integrins to the plasma membrane after internalization. Three major pathways are depicted that act synergistically to traffic various integrin isoforms in either their ligand-bound state or unbound state back to the plasma membrane. The Rab4 pathway specializes in rapid re-expression of ligand-unbound integrins to the plasma membrane. On the other hand, the Rab11 pathway is much slower in the process of trafficking as integrins are re-routed to perinuclear recycling compartments (PNRC) before being re-expressed back on the plasma membrane. The Rab11 pathway specializes in trafficking integrins in their ligand-bound state, thereby ensuring spatially directed recycling and polarized delivery. Finally, the Rab6 pathway traffics integrins retrogradely through the TGN to be re-expressed on the plasma membrane in a highly polarized manner. The only currently known integrin isoform to be trafficked retrogradely is the unbound form of α5β1 integrin. Since the Rab6 pathway has only recently been uncovered, further research is required to determine the pool of integrins that employ this pathway. Figure was generated by Biorender,

Recent advances have enhanced our understanding of trafficking mechanisms that recycle integrins back to the plasma surface and the role Rab GTPases play therein. These pathways and their Rab GTPases vary depending on the cell type, integrin conformation, ligand-bound state, and heterodimer type (149).

Most research on integrin recycling focuses on two primary routes: the short loop governed by Rab4 and the long loop governed by Rab11 (150, 151). Additional trafficking pathways include the Rab7 degradation pathways, which directs integrins from late endosomes to lysosomes for degradation.

1.16 The Rab4 pathway - fast recycling

Integrins are rapidly recycled back to the plasma membrane via the Rab4 pathway, maintaining their availability at the leading edge of migrating cells, thereby ensuring directional migration and quick adhesion turnover (Fig. 4) (152). This fast-recycling route directly reroutes integrins from early endosomes back to the plasma membrane. Through dynamic adhesion turnover, the Rab4 pathway selectively traffics integrins that are associated with cellular migration, wound healing, and rapid adhesion renewal.

Table 3. Summary of integrin trafficking routes governed by their respective small Rab GTPase. Integrin trafficking is strongly affected by the integrin isoform, conformational state, ligand-bound state, and cell type. These attributes specify the trafficking pathway integrins are destined to take, to facilitate cellular migration and adhesion.

Feature	Rab4 (fast recycling)	Rab11 (slow recycling)	Rab6 (retrogradely recycling)
Speed	Rapid	Slower	Slower
Recycling route	Directly from early endosomes to the plasma membrane	Through recycling endosomes before returning to the membrane	Through the TGN before returning to the plasma membrane
Function	Supports quick adhesion turnover	Ensures spatially directed recycling and polarized delivery	Polarized redistribution of integrins to the leading edge of the cell
Integrin isoform	αvβ3, α5β1, and other β1 integrins	α5β1, α6β4, αvβ3, and α2β1	α5β1
Ligand bound state	Ligand-unbound state	Ligand-bound state	Ligand-unbound state
Cellular context	Dynamic adhesion, such as during rapid migration or angiogenesis	Sustained migration, directional migration, and tissue remodeling	Unligated integrins are redistributed to the leading edge of the cell to maintain polarized migration

The Rab4 pathway selectively traffics specific ligand-unbound integrin isoforms required for the formation of dynamic adhesions (153). Isoforms like αvβ3, which mediates angiogenesis, tumor migration, and wound healing, as well as integrin α5β1, critical for cellular migration and ECM remodeling, are trafficked via this pathway (152, 153).

1.17 The Rab11 pathway - slow recycling

The Rab11 long loop, unlike the Rab4 pathway, is slower and regulates spatial and temporal expression of integrins on specific regions of the plasma membrane (Fig. 4) (150). Rab11 recycles integrins to the leading edge in a highly polarized manner. Unlike the dynamic adhesion formation via the Rab4 pathway, the Rab11 pathway facilitates stable adhesions. Like the Rab4 pathway, the Rab11 pathway selectively traffics specific integrin isoforms, primarily in their ligand-bound state (154). Integrin isoforms such as α5β1, α6β4, and αvβ3 rely on the Rab11 pathway to sustain long-term cell migration and stabilize focal adhesions. Despite differences, they act synergistically to coordinate adhesion turnover and directional migration of both ligand-bound and -unbound integrins.

1.18 The Rab6 pathway - retrograde recycling

Johannes and colleagues recently identified a novel trafficking pathway for integrin recycling (Fig. 4). They demonstrated that β1 integrins are transported from the plasma membrane to the TGN and re-secreted in a highly polarized manner to the leading edge of migratory cells. Using conformation specific antibodies, the authors showed that the retrograde route is exclusively utilized for the non-ligand bound conformation of α5β1 integrins. They disrupt retrograde trafficking by knocking down Rab6. In the absence of Rab6, integrin surface distribution was significantly impaired. Under physiological conditions, there is a clear gradient of integrins peaking at the leading edge. However, when Rab6 was disrupted, integrins were randomly distributed across the cellular surface. The authors demonstrated the importance of retrograde transport during mouse embryonic development. In the absence of Rab6, there was severe malformation of embryonic layers, highlighting its importance (155).

1.19 The importance of the retrograde pathway

Retrograde transport of proteins is essential for maintaining cellular homeostasis and function and is identified as a preferred invasion route for various pathogens and toxins (156). The retrograde route comprises three steps:

1. Movement of proteins and other molecules from early and recycling endosome to the TGN.
2. Trafficking through the Golgi system (intra-Golgi transport).
3. Transport from Golgi to ER (157).

The primary function of the retrograde route, facilitating transport of proteins and lipids to the TGN and the ER, allows reuse of transport machinery components (e.g., CI-M6PR, Cathepsin D, Furin, SNAREs) (158). This process is essential for organelle identity maintenance by maintaining the distinct composition of the ER and Golgi apparatus through retrieving ER-resident proteins that have escaped (157). Additionally, integrins, especially β1 integrins, rely on the retrograde route for secretion in a highly polarized manner to sustain the leading edge (155).

The retrograde route serves as a prominent invasion route for various pathogens and bacterial toxins (159). To access their cytosolic targets, bacterial toxins have evolved methods to translocate across cell membranes. Cholera toxin (CT), secreted by *Vibrio cholerae*, bypasses the cell membrane by binding to glycosphingolipids on the outer leaflet of the plasma membrane (160). Following the binding, an accumulation of lipids occurs at the binding site, leading to endocytosis. The endocytosed cargo converges at the endosome, where the Retromer complex traffics CT to the TGN before reaching the ER (159, 160).

Shiga (STx) and Shiga like toxins (SLT), secreted by *S. dysenteriae*, follow a similar route to CT (161). Pseudomonas exotoxin A (PE) is secreted by *Pseudomonas aeruginosa* and is its most toxic virulent factor (162). Unlike STx and CT, which bind lipid residues on the outer leaflet, PE first enters cells by binding to the CD91 receptor and then to intracellular KDEL receptors (KDELRs) (163). KDELRs are primarily found on the cis-Golgi surface, lysosomes, and secretory vesicles (164). Their function is in binding and retrogradely

transporting ER-resident proteins containing a C-terminal Lys-Asp-Glu-Leu (KDEL) sequence (159, 165).

Beyond bacterial derived toxins, certain viruses like SV40 and polyoma viruses (Py) utilize retrograde transport to reach the ER (156). These viruses, like CT and STx, bind to glycolipids in the plasma membrane to gain access to the ER (166).

1.20 The Golgi apparatus in the biosynthetic system

The Golgi apparatus is a central component of the biosynthetic secretory system responsible for trafficking approximately 33% of newly synthesized proteins to various cellular destinations (167, 168). Structurally, the Golgi appears as stacked flattened and fenestrated membrane sacs or cisternae (168, 169). The alignment of several cisternae in parallel produces a stack compartmentalized into cis, medial, and trans compartments. The membranes of these compartments display distinct biochemical and functional properties to facilitate protein transport (167, 168). Compartments are distinguished by specific G-proteins, clathrin adaptors, SNAREs, and Golgin tethers (168).

The trans-most cisternae constitute the TGN. While the entire Golgi is dynamic, the TGN shows particular proclivity for the formation of tubular structures that undergo extensions and retractions (168, 170, 171). These tubular structures facilitate exchange of vesicular bodies by enabling tethering, fusion, and scission of vesicles to and from the TGN.

Beyond trafficking, the Golgi is essential for lipid and protein post-translational modifications. These post-translational modifications include glycosylation. The membranes of the Golgi are lined with glycosyltransferases that facilitate the addition of sugar moieties (172). Integrin glycosylation is critical for conformation, activity, and formation of functional dimers (173, 174). The glycosylation status of integrins, particularly α3β1 and α5β1, correlates with their binding strength to ECM ligands, thereby regulating multiple cellular processes including differentiation, apoptosis, and proliferation (173). Maintaining glycosylation patterns on integrins after internalization and re-expression is key to proper integrin functioning. Little is known about glycosylation patterns of internalized integrins or whether retrograde transport functions to reestablish lost glycosylation.

1.21 Cargo sorting at the TGN and tethering mechanisms

Beyond endosomal sorting, the TGN acts as a sorting station since the TGN is utilized by both anterograde and retrograde routes. Shimizu et al., using super-resolution confocal live imaging microscopy (SCLIM), characterized two distinct "zones" at the TGN surface of *Arabidopsis thaliana*. These zones exhibit spatially and temporally distinct distribution of proteins. The first zone is characterized by proteins involved in secretory trafficking, such as VAMP721 (R-SNARE), AP-1 (adaptor protein complex), and clathrin. The second zone specializes in vacuolar trafficking and is characterized by VAMP727 (R-SNARE) and AP-4 (175). However, the study did not identify a unique zone for retrogradely transported proteins, which might be due to discrepancies between plant TGN, which also acts as endosomes, and human TGN (175).

SNAREs act as molecular “zip-codes” that ensure vesicular trafficking to specific compartments. Syntaxins are essential components of SNARE complexes for targeting and fusion of endosomal-derived vesicles to the TGN surface (176). Particularly, Syntaxin-6 facilitates transport from early, recycling, and late endosomes to the TGN through two distinct SNARE complexes (176-178).

The first SNARE complex identified in humans, trafficking cargo from early/recycling endosomes includes the Stx6–Stx16–Vti1a–VAMP4 complex and requires Rab6A/ Rab11 GTPases (177). Transport from late endosomes is regulated by the Stx10−Stx16−Vti1a−VAMP3 complex and requires the Rab9 GTPase (178, 179). The number of SNARE complexes essential for retrograde transport increases as research progresses (180, 181). These SNARE complexes act synergistically with multiple tethering molecules, including elongated coiled-coil tethers of the Golgin family: Golgin-97, Golgin-245, GCC88, and GCC185, which are specific to the TGN surface (176).

1.22 Integrin trafficking defects lead to pathological conditions

Most integrins are recycled back to the cell surface after endocytosis, maintaining a constant pool of active integrins on the plasma membrane for proper cellular functioning. It is more efficient for cells to recycle endocytosed integrins than to expend resources producing new integrin molecules (182).

Failure to re-express integrins on the plasma membrane following internalization leads to pathophysiological conditions affecting migration and immune function. Dysregulation of integrin trafficking represents a hallmark of cancer (183). Given their role in cell adhesion and migration, integrins contribute to tumor progression and metastasis. By initiating intracellular signaling cascades, integrins promote cellular proliferation and survival. In certain breast cancer types, αvβ3 and α6β4 promote survival signaling when improperly recycled or retained at the cell surface (184-186). This involves activation of the EK1/ERK2 MAPK pathway, which regulates cyclin-dependent kinases (CDKs) and cell cycle progression (187). Research shows that dysregulated αvβ3 and α5β1 cause invadopodia formation, facilitating cancer cell breakdown of the ECM, thereby facilitating metastasis (188-193).

Furthermore, epithelial-to-mesenchymal transition (EMT) is a prominent transformation process in various cancers (194-196). During EMT, adherent cells adopt a mesenchymal phenotype, facilitating migration. Yuan et al. revealed by single particle tracking that during the transition from epithelial to mesenchymal morphology of MCF10A cells, β1 integrins are asymmetrically distributed, favoring front regions. This underscores the importance of integrin distribution during EMT and proposes integrin diffusion as a new hallmark of EMT (197).

1.23 The FWC complex and TBC1D23: novel regulators of retrograde trafficking

Negredo et al. recently identified a novel trimeric complex comprising Fam91A1, WDR11, and C17orf75 (FWC complex) that mediates endosome-to-TGN trafficking. They utilized a forward genetic screen in haploid KM7 cells and expressed a chimeric protein consisting of the extracellular and transmembrane domains of CD8 and the cytoplasmic tail of Furin (CD8-Furin). Furin normally localizes to the TGN, but upon infecting KM7 cells with a gene-trap retrovirus, the chimera CD8-Furin was shifted from the TGN to the cell surface (198). By analyzing cells with higher surface localization of the chimeric protein, by deep sequencing, two hits emerged: WDR11 and AP1M1. The study also demonstrates that WDR11 associates with Fam91A1 and C17orf75, forming a stable complex localized at the TGN. Notably, upon knocking out Fam91A1, the complex disassembles as shown by

reduced protein levels by Western blot and decreased TGN localization in immunofluorescent images (Table 4) (198).

Table 4. FWC dynamics. Fam91A1 appears to be crucial for proper localization to the TGN as well as ensuring stability of the complex. WDR11 has a small impact on proper cellular localization. Finally, C17orf75 does not affect cellular localization or protein stability.

FWC proteins	Needed for localization	Need for stability
WDR11	+	+/-
FAM91A1	+	+
C17orf75	-	-

The study further shows that the FWC complex affects the trafficking of well-known retrogradely trafficked proteins such as cation-independent mannose-6-phsphate receptor (CIMPR) (198).

Electron microscopy revealed that certain cargoes, instead of accumulating on the plasma surface, accumulate in MVBs around the TGN, as demonstrated with Carboxypeptidase D (CPD). CPD belongs to the family of metallocarboxypeptidases that trim peptide chains by cleaving C-terminal amino acids. Despite providing substantial information on the physiology of the FWC complex, the study lacks a functional phenotype for the complex deficiency.

Prior to this work, Shin et al. identified a bridging factor, TBC1D23, connecting the FWC complex to Golgin-245 and Golgin-97, tethering molecules that tether incoming cargo to SNARES on the TGN. Using BioID screens of chimeras consisting of Golgins fused to a mitochondrial localization sequence, the authors demonstrated binding of the FWC complex and TBC1D23 to Golgin-245 and Golgin-97. Through truncation and mutation analysis, the authors uncovered the binding sites between Golgins and TBC1D23 (199).

TBC1D23 binds directly to the N-termini of Golgin-97 and Golgin-245. Upon introducing mutations in the first 21 amino acids (aa) of the Golgins, TBC1D23 failed to localize to the TGN. The authors demonstrated that Fam91A1 binding to TBC1D23 recruits the FWC complex to the TGN and interacts with FAM21A, a member of the WASH complex (199). In summary, Shin et al. established the link between the FWC complex and TBC1D23, demonstrating that TBC1D23 acts as a bridging factor facilitating tethering of incoming

cargo vesicles from the endosomes to the TGN. Golgin-97 and Golgin-245 were identified as the responsible tethering molecules binding TBC1D23 via their N-termini (Fig. 5).

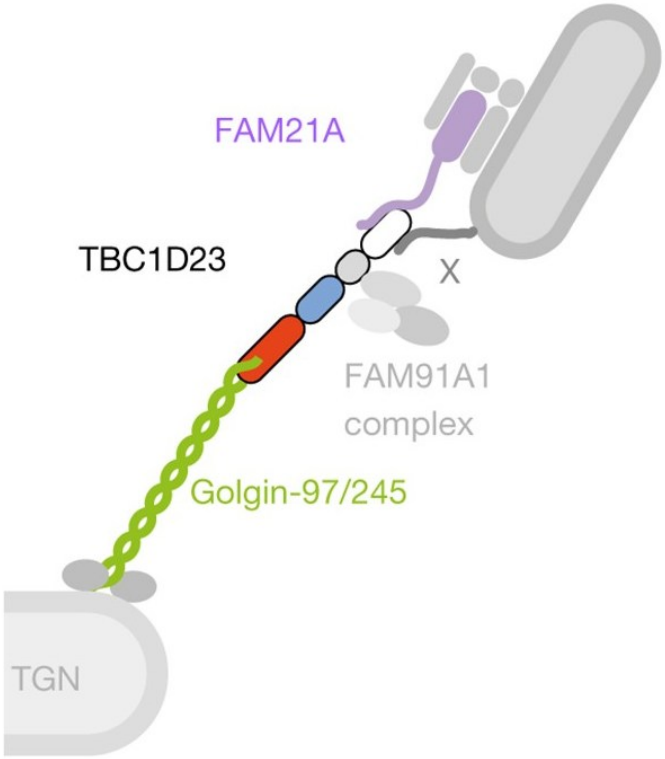

Figure 5. Depiction of FWC complex involvement in the tethering of incoming endosomal vesicles. A proposed model depicting how TBC1D23 functions as a molecular bridge connecting TGN Golgins to vesicles originating from endosomes. To achieve cargo specificity, TBC1D23 is likely to engage with additional vesicular components (indicated as X) besides FAM21, since FAM21 also participates in the formation of endosome-derived vesicles destined for the plasma membrane. The FAM91A1 complex is not essential for tethering, suggesting that it may instead modulate or support the tethering process, act in downstream steps, or function only under specific cellular conditions. Adapted from Shin et. al (199).

Together, these studies establish that the FWC complex and TBC1D23 mediate retrograde trafficking of cargo to the TGN. However, neither study addressed the functional consequences of aberrant retrograde transport nor provided a satisfactory model explaining FWC complex cargo engagement.

Only recently the tertiary structure of the WDR11-Fam91A1 dimer was resolved using cryo-electron microscopy (cryo-EM). The authors used proximity biotinylation to identify additional cargoes trafficked by the FWC complex. These cargoes share a super acidic

cluster (SAC)-containing motif. The SAC is a motif consisting of at least one acidic cluster with 6-10 E/D/S residues flanked by at least one bulky hydrophobic residue. Mutating these motifs reduced binding affinity between WDR11 and cargo. Newly identified proteins include ATG9, TMEM87B, SV2A, MERTK, and VAMP4. The study also addresses the biological relevance of aberrant retrograde trafficking caused by loss of the FWC complex, albeit the findings not being novel. Using zebrafish, they showed that loss of WDR11 causes significant neuronal defects. Axonal length was significantly reduced, but the underlying cause remains unknown (200).

1.24 Fam91A1 associated mutation in pontocerebellar hypoplasia (PCH)

The same group previously demonstrated an identical phenotype in neuronal development of zebrafish in the absence of Fam91A1 (201). The authors sought to determine whether Fam91A1 mutations act as drivers of pontocerebellar hypoplasia (PCH), given that TBC1D23 mutations are already established contributors to the disease. (201-203). The mutations R61A, $KD^{AA,}$ and D198R identified in PCH patients, fail to bind to TBC1D23 on the TGN surface, suggesting that aa residues 61 and 198 are required for TBC1D23 binding.

PCH patients exhibit severe hypoplasia or atrophy of the brain, most prominently affecting the pons and cerebellum (201, 204-206). The observed phenotypes may arise from aberrant protein trafficking caused by impaired *TBC1D23* interaction with the FWC complex.

1.25 WDR11 mutations in Kallmann syndrome

Fam91A1 is not the only FWC complex member associated with disease. Extensive data links *WDR11* mutations to the hormonal disorders Kallmann syndrome (KS) and idiopathic hypogonadotropic hypogonadism (IHH) (207-209). KS is a genetic disorder characterized by inadequate production and maturation of gonadotropin-releasing hormone (GnRH) neurons. GnRH production is crucial for initiation of puberty; failure to produce GnRH leads to reduced or absent sexual development and reproductive function (210). GnRH neurons

originate in the olfactory placode and migrate to the hypothalamus during embryonic development. The hypothalamus then releases GnRH to regulate the secretion of gonadotropins such as luteinizing hormone (LH) and follicle-stimulating hormone (FSH) from the anterior pituitary gland. These hormones stimulate the gonads to produce sex hormones such as estrogen and testosterone. The underlying cause of KS is impaired migration of GnRH neurons to the hypothalamus (211). This faulty migration also affects the olfactory bulbs, causing anosmia or hyposmia that frequently accompanies KS. Anosmia refers to partial or total loss of smell. The connection between sexual development and smell in KS results from the common developmental pathway of olfactory bulbs and GnRH neurons (210, 211).

Clinical manifestations of KS typically appear during adolescence, when affected individuals fail to undergo normal puberty. Various clinical features characterize KS, including stunted development of primary and secondary sex organs and infertility (210). Additional manifestations include neurological and cognitive symptoms such as ataxia or intellectual impairment.

Table 5. Effects of Kallmann syndrome (KS) on male and female development. The delayed or complete shutdown of puberty has detrimental consequences on the development of young adults. Besides the neurological and cognitive impairments that are commonly seen in patients suffering from KS, infertility, anosmia, and the lack of sexual organ development are hallmarks of KS.

Males	Females
Lack of testicular enlargement	Amenorrhea
Infertility	Infertility
Anosmia/Hyposmia	Anosmia/Hyposmia
Neurological and cognitive impairments	Neurological and cognitive impairments

Multiple genetic determinants cause KS. Various genes have been identified in patients with KS, and research supports a genetically heterogeneous etiology (210). Despite this heterogeneity, multiple mutations in the *WDR11* gene have been observed in KS patients, leading to a defective hypothalamic-pituitary-gonadal axis (210-212). Some controversial papers claim that WDR11 interacts with the transcription factor EMX1, essential for

Hedgehog (Hh) signaling and ciliogenesis, as the root cause of KS (207, 208, 213). However, these interactions with transcription factors have not been replicated by other groups, and the phenotypes reported concerning ciliated tissues could also result from dysfunctional protein trafficking. A recent study observed a significant decrease in cellular motility of primordial germ cells (PGCs) in WDR11-deficient embryos (208). Integrins are essential for the formation and maintenance of ciliated tissues by controlling cytoskeletal tension during initial cilia assembly (214, 215). The observed phenotypes, therefore, might reflect faulty recycling of integrins during embryonic development (216-220).

2. Aim of the doctoral thesis

The retrograde trafficking pathway represents a specialized route for polarized protein delivery, yet its role in integrin biology remains unexplored. While canonical recycling pathways via Rab4 and Rab11 have been extensively characterized, the molecular machinery and functional significance of integrin retrograde trafficking through the trans-Golgi network are unknown. This thesis addresses this fundamental gap by investigating whether the FWC complex mediates retrograde trafficking of α5β1 integrins and examining the cellular and developmental consequences of disrupting this pathway.

This work examines the role of the FWC complex in retrograde trafficking of α5β1 integrins and its effects on cellular motility and polarization. The significance of the retrograde route lies in its ability to traffic proteins in a highly polarized manner. Since integrin function depends critically on their spatial positioning on the cell surface, this thesis investigates how the spatial and temporal distribution of α5β1 integrins is affected by loss of the FWC complex function.

Specifically, this thesis aims to:

1. Determine whether α5β1 integrins utilize the FWC complex for retrograde trafficking.
2. Characterize the molecular interactions between FWC complex components and integrin trafficking machinery.
3. Examine the functional consequences of FWC deficiency on integrin-dependent cellular processes.
4. Establish the physiological relevance of retrograde integrin trafficking in development and disease.

By addressing these objectives, this work will establish whether disrupted retrograde trafficking contributes to the severe developmental phenotypes observed in FWC-associated disorders and provide mechanistic insights into how cells spatially organize their adhesion machinery through specialized trafficking pathways.

3. Material and Methods

3.1 General materials

Consumables used for both sterile and non-sterile laboratory procedures were sourced from the following manufacturers: Bioplastics, Bio-Rad, Biozym, Corning, Greiner, Labomedic, Neolab, Sarstedt, and VWR.

3.1.1 Chemicals and reagents

Table 6. Chemical and reagent list

Chemical/Reagent Supplier	Chemical/Reagent Supplier
6X Loading Dye	Thermo Fisher Scientific
Acetic Acid	Roth
Agarose powder	Biozym
BD Pharm Lyse™	BD Biosciences
Bromphenolblue	Roth
BSA	Roth
CaCl2 Roth	Roth
CompleteTM Protease Inhibitor Cocktail	Roche
DMSO	Roth
DNA Ladder	Thermo Fisher Scientific
Doxycyclin Hyclate	Sigma-Aldrich
DTT	Roth
EDTA (0,5 M pH = 8 solution)	Life Technologies
EDTA powder	Roth
Ethanol	Roth
Gene Ruler 1kb or 100bp	Thermo Fisher Scientific
Glycerol	Roth
Glycin	Roth
HCl	Roth
Isopropanol	Roth
KCl	Roth
LB	Roth
LB agar	Roth
MgCl2	Roth
Na2HPO4	Roth
NaCl	Roth
PageRuler™ Prestained Protein Ladder	Thermo Fisher Scientific
Pierce ECL WB substrate	Thermo Fisher Scientific
Ponceau S staining	Sigma-Aldrich
RNase A	Life Technologies

SDS	Roth
TRIS	Roth
Triton X 100	Roth
Trypsin EDTA	Gibco
Tween 20	Roth

3.1.2 Enzymes and enzyme buffers

Table 7. Enzymes and buffers

Enzyme or buffer	Supplier
Fast digest restriction enzymes and buffers	NEB
Phusion Polymerase and buffer	Thermo Fisher Scientific
Q5® Hot Start High-Fidelity DNA Polymerase	NEB
T4 DNA Ligase and buffer	Thermo Fisher Scientific
T4 DNA polymerase	Thermo Fisher Scientific

3.1.3 Kits

Table 8. Molecular kit list

Kit	Supplier
QIAquick gel extraction kit	Qiagen
QIAquick PCR purification kit	Qiagen
BCA assay kit	Thermo Fisher Scientific
PureLink Maxi-Prep kit	Invitrogen

3.1.4 Buffers and solutions

Table 9. Buffers and solutions

Buffer/Solution	Components
10X PBS	1.37M NaCl, 27mM KCl, 80mM Na_2HPO_4, 20mM KH_2HPO_4, adjust to pH 7.4
10X TBS	500mM Tris-base, 1.5M NaCl add water to 10L adjust to pH 7.6
10X Tris-Glycine buffer	250mM Tris-base, 1.92M Glycine, add water to volume 10 L
2X Laemmli Sample buffer	150mM Tris-HCl pH 6.8, 200 mM DTT, 4% SDS, >0.02% Bromophenol Blue, 20% Glycerol, add water to final volume 100ml
50X TAE Buffer	2M Tris-base, 1M Acetic acid, 50mM EDTA, adjust to pH 8
Direct Lysis Buffer	0.2mg/ml Proteinase K, 1mM $CaCl_2$, 3mM $MgCl_2$, 1mM EDTA, 1% Triton X-100, 10 mM Tris pH 7,5
LB agar	20g LB, 15g Agar, 1 L H_2O, autoclaved before use
LB medium	20g LB, 1L H_2O, autoclaved before use
FACS buffer	2 mM EDTA, 2% FCS in PBS
1X TBS-T	100mL 10X TBS, 5 mL Tween-20, add water to 1L

1X Western Blot transfer buffer	100mL of 10x Tris-Glycine buffer, 200mL Ethanol, add water to 1L
1X RIPA buffer	50mMTris-HCL pH8, 150mM NaCl, 1mM EDTA, 1% Triton X-100, 0.5% Sodium deoxycholate, 0.1% SDS
IP buffer	50mM Tris pH 8.0, 150mM NaCl, 0.5mM EDTA, 1% NP-40
Wash buffer	50mM Tris pH 8.0, 150mM NaCl, 0.5mM EDTA
1X HEPES buffer	25mM HEPES, 150mM NaCL, adjust to pH 7.2

3.1.5 Primary antibodies

Table 10. Primary antibodies

Antibody	Supplier	Application	Dilution
WDR11 (ab93871)	Abcam	WB, IF	1:1000WB/1:300 IF
Fam91A1 (27738-1-AP)	Proteintech	WB	1:1000 WB
C17orf75 (SAB1405246)	Sigma	WB	1:1000 WB
TBC1D23 (PA5-106439)	Invitrogen	WB	1:1000
Kindlin-2 (K3269)	Sigma	WB	1:1000
Talin (T3287)	Sigma	WB	1:1000
Vinculin (sc-5573)	Santa Cruz	WB	1:1000
Gapdh (CB1001)	Calbiochem	WB	1:5000
Integrin β1(clone 18)	BD biosciences	WB	1:1000
Integrin α5 (#4705)	Cell Signaling	WB	1:1000
aGFP-Rat (A10262)	Invitrogen	IF	1:5000
GFP-Rabbit (A10262)	Invitrogen	IF	1:5000
TGN46 (AHP500GT)	BIO RAD	WB	1:1000
Integrin β1 clone mAB13 (552828)	BD Pharmingen	IF	1:500
Integrin β1 clone 9EG7(550531)	BD Pharmingen	IF	1:500
Integrin α5 VC5 (555651)	BD Pharmingen	IF	1:500
GM-130 (610822, clone 35)	BD Biosciences	IF	1:250
Phalloidin (P1951)	Sigma	IF	1:500
Phalloidin (A12379)	Molecular Probes	IF	1:500
Integrin α2 (AK7)	Abcam	FACS	1:500
Integrin β1 (556049, CD29) Clone Huts-21	BD Biosciences	FACS	1:500
Integrin α5 (563578, CD49e) Clone IIA1	BD Biosciences	FACS	1:500
IgG1 mouse k isotype Ctrl (400111) Clone MOPC-21)	BioLegend	FACS	1:500
IgG1 mouse k isotype Ctrl (565571) Clone MOPC-21)	BD Biosciences	FACS	1:500

3.1.6 Secondary antibodies

Table 11. Secondary antibodies

Antibody	Host	Reactivity	Supplier	Application	Dilution
AlexaFluor 488 (A11029)	Goat/IgG	Mouse	Invitrogen	IF	1:500
AlexaFluor 488 (A11008)	Goat/IgG	Rabbit	Invitrogen	IF	1:500
AlexaFluor 488 (A11039)	Goat/IgG	Chicken	Invitrogen	IF	1:500
AlexaFluor 488 (A11006)	Goat/IgG	Rat	Invitrogen	IF	1:500
Alexa Fluor 647+ (A32733)	Goat/IgG	Rabbit	Invitrogen	IF	1:500
Cy3 (AC112C)	Sheep/IgG	Human	Sigma	IF	1:500
Anti-rabbit IgG, HRP linked Antibody (#7074)	Goat/IgG	Rabbit	Cell Signaling Technology	WB	1:5000
Anti-mouse IgG, HRP linked Antibody (#7076)	Goat/IgG	Mouse	Cell Signaling Technology	WB	1:5000

3.1.7 Cloning primers

Table 12. Cloning primers

Name	Sequence
pAA40.Xho1_Nhe1_WDR11_Fw	CTCGAGGCTAGCATGTTACCCTACACCGTAAACTTCAAGGTGTCAGCGCGC
pAA19_Not1_Kpn1_mWDR11_Rv	TAACTAGGTACCTCGGCCGCACTTTCCGTTAG
pAA46_Nhe1_KpnI_WDR11_Fw	GCTAGCGGTACCATGTTACCCTACACCGTAAACTTCAAGGTGTCAGCGCGC
pAA47_BamHI_WDR11_Rv	GCGGGATCCACTTTCCGTTAGCTCTTCCTTGG
pAA68_FAM91A1-Xho1-HindIII-Fw	AAGCTTCTCGAGGCATGAACATCGACGTTGAGTTCCAC
pAA63_FAm91A1_Stop-Rv	TTATCTAGATCCGGTGGATCCCGG
pAA74_C17orf75_SACI_Fw	CCGGAGCTCCTACCGGACTCAGATCTACCGCC
pAA38_mC17orf75_AgeI_BamHI_XmaI_Rv	CGGTGGATCCCGGGCCCGC
pAA87.WDR11.Kpn1.Xho1-FW	GCGCTCGAGGACGGTACCATGTTACCCTAC
pAA93_WDR11_400_BamH1-Rv	GCGGGATCCCACACCGGAACTGTTCCGTGC
pAA92_WDR11_500_BamH1_Rv	GCGGGATCCGTGGTACACCAGGACAGAACC
pAA90.WDR11_BamH1-Rv	GCGGGATCCTTCCTTGGTTACCACTGTGTC
pAA91.WDR11_953_KPNI-Fw	GCGGGTACCGCTCCTAAGGACAGGCTGAGC
pAA.88_WDR11-BamH1 Rv	GGTGGATCCACTTTCCGTTAGCT
pAA89.WDR11_KPN1-Rv	GCGGGTACCAACAGCATCTGTACTACATCAAAT
pAA94_WDR11-XhoI-KpnI-Fw	GCGCTCGAGGACGGTACCATGTTACCCTACACCGTA
pAA95_WDR11-XhoI-KpnI-Fw	GCGGCCGCTGGATCCACTTTCCGTTAG
pAA96_Fam91A(p.750)_Kpn1_Rv	GCGGGTACCGCACAGGCCATGGGTAGCTATTTT
pAA97_Fam91A1(p.800)_Kpn1_Rv	GCGGGTACCGCAGGGCGACTGTGAAAGCAC

pAA98_Fam91A1_(p.823)_Kpn1_Rv	GCGGGTACCGCTCCACTCTGATAAGACACCATC
pAA99_Fam91A1_(p.830)_Kpn1_Rv	GGTACCCAGGGAGGAAGGTGAGCGTCC
pAA100_Fam91A1_(p.835)_Kpn1_Rv	GCGGGTACCGAGACTAGCGATGAGCAGGGA
pAA101_Fam91A1_(p.810)_Kpn1_Rv	GCGGGTACCTTTGGCCGGAAGTGGAACTCC
pAA81_C17orf75(Δ1-65aa)	AGTGAGCTCATGGACGTTCAGGTGGCATAAATGC
pAA82_c17orf75(Δ136-400aa)	GCCGAGCTCGCCTTTTCCAACAGGAAAAACTGCTT
pAA83_C17orf75(Δ136-400aa) _Rv	GCGGGATCCAAGCAGTTTTTCCTGTTGGAAAAGGCA
pAA84_C17orf75(Δ136-400aa) _Rv	GCGGGATCCGGAAGCAGTTTTTCCTGTTGGAAAAGGCA
pAA85_C17orf75(Δ300-400aa) _Rv	GGTACCGCGGGATCCTGCATCCAGTCCTCACAAAAACG
pAA86_C17orf75(Δ1-135aa) _Fw	GCGCTCGAGGCGGCTAGCTGCCTTTTCCAACAGGAAAAACTGCTT

3.1.8 Mutagenesis primers

Table 13. Mutagenesis primers

Name	Sequence
mt.pAA53_Fam91A1_R61A-Fw	CATGTCAAGAAAGATGAAgGCAAGTACTATGAGGAGCTGCTC
mt.pAA54_Fam91A1_R61A-Rv	GAGCAGCTCCTCATAGTACTTGCcTTCATCTTTCTTGACATG
mt.pAA55_Fam91A1_D198R-Fw	GGCGCCATTGATAAGATCATCcgCTCAGGTCCTCAGCTCTCTGGG
mt.pAA56_Fam91A1_D198R-Rv	AGAGAGCTGAGGACCTGAGcgGATGATCTTATCAATGGC
mt.pAA45_Fam91A1_R569Q-Fw	ATATTCCAGGGTTATGATCAGTTACTTATAACCTCTTGGggcc
mt.pAA46_Fam91A1_R569Q-Rv	ggccCCAAGAGGTTATAAGTAACTGATCATAACCCTGGAATAT
mt.pAA83_WDR11_R395W_Fw	TGCAGTCGAAATGCAtGGAACAGTTCCGGTGTG
mt.pAA84_WDR11_R395W_Rv	CACACCGGAACTGTTCCaTGCATTTCGACTGCA
mt.pAA97_WDR11_I435V_Fw	ATCGGGCAAAGTGCAgTTGCTGGGGAAGAACAC
mt.pAA98_WDR11_I435V_Rv	GTGTTCTTCCCCAGCAAcTGCACTTTGCCCGAT
mt.pAA23_WDR11_436A>T_Fw	GGGCAAAGTGCAATTACTGGGGAAGAACACCCC
mt.pAA24_WDR11_436A>T_Rv	GGGGTGTTCTTCCCCAGTAATTGCACTTTGCCC
mt.pAA85_WDR11_E448Q_Fw	GGCTCCATTCTGCAGcAAGTGCACCTCAAGTTC
mt.pAA86_WDR11_E448Q_Rv	GAACTTGAGGTGCACTTgCTGCAGAATGGAGCC
mt.pAA21_WDR11_450H>R_Fw	TCCATTCTGCAGGAAGTGCGCCTCAAGTTCCTGCTGACG
mt.pAA22_WDR11_450H>R_Rv	CGTCAGCAGGAACTTGAGGCGCACTTCCTGCAGAATGGA
mt.pAA31_WDR11_H690Q_Fw	AATGATGGCCAAGTTTATCAaCTCACTGTTGAAGGAAATTCT
mt.pAA32_WDR11_H690Q_Rv	AGAATTTCCTTCAACAGTGAGtTGATAAACTTGGCCATCATT
mt.pAA99_WDR11_R755H_Fw	TGGGTGAGGAAGATTCaCTTTGCCCCTGGCAAG
mt.pAA100_WDR11_R755H_Rv	CTTGCCAGGGGCAAAGtGAATCTTCCTCACCCA
mt.pAA13_WDR11_966Y>A_969L>A	CCCACTGGACATCTGCCGCGATGTGCGCTGTGAGAACACC
mt.pAA14_WDR11_966Y>A_969L>A	GGTGTTCTCACAGCGCACATCGCGGCAGATGTCCAGTGGG

3.1.9 sgRNAs

Table 14. sgRNAs

Name	Sequence
oAA15_WDR11_gN19-gN20-guideRNA49fwU6sensepX330	CACCGGTCGGCGCGCACCCTCACG
oAA16_WDR11_gN19-gN20-guideRNA49fwU6antisensepX330	AAACCGTGAGGGTGCGCGCCGACC
oAA17_fam91-utr_gN20-guideRNA15rvU6sensepX330	CACCGCGTCTATGTTCATGATGCCG
oAA18_fam91-utr_gN20-guideRNA15rvU6antisensepX330	AAACCGGCATCATGAACATAGACGC
oAA19_fam91-utr_gN19-gN20-guideRNA15rvU6sensepX330	CACCGGTCTATGTTCATGATGCCG
oAA20_fam91-utr_gN19-gN20-guideRNA15rvU6antisensepX330	AAACCGGCATCATGAACATAGACC
oAA21_fam91A1_Shin_gRNA_Fv	CACCGTTGATAAGATCATCGATTC
oAA22_fam91A1_Shin_guideRNA	AAACGAATCGATGATCTTATCAAC
oAA5 C17orf75	CACCGTAACAACCAACTCGGTAACCTGG
oAA6 C17orf75	AAACCCAGGTTACCGAGTTGGTTGTTAC
oAA7 C17orf75	CACCGTGTAGATTGGCACAGCAACGAGG
oAA8 C170rf75	AAACCCTCGTTGCTGTGCCAATCTACAC

3.1.10 Recombinant protein production primers

Table 15. Primers for the cloning of Fam91A1, WDR11 and C17or75 constructs with HIS-,FLAG- and GST-tags

Name	Sequence
pGib1-HIS-WDR11-Fw	ATCACCATCACCATCACCATATGTTACCCTACACCGTAAACTTCAAG
pGib2-HIS-WDR11-Rev	CGTCGACGTAGGCCTTTGAATTAACTTTCCGTTAGCTCTTCCTTGGTG
pGib3-pLib-HIS-WDR11-Fw	AAGAGCTAACGGAAAGTTAATTCAAAGGCCTACGTCGACG
pGib4-pLib-HIS-Rv	TTTACGGTGTAGGGTAACATATGGTGATGGTGATGGTGATGGTGC
pGib5-HIS-FAM91A1-Fw	ATCACCATCACCATCACCATATGAACATCGACGTTGAGTTCCAC
pGib6-HIS-FAM91A1_Rv	CGTCGACGTAGGCCTTTGAATTAGGTACCCAAATGGAGACTAGCG
pGib7-pLib-HIS-FAM91A1-Fw	GTCTCCATTTGGGTACCTAATTCAAAGGCCTACGTCGACGAG
pGib8-pLib-HIS-FAM91A1-Rv	AACTCAACGTCGATGTTCATATGGTGATGGTGATGGTGATGGTGC
pGib9-HIS-C17orf75-Fw	ATCACCATCACCATCACCATATGCTCCCGTCTTTGCAGG
pGib10-HIS-C17orf75-Fv	CGTCGACGTAGGCCTTTGAATTATACCTGGACAAGCGCTTCT
pGib11-pLib-HIS-C17orf75-Fw	AAGCGCTTGTCCAGGTATAATTCAAAGGCCTACGTCGACG
pGib12-pLib-HIS-C17orf75-Rv	TCCTGCAAAGACGGGAGCATATGGTGATGGTGATGGTGATGGTGC
pGib13-FLAG-WDR11-Fw	GTAGTGGAGGTAGTAGTGGAATGTTACCCTACACCGTAAACTTCAAG
pGib14-FLAG-WDR11-Fv	CGTCGACGTAGGCCTTTGAATTAACTTTCCGTTAGCTCTTCCTTGGTG
pGib15-pLib-FLAG-WDR11-Fw	AAGAGCTAACGGAAAGTTAATTCAAAGGCCTACGTCGACG
pGib16-pLib-FLAG-WDR11-Rv	TTTACGGTGTAGGGTAACATTCCACTACTACCTCCACTACTACCTT
pGib17-FLAG-FAM91A1-Fw	GTAGTGGAGGTAGTAGTGGAATGAACATCGACGTTGAGTTCCACA
pGib18-FLAG-FAM91A1-Rv	CGTCGACGTAGGCCTTTGAATTAGGTACCCAAATGGAGACTAGCG
pGib19-pLib-FLAG-FAM91A1-Fw	GTCTCCATTTGGGTACCTAATTCAAAGGCCTACGTCGACG
pGib20-pLib-FLAG-FAM91A1-Rv	AACTCAACGTCGATGTTCATTCCACTACTACCTCCACTACTACCTT
pGib21-FLAG-C17orf75-Fw	GTAGTGGAGGTAGTAGTGGAATGCTCCCGTCTTTGCAGG

pGib22-FLAG-C17orf75-Rv	CGTCGACGTAGGCCTTTGAATTATACCTGGACAAGCGCTTCT
pGib23-pLib-FLAG-C17orf75-Fw	AAGCGCTTGTCCAGGTATAATTCAAAGGCCTACGTCGACG
pGib24-pLib-FLAG-C17orf75-Rv	TCCTGCAAAGACGGGAGCATTCCACTACTACCTCCACTACT
pGib25-GST-WDR11_For	TTCAGGGATCCGGTGGCTCTATGTTACCCTACACCGTAAACTTCAAGG
pGib26-GST-WDR11-Rv	CGACGTAGGCCTTTGAATTCTTAACTTTCCGT
pGib27-pLib-GST-WDR11-Fw	AAGAGCTAACGGAAAGTTAAGAATTCAAAGGCCTACGTCGACGAG
pGib28-pLib-GST-WDR11-Rv	TTTACGGTGTAGGGTAACATAGAGCCACCGGATCCCT
pGib29-GST-Fam91A1-Fw	TTCAGGGATCCGGTGGCTCTATGAACATCGACGTTGAGTTCCACA
pGib30-GST-Fam91A1-Rv	CGACGTAGGCCTTTGAATTCTTAGGTACCCAAAT
pGib31-pLib-GST-Fam91A1-Fw	GTCTCCATTTGGGTACCTAAGAATTCAAAGGCCTACGTCGACG
pGib32-pLib-GST-Fam91A1-Rv	AACTCAACGTCGATGTTCATAGAGCCACCGGATCCCT
pGib33-GST-C17orf75-Fw	TTCAGGGATCCGGTGGCTCTATGCTCCCGTCTTTGCAGGAA
pGib34-GST-C17orf75-Rv	CGACGTAGGCCTTTGAATTCTTATACCTGGACAAG
pGib35-pLib-GST-C17orf75-Fw	AAGCGCTTGTCCAGGTATAAGAATTCAAAGGCCTACGTCGAC
pGib36-pLib-GST-C17orf75-Rv	TCCTGCAAAGACGGGAGCATAGAGCCACCGGATCCCT
pGib37-GST-WDR11-Fw	ATTTTCAGGGATCTGGTGGCATGTTACCCTACACCGTAAACTTCAAG
pGib38-GST-WDR11-Rv	GTCAGTCACGATGCGGCCGCTTAACTTTCCGTTAGCTCTTCCTTGGTG
pGib39-pGEX-WDR11-Fw	AAGAGCTAACGGAAAGTTAAGCGGCCGCATCGTGACT
pGib40-pGEX-WDR11-Rv	TTTACGGTGTAGGGTAACATGCCACCAGATCCCTGAAAA
pGib41-GST-Fam91A1-Fw	ATTTTCAGGGATCTGGTGGCATGAACATCGACGTTGAGTTCCAC
pGib42-GST-Fam91A1-Rv	GTCAGTCACGATGCGGCCGCTTAGGTACCCAAATGGAGACTAGCGA
pGib43-pGEX-Fam91A1-Fw	GTCTCCATTTGGGTACCTAAGCGGCCGCATCGTGACT
pGib44-pGEX-Fam91A1-Rv	AACTCAACGTCGATGTTCATGCCACCAGATCCCTGAAAA
pGib45-GST-C17orf75-Fw	ATTTTCAGGGATCTGGTGGCATGCTCCCGTCTTTGCAGG
pGib46-GST-C17orf75-Rv	GTCAGTCACGATGCGGCCGCTTATACCTGGACAAGCGCTTCTCTC
pGib47-pGEX-C17orf75-Fw	AAGCGCTTGTCCAGGTATAAGCGGCCGCATCGTGACT
pGib48-pGEX-C17orf75-Rv	TCCTGCAAAGACGGGAGCATGCCACCAGATCCCTGAAAA

3.1.11 Plasmid list

Table 16. Plasmid list

Name	Sequence
pmegfp-C1-wdr11-FL	N-terminally attached meGFP to WDR11 gene
pmegfp-wdr11-1-400aa	N-terminally attached meGFP to truncated WDR11 gene
pmegfp-WDR11-1-500aa	N-terminally attached meGFP to truncated WDR11 gene
pmegfp-WDR11-1-955aa	N-terminally attached meGFP to truncated WDR11 gene
pmegfp-WDR11-321-122aa	N-terminally attached meGFP to truncated WDR11 gene
pmegfp-WDR11-953-122aa	N-terminally attached meGFP to truncated WDR11 gene
pmegfp-WDR11_436A>T	N-terminally attached meGFP to mutated WDR11 gene
pmegfp-WDR11_448E>Q	N-terminally attached meGFP to mutated WDR11 gene
pmegfp-WDR11_451H>R	N-terminally attached meGFP to mutated WDR11 gene
pmegfp-WDR11_690T>A	N-terminally attached meGFP to mutated WDR11 gene
pmegfp-WDR11_755R>H	N-terminally attached meGFP to mutated WDR11 gene
pmegfp-WDR11_756I>H	N-terminally attached meGFP to mutated WDR11 gene

pmegfp-WDR11_966Y>A,969L>A	N-terminally attached meGFP to mutated WDR11 gene
pmegfp-N1-wdr11-FL	C-terminally attached meGFP to WDR11 gene
pmegfp-Fam91A1_1-60aa deletion	N-terminally attached meGFP to truncated Fam91A1gene
pmegfp-Fam91A1_1-370aa deletion	N-terminally attached meGFP to truncated Fam91A1gene
pmegfp-Fam91A1_600-839aa deletion	N-terminally attached meGFP to truncated Fam91A1gene
pmegfp-Fam91A1_700-839aa deletion	N-terminally attached meGFP to truncated Fam91A1gene
pmegfp-Fam91A1_1-750aa	N-terminally attached meGFP to truncated Fam91A1gene
pmegfp-Fam91A1_1-800aa	N-terminally attached meGFP to truncated Fam91A1gene
pmegfp-Fam91A1_1-810aa	N-terminally attached meGFP to truncated Fam91A1gene
pmegfp-Fam91A1_1-823aa	N-terminally attached meGFP to truncated Fam91A1gene
pmegfp-Fam91A1_1-835aa	N-terminally attached meGFP to truncated Fam91A1gene
pmegfp-Fam91A1_L807N	N-terminally attached meGFP to mutated Fam91A1 gene
pmegfp-Fam91A1_A809N	N-terminally attached meGFP to mutated Fam91A1 gene
pmegfp-Fam91A1_R825D	N-terminally attached meGFP to mutated Fam91A1 gene
pmegfp-Fam91A1_R512W	N-terminally attached meGFP to mutated Fam91A1 gene
pmegfp-Fam91A1_R569Q	N-terminally attached meGFP to mutated Fam91A1 gene
pmegfp-Fam91A1_T589M	N-terminally attached meGFP to mutated Fam91A1 gene
pmegfp-Fam91A1_R61A	N-terminally attached meGFP to mutated Fam91A1 gene
pmegfp-Fam91A1_D198R	N-terminally attached meGFP to mutated Fam91A1 gene
pmegfp-Fam91A1_R569Q	N-terminally attached meGFP to mutated Fam91A1 gene
pmegfp-Fam91A1_T589M	N-terminally attached meGFP to mutated Fam91A1 gene
pmegfp-C17orf75-FL	N-terminally attached meGFP to C17orf75 gene
pmegfp-C17orf75-1-135aa deletion	N-terminally attached meGFP to truncated C17orf75 gene
pmegfp-C17orf75-136-400aa deletion	N-terminally attached meGFP to truncated C17orf75 gene
pmegfp-C17orf75-300-400aa deletion	N-terminally attached meGFP to truncated C17orf75 gene
pLIB-HIS-WDR11	Gateway-compatible donor vector for the biGBac system
pLIB -WDR11-HIS	Gateway-compatible donor vector for the biGBac system
pLIB-HIS-Fam91A1	Gateway-compatible donor vector for the biGBac system
pLIB -Fam91A1 -HIS	Gateway-compatible donor vector for the biGBac system
pLIB-HIS-C17oef75	Gateway-compatible donor vector for the biGBac system
pLIB -C17orf75 -HIS	Gateway-compatible donor vector for the biGBac system
pLIB-FLAG-WDR11	Gateway-compatible donor vector for the biGBac system
pLIB -WDR11-FLAG	Gateway-compatible donor vector for the biGBac system
pLIB-FLAG-Fam91A1	Gateway-compatible donor vector for the biGBac system
pLIB -Fam91A1 -FLAG	Gateway-compatible donor vector for the biGBac system
pLIB-FLAG-C17oef75	Gateway-compatible donor vector for the biGBac system
pLIB -C17orf75 -FLAG	Gateway-compatible donor vector for the biGBac system
pLIB-GST-WDR11	Gateway-compatible donor vector for the biGBac system
pLIB -WDR11-GST	Gateway-compatible donor vector for the biGBac system
pLIB-GST -Fam91A1	Gateway-compatible donor vector for the biGBac system
pLIB -Fam91A1 -GST	Gateway-compatible donor vector for the biGBac system
pLIB-GST -C17oef75	Gateway-compatible donor vector for the biGBac system
pLIB -C17orf75 -GST	Gateway-compatible donor vector for the biGBac system

3.2 Cell culture methods

3.2.1 Cell lines

Table 17. Cell lines

Name	Origin
U2OS WT	ATCC®HTB-96™
U2OS WDR11 KO #1	Generated for this thesis
U2OS WDR11 KO #2	Generated for this thesis
U2OS Fam91A1 KO #1	Generated for this thesis
U2OS Fam91A1 KO #2	Generated for this thesis
U2OS C17orf75 KO #1	Generated for this thesis
U2OS C17orf75 KO #2	Generated by Alexandros Anastasakis
U2OS WT-mEGFP	Generated for this thesis
U2OS WDR11 KO #1+mEGFP_WDR11	Generated for this thesis
U2OS WDR11 KO #2+mEGFP_WDR11	Generated for this thesis
U2OS Fam91A1 KO #1+mEGFP_Fam91A1	Generated for this thesis
U2OS Fam91A1 KO #2+mEGFP_Fam91A1	Generated for this thesis
U2OS C17orf75 KO #1+mEGFP_C17orf75	Generated for this thesis
U2OS C17orf75 KO #2+mEGFP_C17orf75	Generated for this thesis
Mouse fibroblast	Provided by Dr. Ralph Böttcher
Mouse fibroblast Talin1/2 KO	Provided by Dr. Ralph Böttcher
Mouse fibroblast_Itgα5-BioID	Provided by Dr. Ralph Böttcher
HEK 293T	ATCC®CRL-3216™
Sf9	Protein core facility at the MPI of Biochemistry
Hi5	Protein core facility at the MPI of Biochemistry

3.2.2 Cell culture conditions

All cell lines were cultured in Dulbecco's Modified Eagle Medium (DMEM, Gibco #61965059) supplemented with 10% heat-inactivated fetal calf serum (FCS, Gibco #A5256701) and 1% penicillin-streptomycin (Thermo Fisher Scientific #15140122). Cells were maintained at 37°C in a humidified atmosphere containing 5% CO_2. Cell passaging was performed at 70-80% confluence using 5mM EDTA in PBS for cell detachment. All cell lines were routinely tested for mycoplasma contamination using the MycoAlert™ Mycoplasma Detection Kit (Lonza #LT07-318) every two months.

3.2.3 Generation of knock-out cell lines

Knock-out (KO) cell lines were generated using CRISPR/Cas9 technology following established protocols (221). Guide RNAs (gRNAs) targeting early coding exons were designed using CRISPOR (http://crispor.tefor.net/) to maximize on-target efficiency while minimizing off-target effects. The gRNA sequences are listed in Table 22.

Transfection and selection: U2OS cells were seeded at 2 × 10^5 cells per well in 6-well plates 24 hours before transfection. Cells were transfected with 2µg of pSpCas9(BB)-2A-Puro plasmid containing the respective gRNA using Lipofectamine 2000 (Invitrogen, #11668019) according to the manufacturer's instructions. 24 hours post-transfection, cells were selected with 2µg/mL puromycin (Sigma, #P8833) for 48 hours. Surviving cells were allowed to recover in complete medium without selection for 5 days.

Single clone isolation: Single cell clones were obtained by limiting dilution. Cells were diluted to 0.5 cells per 100µL in complete medium and plated in 96-well plates (200µL per well). Wells containing single colonies after 10-14 days were expanded progressively through 24-well, 6-well, and 10cm dishes.

Genotyping and Validation: Genomic DNA was extracted using the DNeasy Blood & Tissue Kit (Qiagen, #69504). The targeted regions were amplified by PCR using primers flanking the gRNA cut sites (300-500 bp amplicons). PCR products were purified using QIAquick PCR Purification Kit (Qiagen, #28104) and analyzed by Sanger sequencing (Eurofins Genomics). Knock-out efficiency was confirmed by Western blot analysis using antibodies listed in Table 10. At least two independent knock-out clones per gene were selected for further experiments.

3.2.4 Transient transfection

Cells were seeded at 2-3 × 10^5 cells per well in 6-well plates and cultured overnight to reach 70-80% confluence. Transfection mixtures were prepared by combining 2µg plasmid DNA with 150µL Opti-MEM (Invitrogen, #31985062) and separately mixing 6µL Lipofectamine 2000 with 150µL Opti-MEM. After 5 minutes incubation at room temperature, both mixtures were combined and incubated for an additional 10 minutes. The transfection mixture was

added dropwise to cells in 2mL complete medium. Cells were analyzed 48 hours post-transfection.

3.2.5 Retroviral transduction

Retroviral particles were produced by the Max Planck Institute Viral Core Facility using a third-generation packaging system. HEK293T cells were co-transfected with pRetroQ-mEGFP constructs and packaging plasmids. Viral supernatants were collected 48- and 72-hours post-transfection, filtered through 0.45µm filters, and concentrated by ultracentrifugation.

Target cells were seeded at 1-3×10⁵ cells per well in 6-well plates 24 hours before transduction. Cells were infected with viral particles in the presence of 8µg/mL polybrene (Sigma, #H9268) for 24 hours. Successfully transduced cells were selected using 2µg/mL puromycin for 72 hours and expanded for further analysis.

3.3 Molecular biology methods

3.3.1 Electrophoresis run on agarose gel

PCR reactions were performed using either Phusion High-Fidelity DNA Polymerase (Thermo Fisher Scientific, #F530S) or Q5 Hot Start High-Fidelity DNA Polymerase (NEB, #M0493S) according to manufacturers' protocols.

Table 18. Standard PCR reaction setup

Component	Volume (µL)	Final Concentration
5X Phusion/Q5 Buffer	10	1x
10mM dNTPs	1	200µM
Forward primer (10µM)	2.5	0.5µM
Reverse primer (10µM)	2.5	0.5µM

Table 19. PCR cycling conditions

Step	Temperature	Time	Cycles
Initial denaturation	98°C	30 s	1
Denaturation	98°C	10 s	30-35
Annealing	55-72°C*	30 s	30-35
Extension	72°C	30 s/kb	30-35
Final extension	72°C	5 min	1
Hold	4°C	∞	-

*Annealing temperature was calculated based on primer Tm values

3.3.2 Agarose gel electrophoresis

DNA fragments were separated on 0.8-1.5% (w/v) agarose gels in 1xTAE buffer containing 0.5µg/mL ethidium bromide. Samples were mixed with 6X loading dye (Thermo Fisher Scientific, #10816015) and loaded alongside GeneRuler DNA ladders. Electrophoresis was performed at 100-120V for 30-45 minutes. Gels were visualized using a ChemiDoc™ XRS+ System (Bio-Rad) with Image Lab software version 6.1.

3.3.3 DNA purification

PCR products were purified using QIAquick PCR Purification Kit (Qiagen, #28104). DNA fragments from agarose gels were extracted using QIAquick Gel Extraction Kit (Qiagen, #28704). All procedures followed the manufacturer's protocols. DNA concentrations were determined using a NanoDrop 2000 spectrophotometer (Thermo Fisher Scientific).

3.3.4 Restriction enzyme digestion and ligation

Restriction digestions were performed using FastDigest enzymes (Thermo Fisher Scientific) at 37°C for 1-2 hours. Reactions contained 1µg DNA, 2µL 10X FastDigest buffer, 1µL each enzyme, and H_2O to 20µL. After 30 minutes, reactions were transferred to fresh tubes to minimize star activity.

Ligations were performed using T4 DNA Ligase (Thermo Fisher Scientific, #EL0011) with vector:insert molar ratios of 1:3 to 1:5. Reactions contained 100ng linearized vector,

appropriate amount of insert, 2µL 10X T4 Ligase buffer, 1µL T4 DNA Ligase, and H_2O to 20µL. Ligations were incubated at room temperature for 1 hour or at 16°C overnight.

Table 20. Ligation reaction mix

Component	Volume/reaction
10X Ligase Reaction Buffer	4µL
ddH_2O	3.8µL
Insert:Vector	Ratio 5:1
Vector	100ng
H_2O	Adjust volume to 10µL
Reaction time: 1 hour at room temperature	

3.3.5 Gibson assembly

Gibson assembly reactions were performed using NEBuilder HiFi DNA Assembly Master Mix (NEB, #E2621). PCR fragments with 15-40 bp overlapping regions were generated using primers listed in Table 12. After PCR amplification, products were treated with DpnI (NEB, #R0176S) at 37°C for 1 hour to remove template DNA. Assembly reactions contained 50-100ng total DNA fragments in equimolar ratios, 10µL 2X Gibson Assembly Master Mix, and H_2O to 20µL. Reactions were incubated at 50°C for 60 minutes.

Table 21. Gibson assembly mix

Component	Final Concentration	Volume (for 20 µL reaction)
DNA fragments (total)	50-100ng	Variable (~5-10µL)
Gibson Assembly Master Mix	1X	10µL
DNA Backbone	10-20ng	1µL
Nuclease-Free Water	-	To final 20µL

3.3.6 Site-directed mutagenesis

Point mutations were introduced using overlap extension PCR with primers containing the desired mutation (Table 13). The entire plasmid was amplified using high-fidelity polymerase with primers designed to have 15-20bp overlaps flanking the mutation site.

PCR products were DpnI-treated, purified, and circularized using Gibson assembly as described above.

3.3.7 Bacterial transformation

Chemically competent *E. coli* DH5α cells were thawed on ice. For each transformation, 50µL of cells were mixed with 2µL ligation or assembly reaction and incubated on ice for 30 minutes. Heat shock was performed at 42°C for 60 seconds, followed by 2 minutes on ice. Cells were recovered in 950µL SOC medium at 37°C for 1 hour while shaking (220rpm). Transformed cells were plated on LB agar containing appropriate antibiotics (100µg/mL ampicillin or 50µg/mL kanamycin) and incubated overnight at 37°C.

3.3.8 Plasmid DNA isolation

Single colonies were inoculated in 5mL LB medium with antibiotics and cultured overnight at 37°C with shaking. Plasmid DNA was isolated using QIAprep Spin Miniprep Kit (Qiagen, #27104). Positive clones were verified by restriction digestion and Sanger sequencing (Eurofins Genomics). For large-scale preparations, 200mL cultures were processed using PureLink HiPure Plasmid Maxiprep Kit (Invitrogen, #K210007).

3.3.9 RNA isolation and qRT-PCR

Total RNA was extracted using RNeasy Mini Kit (Qiagen, #74104) from cells at 80% confluence. RNA concentration and purity were assessed using NanoDrop 2000. cDNA synthesis was performed using iScript cDNA Synthesis Kit (Bio-Rad, #1708891) with 1µg total RNA per reaction.

Quantitative RT-PCR was performed on a LightCycler 480 Instrument II (Roche) using SYBR Green I Master Mix (Roche, #04707516001). Each 20µL reaction contained 10µL SYBR Green Master Mix, 0.6µL each primer (10µM), 5µL cDNA (diluted 1:10), and 3.8µL H_2O. All samples were analyzed in technical triplicates. Relative expression was calculated using the 2^-ΔΔCt method with GAPDH as a reference gene.

Table 22. qRT-PCR primers

Primer pair		Product length
Integrin β1	Fwd:5'-GTGGTTGCTGGAATTGTTCTTATTGG-3' Rvs: 5'-CATACTTCGGATTGACCACAGTTGT-3'	138bp
Integrin α5	Fwd: 5'-AGGGCAAACGTGTGAGATGT -3' Rvs: 5'-GGGACACAGGATCAGGTTGG -3'	137bp
GAPDH	Fwd: 5'-GTCTCCTCTGACTTCAACAGCG-3' Rvs: 5'-ACCACCCTGTTGCTGTAGCCAA-3'	131bp

Table 23. qRT-PCR protocol

Component	Volume/reaction	Reaction setup	
cDNA	5µL	95°C – 5min	
ddH_2O	3.8µL	95°C – 15sec	40 cycles
Primer Fwd	0.6µL	57°C – 15sec	
Primer Rvs	0.6µL	95°C – 15sec	
SYBR green	10µL	60°C – 15sec	
		95°C – 15sec	
		4°C – ∞	

3.4 Biochemical Methods

3.4.1 Protein extraction and quantification

Cells were washed twice with ice-cold PBS and lysed in RIPA buffer (50mM Tris pH 8.0, 150mM NaCl, 1% Triton X-100, 0.1% SDS, 1mM EDTA) supplemented with cOmplete Protease Inhibitor Cocktail (Roche, #04693159001). Cells were scraped, collected in 1.5mL tubes, and incubated on ice for 30 minutes with occasional vortexing. Lysates were clarified by centrifugation at 15,000×g for 15 minutes at 4°C. Protein concentration was determined using Pierce BCA Protein Assay Kit (Thermo Fisher Scientific, #23225) with BSA standards. Absorbance was measured at 562nm using a SpectraMax ABS Plus microplate reader (Molecular Devices).

3.4.2 SDS-PAGE and Western blot analysis

Protein samples were prepared by mixing with 4X Laemmli sample buffer and heating at 95°C for 10 minutes. Equal amounts of protein (20-50µg) were separated on 4-15% Mini-PROTEAN TGX Precast Gels (Bio-Rad, #4561086) in Tris-Glycine running buffer at 100-120V for 90 minutes.

Proteins were transferred to 0.45µm PVDF membranes using Trans-Blot Turbo Transfer System (Bio-Rad, #1704150) with the mixed molecular weight program (7 minutes, 2.5A, 25V). Membranes were blocked in 5% BSA in TBS-T for 1 hour at room temperature. Primary antibodies (Table 10) were incubated overnight at 4°C with gentle rocking. After three 10-minute washes in TBS-T, membranes were incubated with HRP-conjugated secondary antibodies (1:5000) for 1 hour at room temperature. Following three additional washes, proteins were detected using Pierce ECL Western Blotting Substrate (Thermo Fisher Scientific, #32106) and visualized on an Amersham AI600 imager (GE Healthcare). Band intensities were quantified using Image Lab software version 6.1 (Bio-Rad) or Image Studio Lite version 5.2.5 (LI-COR).

3.4.3 Immunoprecipitation

HEK293T cells transiently expressing GFP-tagged proteins were lysed in IP buffer (50mM Tris pH 8.0, 150mM NaCl, 0.5mM EDTA, 1% NP-40) with cOmplete Protease Inhibitor Cocktail (Roche, #04693159001). Lysates were sonicated (Sonopuls, Bandelin) at 30% intensity for 10 seconds and clarified by centrifugation. For each IP, 500µg protein lysate was incubated with 30µL GFP-Trap agarose beads (ChromoTek, #gta-20) for 3 hours at 4°C with rotation. Beads were washed three times with wash buffer (50mM Tris pH 8.0, 150mM NaCl, 0.5mM EDTA). Bound proteins were eluted by boiling in 50µL 2X Laemmli buffer for 5 minutes.

3.4.4 Peptide pull-down assays

Biotinylated integrin β1 tail peptides (WT, Y783A, Y795A, Y783/795AA, scrambled control) were provided by Dr. Ralph Böttcher. Peptides were dissolved at 2mM in peptide buffer

(50mM Tris-HCl pH 7.4, 150mM NaCl). For each pull-down, 5nmol peptide was coupled to 50µL streptavidin magnetic beads (Cytiva, #28985799) for 1 hour at 4°C. Beads were washed three times with lysis buffer to remove unbound peptide.

Cell lysates (500µg protein) were incubated with peptide-coupled beads for 2 hours at 4°C with rotation. Beads were washed four times with lysis buffer containing 0.1% Triton X-100. Bound proteins were eluted with 50µL 2X Laemmli buffer at 95°C for 5 minutes and analyzed by Western blot.

3.4.5 Recombinant protein production

The BiGBac baculovirus expression system was used for large-scale protein production (233). Expression constructs in pLIB vectors were transformed into *DH10Bac E. coli* cells. Bacmid DNA was isolated and transfected into Sf9 insect cells to generate baculovirus. *Trichoplusia ni* (Hi5) cells were infected at MOI 1-2 and harvested 72 hours post-infection. All constructs were co-expressed in Hi5 insect cells using the MultiBac-derived BigBac system at a 1:1:1 molar ratio.

Cells were lysed by sonication in buffer containing 30mM Tris pH 8.0, 200mM NaCl, 3mM DTT, protease inhibitors, and DNase. Lysates were clarified by centrifugation at 20,000×g for 40 minutes at 4°C. His-tagged proteins were captured on Ni-NTA magnetic beads (Cytiva, #11530894) and eluted with 300mM imidazole. GST-tagged proteins were purified using Glutathione Sepharose 4B (Cytiva, #17075601). Tags were removed by TEV protease cleavage overnight at 4°C. Final purification was performed by size exclusion chromatography on a Superose 6 10/300 GL column (Cytiva) using an NGC Quest 10 Plus system (Bio-Rad).

3.5 Cell Biology Methods

3.5.1 Immunofluorescence microscopy

Cells were seeded on fibronectin-coated coverslips (5µg/mL in PBS, 1 hour at 37°C) at 2-3 × 10^4 cells per coverslip in 24-well plates. After overnight culture, cells were fixed with 4% paraformaldehyde in PBS for 10 minutes at room temperature. Following three PBS

washes, cells were permeabilized with 0.1% Triton X-100 in PBS for 10 minutes and blocked with 5% BSA in PBS for 1 hour.

Primary antibodies diluted in 1% BSA/PBS were applied overnight at 4°C. After three 5 minutes PBS washes, appropriate fluorophore-conjugated secondary antibodies (1:500) were applied for 1 hour at room temperature in the dark. Nuclei were stained with DAPI (1:10,000) for 10 minutes. After final PBS washes, coverslips were mounted using ProLong Gold Antifade Mountant (Invitrogen, #P36930).

Images were acquired on a Zeiss LSM 780 confocal microscope using Plan-Apochromat 63×/1.4 NA or 100×/1.46 NA oil immersion objectives. Image acquisition was performed using ZEN Black software version 2.3. Colocalization analysis was performed using the JACoP plugin in Fiji/ImageJ version 2.3.0, calculating Pearson correlation coefficients from at least 30 cells per condition.

3.5.2 Live cell antibody labeling for integrin trafficking

Cells on fibronectin-coated coverslips were incubated with integrin-specific antibodies (mAb13, 9EG7, or VC5; 1:500 in 5% FBS/PBS) for 1 hour on ice to allow antibody binding. After three PBS washes, cells were returned to complete medium for 45 minutes to allow trafficking. Cells were then fixed and processed for immunofluorescence as described above, using fluorophore-conjugated secondary antibodies to detect internalized integrins.

3.5.3 Flow cytometry

Cells were detached using 5mM EDTA in PBS, washed twice with cold PBS, and resuspended at 1×10^6 cells/mL in FACS buffer (PBS with 2% FCS, 2mM EDTA). For each sample, 5×10^5 cells in 100µL were incubated with primary antibodies (1:400) or isotype controls for 30 minutes on ice in the dark. After two washes with cold FACS buffer, cells were resuspended in 400µL FACS buffer and analyzed immediately on a BD LSRFortessa X-20 flow cytometer. Data from 10,000 events per sample were analyzed using FlowJo software version 10.10 (BD Biosciences).

3.5.4 Wound healing assay

Cells were seeded at 7 × 10^4 cells per well in fibronectin-coated 24-well plates containing Culture-Insert 2 Well silicone inserts (ibidi, #81176) and cultured overnight to form confluent monolayers. Inserts were carefully removed with sterile forceps, and cells were washed twice with PBS to remove debris. Migration was monitored in complete medium containing 5µg/mL mitomycin C (Sigma, #M4287) to inhibit proliferation. Images were captured at 0 and 24 hours using an EVOS FL Auto 2 imaging system (Thermo Fisher Scientific) with a 10× objective. Wound closure was quantified using the MRI Wound Healing Tool in Fiji/ImageJ.

3.5.5 Micropattern generation using deep UV lithography

Glass coverslips (18×18mm, Menzel-Gläser) were cleaned by sonication in ethanol for 10 minutes, followed by sequential washing with ethanol, isopropanol, and deionized water. Coverslips were dried with precision wipes (Kimtech) and exposed to deep UV (185nm) for 5 minutes in a UV-ozone cleaner.

Clean coverslips were incubated with 0.1mg/mL PLL-g-PEG (SuSoS #PLL(20)-g[3.5]-PEG(2)) in 10mM HEPES pH 7.4 for 1 hour at room temperature. The PEGylated surface was placed in contact with chrome photomasks containing 5 or 10µm wide lines with 35µm interspacing. The assembly was exposed to deep UV for 5 minutes to locally degrade PEG in exposed regions. After separation in water, patterned coverslips were incubated with 20µg/mL fibronectin in PBS for 30 minutes at 37°C before cell seeding (Fig. 6).

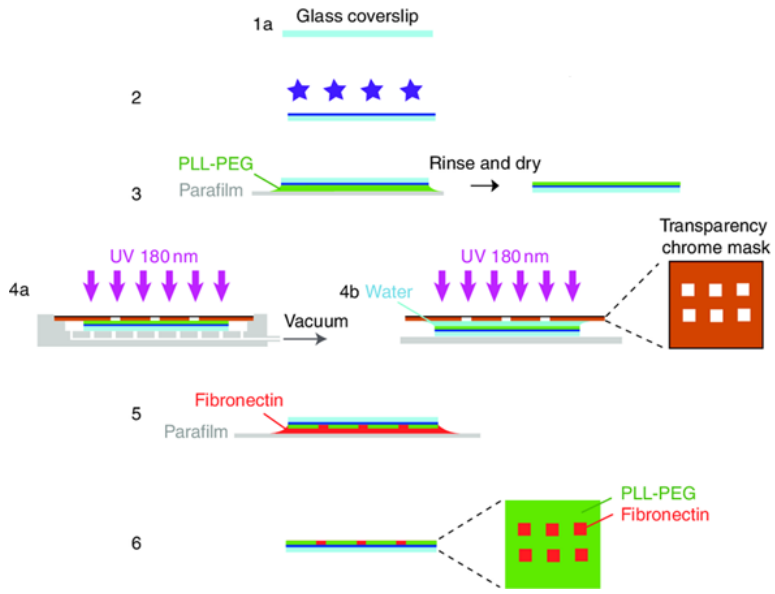

Figure 6. Deep UV-micropattern fabrication protocol. This scheme outlines the step-by-step process for micropattern fabrication. Micropatterning can be carried out on different substrates, typically on a glass coverslip. Preparation of substrate (1): use a clean glass coverslip and proceed to step. (2) Surface oxidation: treat the glass coverslip with a plasma cleaner (30W for 10 seconds). (3) Apply PLL-PEG Coating by incubating the glass coverslip in PLL-PEG solution (0.1mg/mlL in HEPES buffer, pH 7.4) for 30 minutes, then rinse with MilliQ water. Proceed with micropatterning with UV exposure. Place the coverslip and the chrome mask on a mask holder (4a). Alternatively, position the coverslip in direct contact with the chrome mask using a drop of water (4b). Expose the assembly to 180nm UV light for 5 minutes to oxidize the PLL-PEG in the transparent regions. Before seeding cells, immerse the glass coverslip in a fibronectin solution (20µg/mL in $NaHCO_3$ buffer, pH 8.5) for 30 minutes (5). Finally, rinse and dry the glass coverslip by washing the substrate in $NaHCO_3$ buffer and allowing it to dry (6). Figure adapted from Azioune et. al. (222).

3.6 Proteomics Methods

3.6.1 Cell surface proteomics

Surface proteins were labeled by incubating cells with 0.2mg/mL EZ-Link Sulfo-NHS-SS-Biotin (Thermo Fisher Scientific, #21217) in cold PBS for 20 minutes at 4°C. After quenching with 100mM glycine and washing, cells were lysed in proteomics lysis buffer. Biotinylated proteins were captured on streptavidin magnetic beads (Cytiva, #28985799) for 2.5 hours at 4°C. Beads were washed extensively and proteins were digested on-bead with trypsin before LC-MS/MS analysis at the Max Planck Institute Proteomics Core Facility.

3.6.2 Proximity-dependent biotin identification (BioID)

Cells expressing miniTurbo-tagged proteins were incubated with 50µM biotin for 30 minutes at 37°C. After washing and lysis, biotinylated proteins were captured on streptavidin beads and processed for mass spectrometry as described for surface proteomics.

3.6.3 Whole cell proteomics

Cell pellets from four biological replicates were lysed in 8M urea, 50mM Tris pH8.0 with protease inhibitors. Proteins were reduced with 10mM DTT, alkylated with 55mM iodoacetamide, and digested with trypsin. Peptides were analyzed by LC-MS/MS on a Bruker timsTOF Pro mass spectrometer at the Max Planck Institute Proteomics Core Facility.

3.7 Biophysical methods

3.7.1 Mass photometry

Protein samples (20nM in PBS) were analyzed on a TwoMP mass photometer (Refeyn) at room temperature. Data were acquired using AcquireMP software version 2.5 and analyzed with DiscoverMP software version 2.5.

3.7.2 Cryo-electron microscopy

Protein samples (3µL at 0.5mg/mL) were applied to glow-discharged Quantifoil grids and vitrified using a Vitrobot Mark IV (Thermo Fisher Scientific). Data collection was performed on a Glacios Cryo-TEM (Thermo Fisher Scientific) operated at 200kV with a Gatan K3 detector. Images were collected at 22,000×magnification (1.871Å/pixel) with a total dose of 40e^{-}/Å^{2}. Data processing was performed using cryoSPARC version 4.2.

3.8 Statistical analysis

Statistical analyses were performed using GraphPad Prism version 9.5.0. Data from at least three independent experiments are presented as mean ± standard deviation (SD). For

comparisons between two groups, unpaired Student's t-test was used. For multiple comparisons, one-way or two-way ANOVA with Tukey's or Šidák's post-hoc test was applied as appropriate. For paired microscopy data comparing two signals in the same cell, paired t-test was used. Statistical significance was defined as: p-Value<0.05. Sample sizes, specific statistical tests, and exact P values are reported in figure legends.

4. Results

4.1 The FWC complex binds to multiple β-subunits

A potential interaction between the FWC complex and integrins was first observed by Meves et al. (2013) in the Department of Molecular Medicine at the Max Planck Institute of Biochemistry (MPIB). Dr. Meves employed comparative interactome analysis of the β1 integrin cytosolic domain using wild-type peptides versus scrambled peptides and peptides with mutations in the conserved NPxY binding sites (β1 Y783A and β1 Y795A) (60). The study elegantly demonstrated the effects of these NPxY binding site mutations on interactions with known Itgβ1 binding proteins. The Y783A mutation (proximal NPxY) abolished Talin binding while retaining Kindlin-2 binding. Similarly, the Y795A mutation (distal NPxY) eliminated Kindlin-2 binding while retaining Talin binding. The double mutant lost binding to both Talin and Kindlin-2. These findings confirmed that the membrane-proximal NPxY motif (Y783) is essential for Talin binding, while the membrane-distal NPxY motif (Y795) is essential for Kindlin-2 binding. Importantly, mass-spectrometry analysis of the peptide pull-down interactome revealed additional potential interaction partners of Itgβ1, including WDR11 and Fam91A1. However, the researchers did not investigate the role of WDR11 and Fam91A1 in integrin physiology further at the time (60). This provided the foundation for subsequent biochemical and mechanistic investigations to uncover the functional relevance of Fam91A1, WDR11 and C17orf75 in integrin physiology. Fam91A1 and WDR11, together with C17orf75, assemble into a heterotrimeric complex that localizes to the Golgi apparatus (200). In the context of elucidating previously unidentified factors involved in endosomal integrin trafficking, an essential determinant of integrin function, the identification of a Golgi-resident complex with reported roles in retrograde trafficking presented an intriguing avenue for investigation.

To validate and build upon these initial observations, I employed a proximity labeling strategy to delineate the proximity interactome associated with the cytoplasmic tail of β1 integrin. In contrast to the peptide-pulldown approach, I aimed to determine Itgβ1 interaction partners in living cells and confirm the binding between Itgβ1 and Fam91A1 and WDR11 under physiological conditions. For this purpose, I utilized mouse embryonic fibroblasts stably expressing an engineered biotin ligase fused to the C-terminus of Itgα5

(miniTurbo-tagged Itgα5) (223). Cells were either left untreated or incubated with 50µM biotin for 30 min at 37°C, which enables rapid proximity-dependent biotinylation of proteins within living cells, capturing nearby interactors within a ~10 nm radius. Following cell lysis, biotinylated proteins were captured using streptavidin magnetic beads and subsequently identified by mass spectrometry, performed at the MPIB proteomics core facility.

A total of 348 proteins were identified as potential Itgα5 proximity partners, including known interactors Talin and Kindlin-2 (purple) as well as multiple integrin subunits (Itgβ1, Itgα5, Itgα3, ItgαV, Itgβ6) (green). Importantly, this experiment confirmed the presence of Fam91A1 and WDR11 within the Itgα5-associated proximity proteome in intact cells (red) (Fig. 7A).

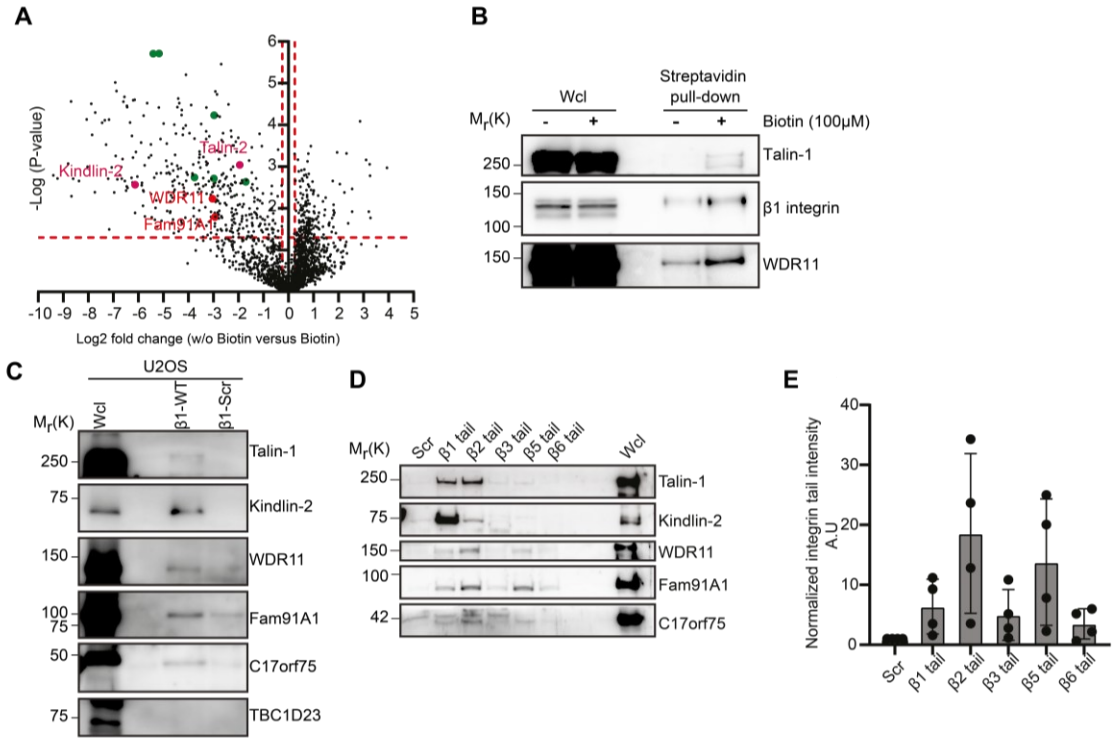

Figure 7. Fam91A1 and WDR11 are novel interactors of β1 integrin tails. **A)** Volcano plot showing enrichment vs significance of potential Itga5 interactors identified by proximity labeling in β1 flox fibroblasts expressing Itgα5-miniTurbo constructs. Comparisons were made between the interactomes of Itga5-miniTurbo expressing cells with and without (control) biotin treatment. Known α5β1 integrin interactors and components of the FWC complex are highlighted in red. Integrin subunits are labeled in green. **(B)** Western blot analysis of proximity labeling assays using Itga5-miniTurbo expressing mouse fibroblasts, either untreated or treated for 30min with 100µM Biotin. Biotinylated proteins were enriched by streptavidin pulldown. Wcl, whole cell lysate. **(C)** Pull-down

using β1 integrin wild type (β1-WT) and scrambled (β1-Scr) cytoplasmic tail peptides in U2OS cells. FWC complex members and TBC1D23 binding to the β1 integrin cytoplasmic tail peptides was detected by Western blotting. Binding of Talin and Kindlin-2 to the β1-WT peptide corroborated functionality of the peptide. **(D)** Integrin β-tail pulldown using isoforms β1, β2, β3, β5 and β6 in U2OS cells. Members of the FWC complex can be detected by Western blot analysis. Kindlin-2 and Talin-1 act as positive binding controls. **(E)** Quantification of FWC signals from β-tail isoform pull-downs, normalized to positive controls (mean ± s.d.; n=4).

These results were corroborated through an independent proximity biotinylation assay followed by Western blot analysis (Fig. 7B). As expected, Talin-1 and Itgβ1 were biotinylated by miniTurbo-tagged Itgα5 after incubation with biotin. Importantly, increasing amounts of WDR11 were pulled-down, confirming the spatial association with the FWC complex. However, even in the control condition without the addition of biotin, relatively high levels of WDR11 and Itgβ1 were detected. This is likely due to the known high background of the miniTurbo variants compared to the earlier BioID2 systems.

After confirming the presence of the FWC complex in the proximity of miniTurbo-tagged Itgα5, I next addressed two related questions: (1) Does the FWC complex associate with β1 integrin tails directly, or does it require the bridging factor TBC1D23? (2) Is this interaction specific to β1 integrins, or does it extend to other β integrin subunits? To examine the first question, I performed peptide pull-down assays using wild-type β1 integrin cytoplasmic tail (β1-WT) and scrambled β1 control peptide (β1-Scr). The β1-WT peptide robustly pulled-down Kindlin-2 and Talin-1, and also enriched all members of the FWC complex (Fig. 7C). In contrast, TBC1D23 was not detected in the pull-down, suggesting that the FWC complex binds β1 integrin tails independently of TBC1D23. Given that TBC1D23 is a known TGN–associated bridging factor, this result supports a model in which the FWC complex assembles on vesicular membranes prior to TGN docking and subsequently engages the TGN via TBC1D23-mediated tethering, rather than being recruited to β1 integrins via TBC1D23.

To determine whether the FWC complex binds exclusively to the β1-cytoplasmic tail or also to other β-subunits, I repeated the pull-down experiments with cytoplasmic tail peptides of various β-integrin subunits (β1, β2, β3, β5, β6) (Fig. 7D). Talin and Kindlin were used as positive controls in the experiments and were successfully pulled-down by all β-tails,

although the association was weaker for β3, β5 and β6. Importantly, all β-subunits tested were able to pull-down FWC complex members, with β1, β2, and β5 exhibiting stronger signals (Fig. 7D, E). Together, these findings indicate that the FWC complex can associate with integrin β cytoplasmic tails, independently of TBC1D23, and that this interaction is not limited to β1 but extends to multiple integrin β-subunits, most likely through the conserved NPXY motifs. This suggests a broader physiological role for the FWC complex in integrin trafficking and regulation of diverse integrin heterodimers.

4.2 WDR11 binds to the membrane proximal NPXY motif

Given that the FWC complex interacts with multiple β integrin subunits, I hypothesized that this binding is mediated by one of the highly conserved NPXY motifs present in the cytoplasmic tails of β integrins. To test whether the FWC complex recognizes β integrin tails via NPXY motifs, I performed peptide pull-down assays using synthesized β1 integrin cytoplasmic tails harboring mutations in either the membrane proximal (Y783A) or distal NPXY (Y795A), followed by Western blot analysis. As positive controls, I confirmed efficient capture of known integrin-binding proteins, Talin and Kindlin. As expected, mutation of the proximal NPXY motif (Y783A) strongly reduced Talin binding, whereas mutation of the distal motif (Y795A) impaired Kindlin binding. Both proteins bound efficiently to the wild-type (WT) β1 tail (Fig. 8A). Strikingly, mutation of the proximal (Y783A) motif caused a substantial reduction in binding of the FWC components Fam91A1 and C17orf75, indicating its importance for FWC interaction (Fig. 8A). Quantification revealed that distal motif mutation (Y795A) also diminished binding, but less severely than the proximal mutation (Fig. 8B). I next examined these interactions in living mouse embryonic fibroblast cells expressing Itgα5-miniTurbo together with β1-WT or β1 in which both NPXY motifs were mutated (YYAA) (Fig. 8C). In β1-WT cells, biotin labeling followed by streptavidin pull-down successfully enriched Talin-1, Fam91A1, and C17orf75. In contrast, the β1-YYAA cell line failed to biotinylate Talin-1 and showed reduced biotinylation of Fam91A1 and C17orf75, resulting in weaker recovery in the streptavidin pull-down (Fig. 8C). Quantification confirmed that Fam91A1 and C17orf75 levels were reduced by approximately 50% β1-YYAA cell line compared to β1-WT (Fig. 8D).

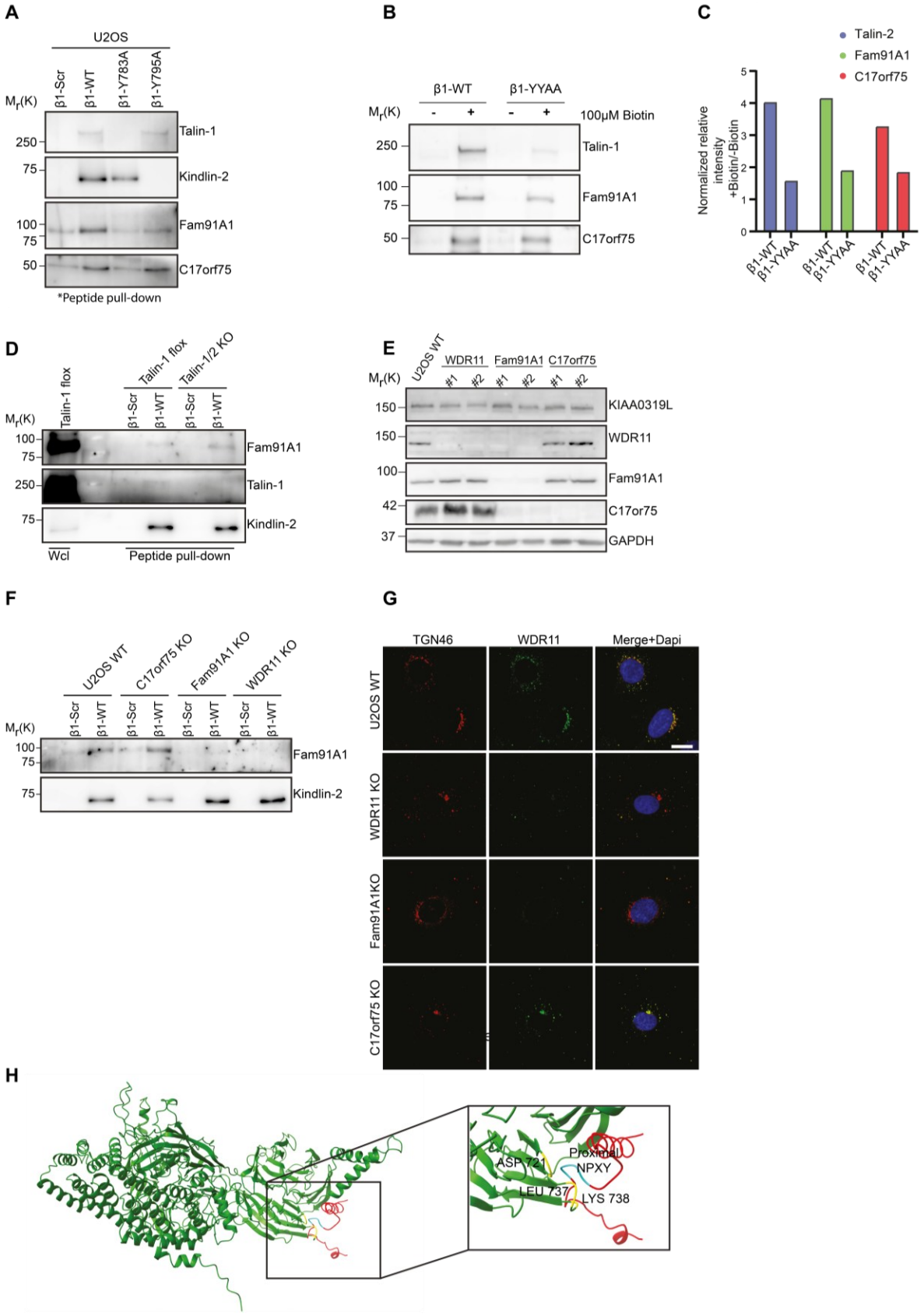
A
U2OS
β1-Scr
β1-WT
β1-Y783A
β1-Y795A
Mr(K)
250
75
100
75
50
Talin-1
Kindlin-2
Fam91A1
C17orf75
*Peptide pull-down
B
β1-WT
β1-YYAA
Mr(K)
- + - +
100μM Biotin
250
100
75
50
Talin-1
Fam91A1
C17orf75
C
Talin-2
Fam91A1
C17orf75
Normalized relative intensity +Biotin/-Biotin
0
1
2
3
4
5
β1-WT
β1-YYAA
β1-WT
β1-YYAA
β1-WT
β1-YYAA
D
Talin-1 flox
Talin-1 flox
Talin-1/2 KO
β1-Scr
β1-WT
β1-Scr
β1-WT
Mr(K)
100
75
250
75
Fam91A1
Talin-1
Kindlin-2
Wcl
Peptide pull-down
E
U2OS WT
WDR11
Fam91A1
C17orf75
#1
#2
#1
#2
#1
#2
Mr(K)
150
150
100
42
37
KIAA0319L
WDR11
Fam91A1
C17or75
GAPDH
F
U2OS WT
C17orf75 KO
Fam91A1 KO
WDR11 KO
β1-Scr
β1-WT
β1-Scr
β1-WT
β1-Scr
β1-WT
β1-Scr
β1-WT
Mr(K)
100
75
75
Fam91A1
Kindlin-2
G
TGN46
WDR11
Merge+Dapi
U2OS WT
WDR11 KO
Fam91A1KO
C17orf75 KO
H
ASP 721
Proximal NPXY
LEU 737
LYS 738

Figure 8. WDR11 interacts with membrane proximal NPXY motif in the integrin β subunit. A) Western blot analysis of peptide pull-down assays illustrating the interaction of β1-Scr, β1-WT, β1-Y783A, and β1-Y795A with FAM91A1 and C17orf75. Talin and Kindlin act as positive controls. **B)** Western blot analysis of mouse fibroblast cells expressing β1-WT or β1-YYAA and Itgα5-miniTurbo. Cells were either untreated or treated for 30 minutes with 100μM biotin before cell lysis followed by a streptavidin pull-down. **C)** Quantification of streptavidin pulled-down signals, normalized to untreated conditions. **C)** Peptide pulldown using β1-Scr, β1-WT in Talin-1 and Talin-2 deficient cells. Samples were analyzed for Talin-1/2, Kindlin-2 and Fam91A1 binding . **E)** Quantification of streptavidin pull-down signals, normalized to untreated levels. **E)** Western blot analysis of U2OS WDR11, Fam91A1, and C17orf75 KO cell lines. Two clones were evaluated for each gene. **F)** Peptide pull-down using β1-Scr and β1-WT integrin tails with U2OS wild type (WT) and FWC KO cell lysates. Samples were analyzed for Kindlin-2 and Fam91A1 binding. **G)** Immunofluorescence analysis of U2OS WT and FWC KO U2OS cells seeded on fibronectin-coated coverslips. Cells were stained with antibodies against TGN46 (red), WDR11 (green), and counter-stained with DAPI (blue). Scale bar: 20μm. **H)** Alphafold2 model depicting WDR11 (green) and Itgβ1 tail (red) binding. The proximal NPXY motif (cyan) interacts with WDR11's Leu737, Lys738, and Asp721 (yellow).

Since the membrane-proximal NPXY motif is the primary Talin-binding site on β integrins, I tested whether FWC complex recruitment requires Talin as an intermediary adaptor. Using Talin-1/Talin-2 double knock-out mouse embryonic fibroblasts, I performed pull-down assays with β1-WT cytoplasmic tail peptides (Fig. 8E). Western blot analysis showed that Fam91A1 binding to the β1 tail persisted in the absence of both Talin isoforms, indicating that FWC complex binding to the membrane-proximal NPXY motif occurs independently of Talin (Fig. 8E).

Finally, I sought to identify which FWC complex component mediates β-tail integrin binding. To dissect the specific contributions of individual FWC complex components to integrin binding, I generated U2OS cell lines with targeted deletions of WDR11, Fam91A1, and C17orf75 using CRISPR-Cas9 technology. Two independent knock-out clones per gene were analyzed to minimize clonal variation artifacts (Fig. 8E). Protein expression analysis of the individual KO cell lines revealed distinct interdependencies within the complex: loss of Fam91A1 strongly reduced WDR11 and C17orf75 levels, whereas deletion of WDR11 or C17orf75 did not affect the abundance of the other members (Fig. 8E).

β1-tail pull-down assays in the KO cell lines demonstrated that C17orf75 is dispensable for β1 binding, as Fam91A1 was still readily recovered in its absence (Fig. 8F). However,

deletion of WDR11 abolished Fam91A1 capture with the β1-WT tail peptides, demonstrating that WDR11 is indispensable for the interaction with β1-tail (Fig. 8F).

Finally, I employed immunofluorescence imaging in the KO cell lines to elucidate the role of individual complex members in FWC complex localization (Fig. 8G). In the immunofluorescence images, the absence of C17orf75 was dispensable for the proper localization of the FWC complex to the TGN, marked by the TGN marker TGN46. In contrast, deletion of Fam91A1 resulted in the loss of WDR11 signal intracellularly. This further corroborates the role of Fam91A1 in stabilizing the complex at the TGN and its potential role in its localization.

To explore the structural basis of this interaction, I employed AlphaFold2 modeling of the β1 integrin cytoplasmic tail with each FWC component (Fig. 8H). Models of the β1 intracellular tail with Fam91A1 and C17orf75 were of low confidence and did not provide a reliable model. In contrast, the β1 intracellular tail - WDR11 complex was modelled with high confidence (confidence score 95), revealing a plausible interaction interface in which the membrane-proximal NPXY motif (position 783, highlighted in cyan) contacts Gly720, Asp721, Leu727, and Lys728 on WDR11 (Fig. 8H). This structural prediction supports a Talin-independent mode of β1 tail recruitment for the FWC complex.

4.3 Loss of the FWC complex impairs integrin recycling and reshapes the surface proteome

Recent studies have shown that the absence of FWC complex components, Fam91A1 and WDR11, leads to aberrant surface expression of retrograde-trafficked proteins (208). To investigate whether the FWC complex also has a role in integrin recycling and to define the surface proteins regulated by the FWC complex, I performed a surface biotinylation assay combined with quantitative proteomics in U2OS FWC complex member KO cell lines. Surface proteins were labeled with Sulfo-NHS-SS-biotin, and biotinylated proteins were then pulled down with streptavidin beads for analysis.

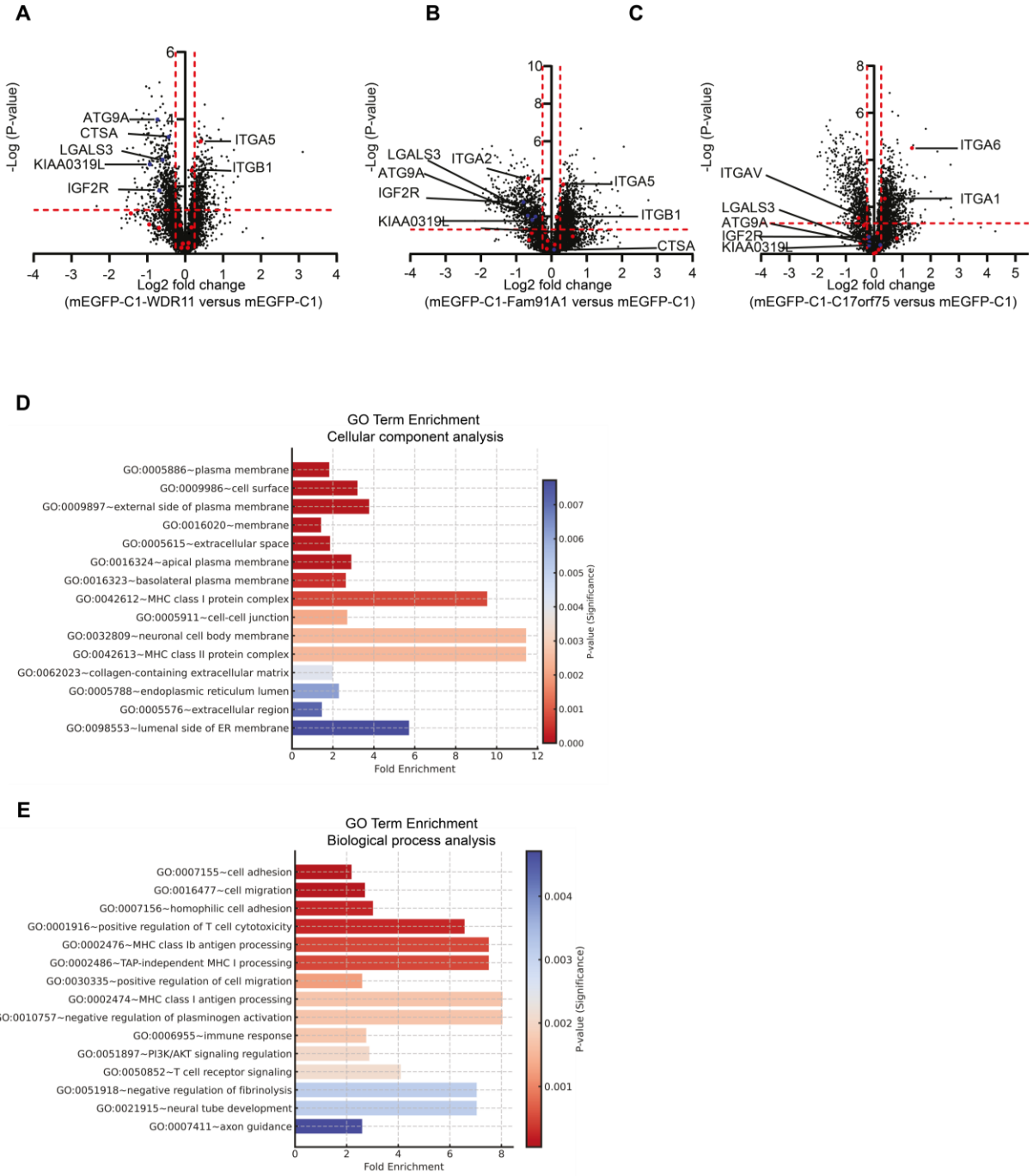

Figure 9. Surface proteome analysis in U2OS cells lacking the FWC complex. A-C) Volcano plots comparing the cell surface proteomes of U2OS WT cells vs U2OS FWC complex member KO cell lines. Integrin isoforms are highlighted in red, control retrogradely trafficked proteins known to increase in surface expression in the absence of the FWC complex (ATG9A, CTSA, LGALS3, KIAA0319L, IGF2R) are shown in blue. **D, E)** GO term enrichment analysis of significant hits from the WDR11 and Fam91A1 datasets, displayed for (D) biological process and (E) cellular components.

This approach successfully validated known changes in retrograde trafficking markers: the cation-independent mannose 6-phosphate receptor (IGF2R) and KIAA0319L both displayed elevated surface levels when FWC-mediated retrograde transport was disrupted (Fig.10A, B). Interestingly, the surface expression of α5β1 integrins was significantly reduced in Fam91A1 and WDR11 KO cells, a phenotype not observed for other retrograde cargoes (Fig. 9A, B). Notably, the WDR11 and Fam91A1 KO datasets reveal strong similarities in the affected surface proteins, while C17orf75 shows a distict phenotype (Fig. 9C).

Among the Fam91A1 and WDR11-mediated retrograde trafficked proteins were ATG9A, LGALS3, and CTSA, which together highlight the breadth of pathways impacted by FWC complex loss. ATG9A, though best known for its role in autophagy and phospholipid transport, is also involved in membrane remodeling and unconventional secretion via the ESCRT machinery. LGALS3 (Galectin-3) modulates cell adhesion, motility, and lysosomal integrity, both through classical and non-classical secretory pathways that may involve FWC-regulated vesicles. Finally, CTSA (Cathepsin A) is a key lysosomal serine carboxypeptidase crucial for degradation, lysosomal stability, and extracellular matrix turnover, suggesting a link between FWC complex function and both degradative and secretory routes.

Crucially, a pronounced surface reduction was seen for Itgα5 and Itgβ1 (Fig. 9A, B). This finding is of particular interest as the majority of research on retrograde transport of proteins focuses on proteins whose surface expression increases. Here for the first time, a decrease in surface integrin abundance is demonstrated as a direct consequence of FWC complex loss.

To further interrogate the surface proteome datasets, I performed a gene ontology (GO) term enrichment analysis on significant hits from the WDR11 and Fam91A1 datasets (Fig. 9D, E). The most highly enriched biological processes include cell adhesion and cell migration ($p<0.05$). Interestingly, the largest group of proteins is associated with major histocompatibility complex (MHC) class I receptors and T-cell cytotoxicity. Cellular component analysis of the surface proteome confirmed a strong enrichment for plasma

membrane and cell surface-localized proteins ($p<0.05$), reinforcing the integral role of the FWC complex in surface protein regulation.

These data indicate that the FWC complex is not only central to cell adhesion and motility, but may also regulate immune responses and signal transduction pathways.

To better characterize the generated KO cell lines and to determine whether the altered surface levels of Itgα5 and Itgβ1 were due to changes in protein production, I performed whole cell proteome analysis on individual U2OS WDR11, Fam91a1, and C17orf75 KO cell lines. I analyzed three independent knock-out cell lines for each gene, with experiments performed in quadruplicate.

Heatmap visualization indicates proteins with decreased abundance compared to the WT (green) and proteins that are upregulated compared to the control (red) (Fig. 10A). The independent knock-out cell lines generated for each gene exhibited comparable protein expression profiles, thereby confirming consistency between individual clones. The whole cell proteome corroborates previous results. Notably, Fam91A1 KO resulted in a pronounced reduction of WDR11 and Syntaxin 17 (STX17), a SNARE (Soluble NSF Attachment Protein Receptor) protein involved in autophagosome–lysosomal fusion, suggesting that Fam91A1 may play a role in autophagy regulation (224). WDR11 KO cells displayed the most pronounced proteomic shift among FWC components compared to WT cells. The GO enrichment analysis revealed that the most significant changes in biological processes involved proteins regulating cell shape and actomyosin organization ($p<0.05$), with lamellipodium membrane proteins prominently represented in the cellular component analysis (Fig. 10B, C). Among the most prominent hits reduced in the WDR11 KO cell lines, modulating cellular migration are ADAM10, EPHA2, FERMT2, Itga5, and TGFB1.

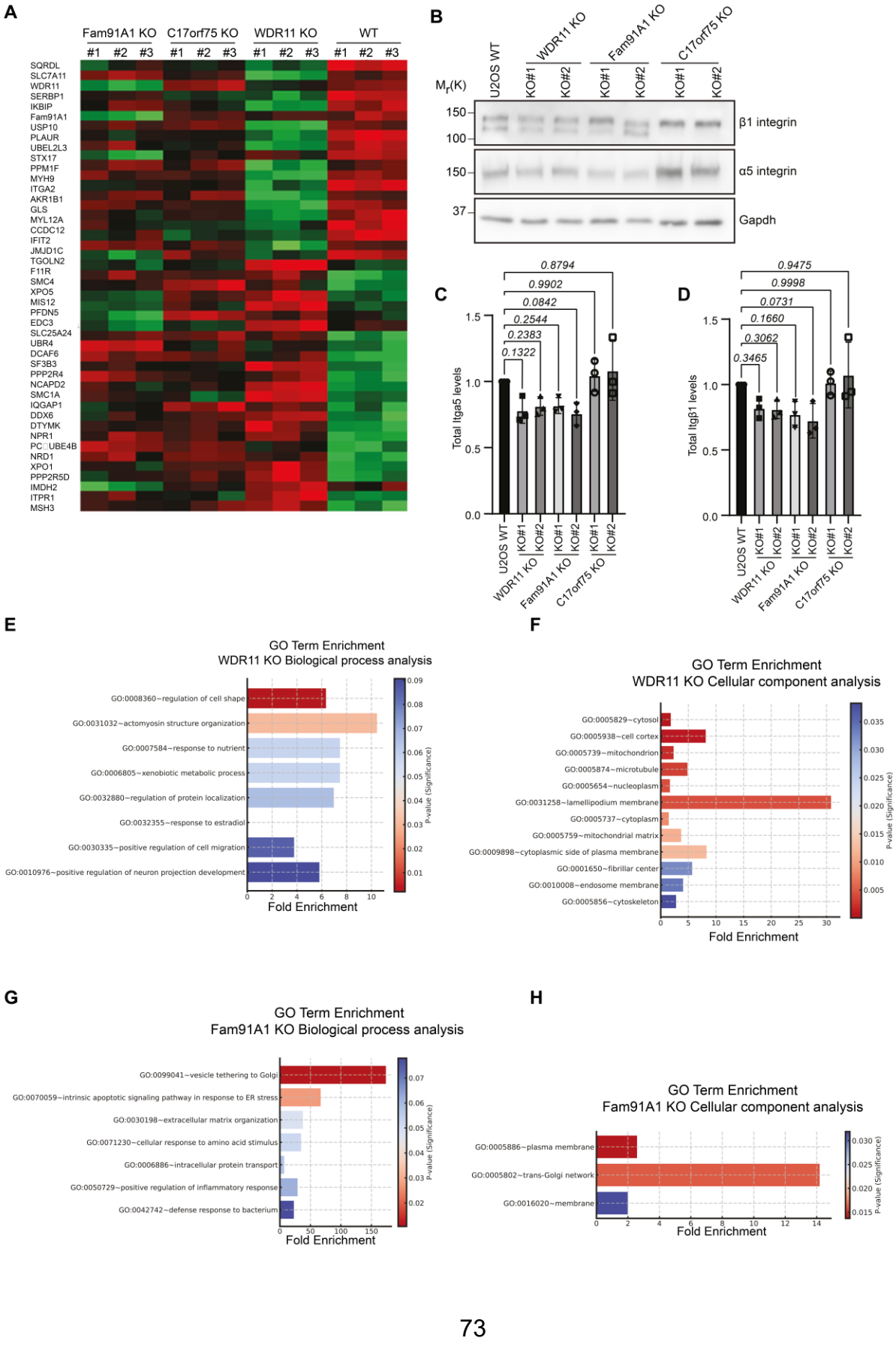
A
Fam91A1 KO
C17orf75 KO
WDR11 KO
WT
#1 #2 #3 #1 #2 #3 #1 #2 #3 #1 #2 #3
SQRDL
SLC7A11
WDR11
SERBP1
IKBIP
Fam91A1
USP10
PLAUR
UBEL2L3
STX17
PPM1F
MYH9
ITGA2
AKR1B1
GLS
MYL12A
CCDC12
IFIT2
JMJD1C
TGOLN2
F11R
SMC4
XPO5
MIS12
PFDN5
EDC3
SLC25A24
UBR4
DCAF6
SF3B3
PPP2R4
NCAPD2
SMC1A
IQGAP1
DDX6
DTYMK
NPR1
PC□UBE4B
NRD1
XPO1
PPP2R5D
IMDH2
ITPR1
MSH3
B
U2OS WT
WDR11 KO
Fam91A1 KO
C17orf75 KO
KO#1
KO#2
M_r(K)
150
100
150
37
β1 integrin
α5 integrin
Gapdh
C
0.8794
0.9902
0.0842
0.2544
0.2383
0.1322
Total Itga5 levels
1.5
1.0
0.5
0.0
U2OS WT
WDR11 KO
Fam91A1 KO
C17orf75 KO
D
0.9475
0.9998
0.0731
0.1660
0.3062
0.3465
Total Itgβ1 levels
E
GO Term Enrichment
WDR11 KO Biological process analysis
GO:0008360~regulation of cell shape
GO:0031032~actomyosin structure organization
GO:0007584~response to nutrient
GO:0006805~xenobiotic metabolic process
GO:0032880~regulation of protein localization
GO:0032355~response to estradiol
GO:0030335~positive regulation of cell migration
GO:0010976~positive regulation of neuron projection development
Fold Enrichment
P-value (Significance)
F
GO Term Enrichment
WDR11 KO Cellular component analysis
GO:0005829~cytosol
GO:0005938~cell cortex
GO:0005739~mitochondrion
GO:0005874~microtubule
GO:0005654~nucleoplasm
GO:0031258~lamellipodium membrane
GO:0005737~cytoplasm
GO:0005759~mitochondrial matrix
GO:0009898~cytoplasmic side of plasma membrane
GO:0001650~fibrillar center
GO:0010008~endosome membrane
GO:0005856~cytoskeleton
Fold Enrichment
P-value (Significance)
G
GO Term Enrichment
Fam91A1 KO Biological process analysis
GO:0099041~vesicle tethering to Golgi
GO:0070059~intrinsic apoptotic signaling pathway in response to ER stress
GO:0030198~extracellular matrix organization
GO:0071230~cellular response to amino acid stimulus
GO:0006886~intracellular protein transport
GO:0050729~positive regulation of inflammatory response
GO:0042742~defense response to bacterium
Fold Enrichment
P-value (Significance)
H
GO Term Enrichment
Fam91A1 KO Cellular component analysis
GO:0005886~plasma membrane
GO:0005802~trans-Golgi network
GO:0016020~membrane
Fold Enrichment
P-value (Significance)

Figure 10. Whole-proteome analysis in cells lacking the FWC complex. A) Heatmap illustrating differences in protein expression between U2OS WT cells and U2OS FWC complex-KO cell lines. **B)** Western blot analysis of endogenous Itgα5 and Itgβ1 protein expression levels in U2OS WT and FWC KO cell lines. **C-D)** qRT-PCR analysis of mRNA expression levels of Itgα5 (C) and Itgβ1 (D) in U2OS WT and U2OS FWC KO cell lines. Data are presented as mean ± s.d. A Student's t-test was performed to assess statistical significance. For each sample, 500ng of total RNA was reverse transcribed and used for cDNA synthesis. **E-F)** GO term enrichment analysis of significantly altered proteins in the WDR11 KO dataset, categorized by (E) biological process and (F) cellular component. **G-H)** GO term enrichment analysis of significantly altered proteins in the Fam91a1 KO dataset, categorized by (G) biological process and (H) cellular component.

Within Fam91A1 KO cell lines, the most significantly altered proteins were involved in vesicle tethering to the Golgi ($p<0.05$), consistent with FWC's function. These proteins were detected both at the plasma membrane and at the TGN ($p<0.05$) (Fig. 10F, H).

Western blotting of cell lysates from U2OS FWC complex KO cell lines confirmed that the total Itgα5 and Itgβ1 protein levels remained unchanged at the whole-cell level, indicating that loss of FWC complex does not degrade or prevent translation of integrins, but rather affects their trafficking to the cell surface (Fig. 10B). As WDR11 has previously been reported to interact with transcription factors, I examined integrin mRNA levels by RT-qPCR. No significant changes in integrin transcript abundance were detected in WDR11 and Fam91A1 KO cells after normalization to GAPDH ($p>0.05$) (Fig. 10C, D).

Taken together, the proteomic data reveal the breadth of FWC complex involvement: not only in cell adhesion and migration but also in the regulation of immune responses and autophagy. Importantly, the observed reductions in surface Itgα5 and Itgβ1 result from trafficking defects rather than changes in transcription or translation, positioning the FWC complex as a vital regulator of integrin recycling.

4.4 FWC complex loss retains inactive α5β1 integrins in vesicles near the TGN

Building on the established role of the FWC complex in retrograde vesicle trafficking at the TGN interface, I sought to clarify the precise mechanisms underlying the reduced plasma membrane expression of Itgα5 and Itgβ1 observed in FWC-deficient cells. A reduction in

integrin surface expression is a well-documented consequence of disruptions in intracellular trafficking pathways (91, 198).

To test this hypothesis, I employed a panel of conformation-specific antibodies: VC5, 9EG7, and mAb13 to visualize the intracellular localization and conformational state of α5β1 integrins paying special attention at the TGN interface (Fig. 11).

Previous work on integrin recycling has shown that inactive α5β1 integrins preferentially traffic through retrograde pathways (155). To assess the involvement of the FWC complex in this process, I utilized mAb13, an antibody that selectively recognizes the inactive conformation of β1 integrins. After incubating living U2OS WDR11 KO, Fam91A1 KO, and C17orf75 KO cells with mAb13 on ice for at least one hour to ensure antibody binding, integrin-antibody conjugates were chased for 45 minutes at 37°C to allow internalization and endosomal trafficking. I assessed their intracellular localization by confocal microscopy. Strikingly, both WDR11 and Fam91A1 KO cells exhibited prominent accumulation of internalized mAb13-labeled integrins in proximity to the TGN, indicating impaired vesicle tethering or fusion at this compartment (Fig. 11B). Quantitative analyses revealed a significant increase in the number of integrin-positive vesicles localized near the TGN in WDR11 and Fam91A1 KO cells compared to wild-type controls ($p<0.05$) (Fig. 11B, C). Measurement of mAB13 signal intensity surrounding the TGN, normalized to the cytoplasmic background, confirmed that the majority of the integrin pool is retained in close proximity to the TGN in the absence of these FWC components. This spatial redistribution is consistent with defective trafficking and aligns with the previous observations of decreased integrin surface expression.

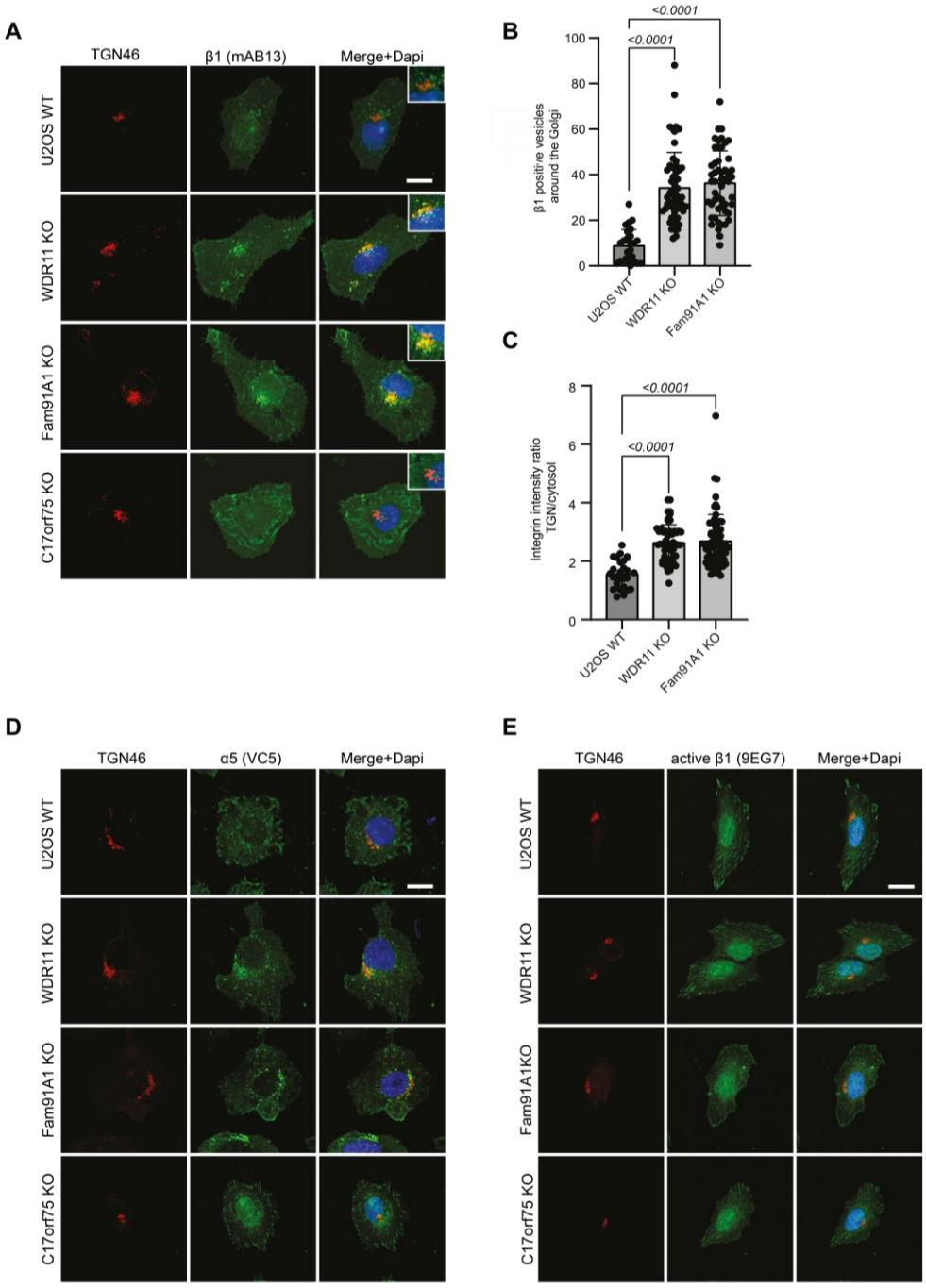

Figure 11. Loss of the FWC complex leads to accumulation of Itgα5- and Itgβ1-positive vesicles near the TGN. A) Immunofluorescence analysis of endocytosed inactive Itgβ1 in U2OS WT and U2OS FWC KO cells. Living cells were incubated for 1 h on ice with an antibody against inactive Itgβ1 (mAB13, green) and chased for 45 minutes at 37°C to allow internalization. The TGN was visualized using an antibody against TGN46 (red). DAPI (blue) was used to stain nuclei. Scale bar: 20µm. **B-C)** Quantification of mAB13 signal intensity around the TGN (B) and ratiometric comparison of TGN-proximal versus cytosolic signal. Data are presented as mean ± s.d. A Student's t-test was performed to assess statistical significance (n=50). **D)** Immunofluorescence analysis of endocytosed Itgα5 signal in U2OS FWC KO cells. Cells were

incubated with the VC5 antibody (green) for 1 h on ice and chased for 45 minutes at 37°C to allow internalization. The TGN was visualized using an antibody against TGN46 (red). DAPI (blue) was used to stain nuclei. Scale bar: 20µm. **E)** Immunofluorescence analysis of endocytosed active Itgβ1 in U2OS WT and U2OS FWC KO cells. Cells were incubated with the 9EG7 antibody for 1 h on ice and chased for 45 minutes at 37°C to allow internalization. The TGN was visualized using an antibody against TGN46 (red). DAPI (blue) was used to stain nuclei. Scale bar: 20µm

To assess whether the accumulation was conformation-dependent, I used the VC5 antibody (detects α5 integrins irrespective of conformational state) and the 9EG7 antibody (recognizing only active, extended-open β1). VC5 labeling showed increased intracellular accumulation of α5-positive vesicles in the proximity of the TGN, similar to the mAB13-staining (Fig. 11D). In contrast, no significant TGN accumulation was observed with 9EG7 antibody (Fig. 11E), indicating active β1 integrins are not retained at the TGN following internalization.

These findings suggest that the retrograde trafficking route mediated by the FWC complex selectively affects inactive β1 integrins, supporting a model where conformation-specific sorting determines integrin fate. Loss of Fam91A1 or WDR11 disrupts retrograde trafficking of inactive α5β1 integrins to the TGN, causing their intracellular retention and decreasing their surface presentation.

4.5 Fam91A1- or WDR11-deficient U2OS cells exhibit reduced migration and impaired polarization

The reduction in α5β1 integrin surface expression observed in Fam91A1 and WDR11 KO cells markedly decreases the functional pool of α5β1 integrins at the plasma membrane, which is crucial for mediating cell adhesion, spreading, and motility. To determine the extent to which the functional pool of α5β1 integrins is compromised, and to directly assess the functional consequences of disrupting the FWC complex on integrin-dependent processes, I performed wound-healing (scratch) assays in U2OS cells deficient in Fam91A1, WDR11, or C17orf75.

To mitigate the confounding influence of cell proliferation on wound closure, all cell lines were pre-treated with 5µg/mL mitomycin for two hours prior to wound infliction. Wounds

were generated using silicone inserts, and closure was monitored over 24 hours by time-lapse microscopy. Fam91A1 and WDR11 KO cells failed to effectively close the wound, demonstrating severely compromised migratory capacity. In contrast, C17orf75-deficient cells retained migration dynamics similar to WT controls. Re-expression of wild-type Fam91A1 or WDR11 in the respective KO cell lines rescued the migratory function, directly linking integrin trafficking defects to lost directional cell motility (Fig. 12A, B).

Detailed analysis of cell behavior during wound closure revealed a marked reduction in migration velocity in Fam91A1 and WDR11 KO cells (Fig. 12F, G). Migration speed was quantified by both measuring front-wall advancement and tracking individual cell trajectories within the wound area. Both analyses confirmed significantly slower migration in KO cells, with migration velocity restored upon gene rescue ($p<0.05$) (Fig. 12F, G).

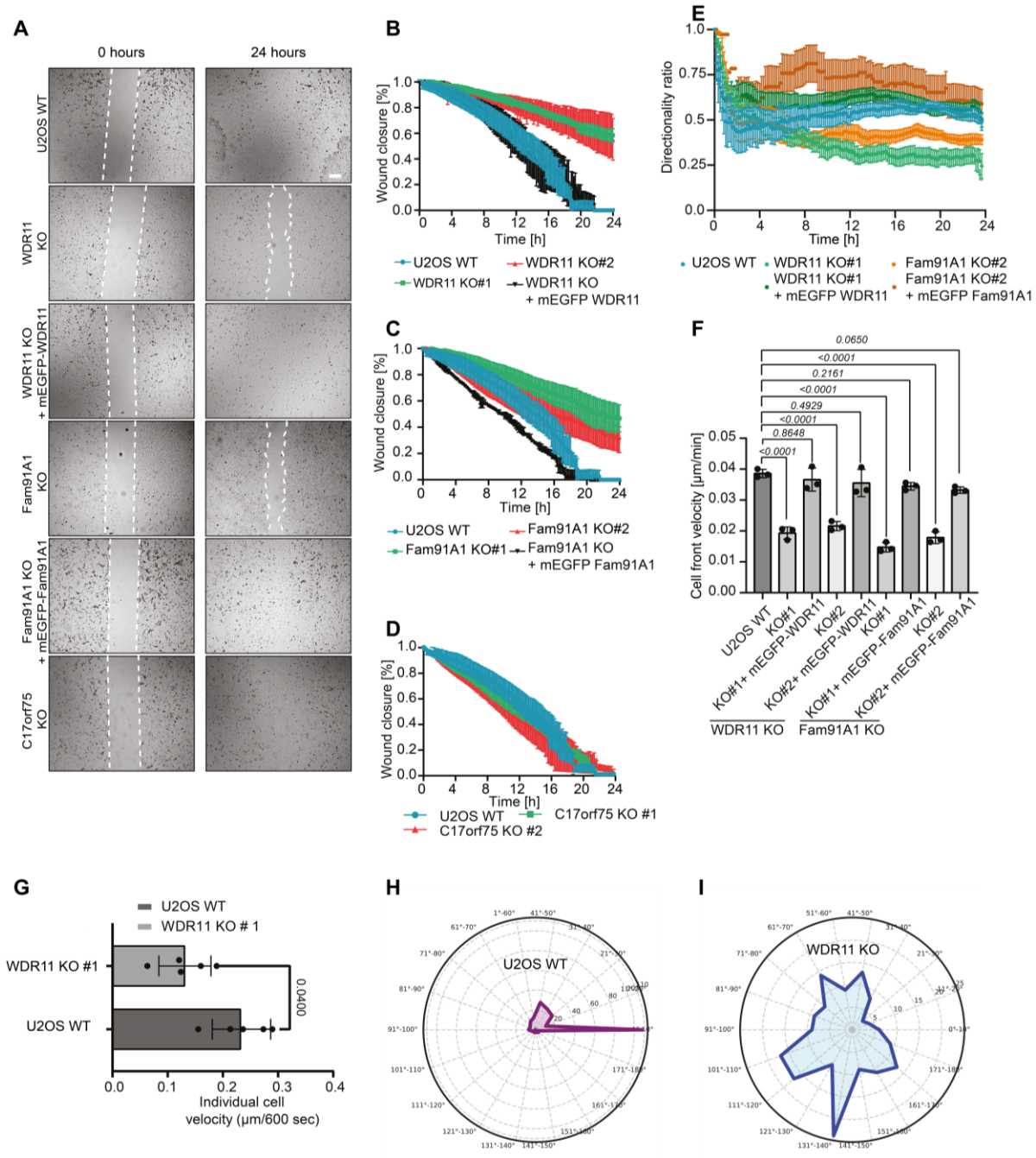

Figure 12. Loss of WDR11 or Fam91A1, but not C17orf75, impairs directed cell migration. A) Wound-healing assay in U2OS WT cells, U2OS FWC complex KO cells, and KO-rescued cell lines. Prior to wound induction, cells were treated with 5µM mitomycin for 2 h to inhibit cell proliferation. Wound closure was monitored over 24h. Scale bar: 100µm. **B-D)** Quantification of wound closure in WDR11 (B), Fam91a1 (C), and C17orf75 (D) KO cell lines over time. Data are presented as mean ± s.d. A Student's t-test was performed to assess statistical significance (n=3). **E)** Directionality ratio calculated from track analysis of individual cells during wound invasion. **F)** Wound cell front velocity of U2OS WT, U2OS FWC complex KO, and KO-rescue cell lines (µm/min). Data are presented as mean ± s.d. A Student's t-test was performed to assess statistical

significance (n=3). G) Individual cell velocity of U2OS WT and U2OS WDR11 KO cells (µm/ 600sec). Data are presented as mean ± s.d. A Student's t-test was performed to assess statistical significance (n=3). **H-I)** Polar plots depicting the relative angle between the Golgi apparatus and the wound in U2OS WT (H) and U2OS WDR11 KO (I) cells, analyzed 6h after wound induction.

To assess migratory directionality, individual cell tracking over 24 hours enabled calculation of the directionality ratio, defined as the shortest linear distance between migration start and endpoint divided by the actual path length. WT cells reoriented their migration axis toward the wound approximately four hours post-scratch, indicative of efficient directed migration. In contrast, Fam91A1 and WDR11 KO cells failed to reorient and displayed disorganized migration, a phenotype that was reversed in rescue cell lines (Fig. 12E).

To further explore the role of WDR11 in cellular polarization, I examined Golgi orientation during a wound healing assay using GM130 (a Golgi marker) and Paxillin (focal adhesion marker) immunostaining. 6 hours post-wound time-point for the analysis was chosen based on prior observations that WDR11-deficient cells require at least 4 hours to initiate reorientation.

In polarized, directionally migrating cells, the Golgi apparatus aligns within a 45° arc facing the wound (225). WT cells predominantly oriented their Golgi apparatus toward the wound edge (between 0–10° relative to the wound) (Fig. 12H, I). In contrast, WDR11 KO cells displayed a randomized Golgi orientation across the 0–180° range, indicative of defective polarization.

Collectively, these results establish that disruption of the FWC complex reduces the surface pool of integrins, leading to impaired integrin-dependent cellular processes, including cell migration, polarization, and spreading. These defects likely arise from intracellular integrin accumulation and compromised recycling to the leading edge, revealing a key mechanistic link between FWC complex function and integrin-dependent regulation of cell movement and architecture.

4.6 One-dimensional migration and integrin polarization are impaired in Fam91A1- and WDR11-deficient U2OS cells

Following the polarity defects observed during wound healing, I next investigated the role of retrograde trafficking in the spatial organization of β1 integrin during directed migration. To do this, I utilized a one-dimensional (1D) migration assay using micropatterned substrates constraining cell movement along linear tracks, enforcing a binary front-rear polarity, and allowing precise evaluation of polarized integrin distribution along the migratory axis.

Micropatterns were generated using deep UV photolithography to create parallel lines (5 or 10μm wide, separated by 35μm) on glass slides coated with 0.1mg/mL PLL-g-PEG (Fig. 13A). To facilitate cell adhesion, the micropatterned regions were functionalized with 5μg/mL fibronectin in PBS for 1 hour at 37°C.

In WT control U2OS cells, non-ligand-bound, inactive β1 integrins, visualized by mAb13 antibody staining, localized preferentially at the leading edge. Quantitative fluorescence profiling along the cell axis showed a gradient of mAB13 β1 integrin signal increasing from rear toward the front, with peak localization at the cell tip (Fig. 13B, C). This pattern reflects efficient retrograde trafficking and polarized recycling of integrins to support sustained directional migration.

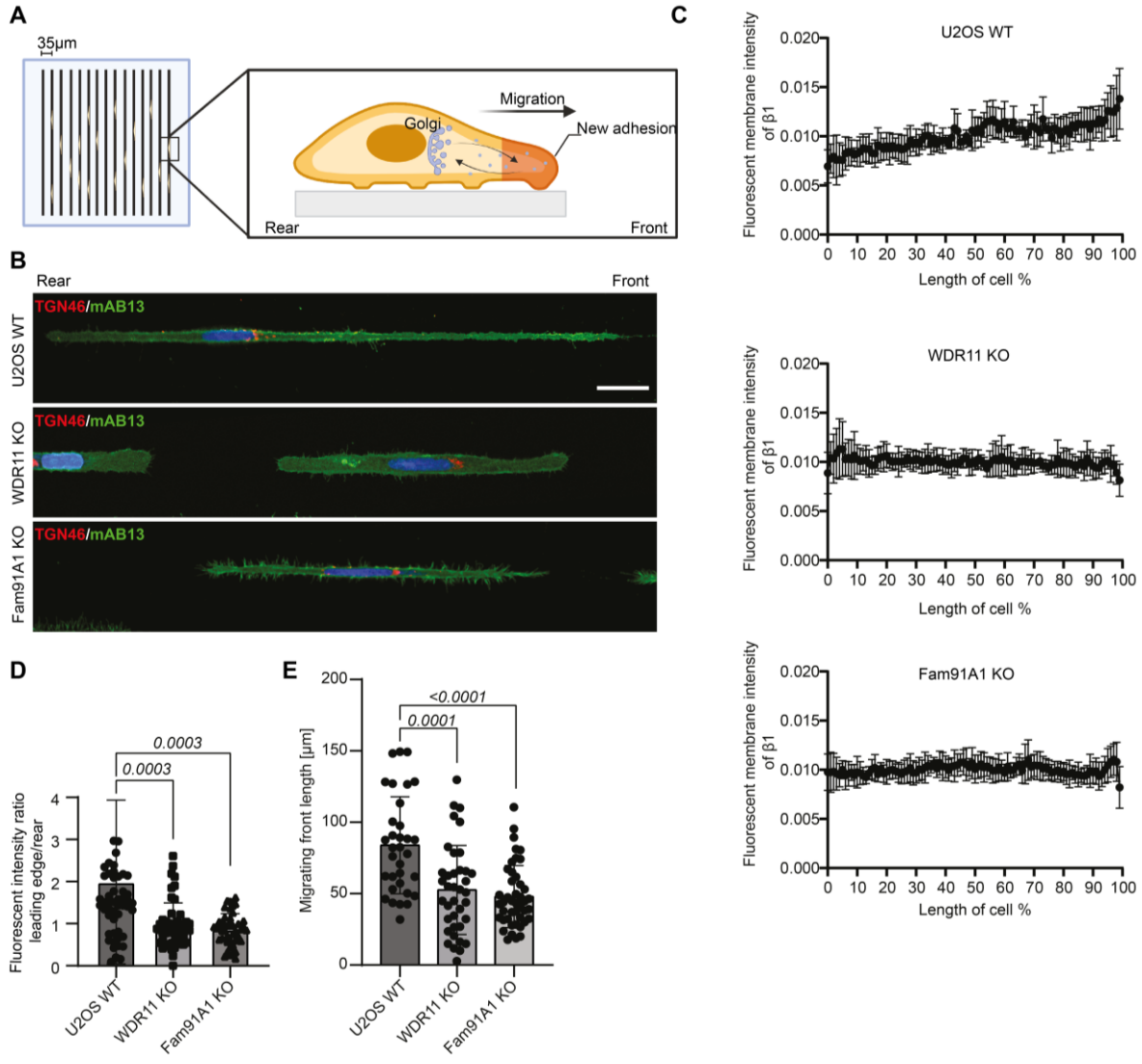

Figure 13. One-dimensional migration of wild-type and FWC complex KO U2OS cells on line patterns. A) Deep UV-lithography was used to generate micropatterned lines with an inter-line distance of 35µm and line widths of 5-10µm. These patterns restrict migration to a bidirectional axis, providing optimal conditions to study polarized migration. The Golgi position was used as a reference to determine the migratory front. **B)** Immunofluorescent images of U2OS WT, WDR11 KO, and Fam91A1 KO cells on micropatterned lines. Surface integrins were stained with mAB13 (inactive Itgβ1, green) antibody before cellular permeabilization. The TGN marker TGN46 was employed to detect TGN position and infer cellular orientation (red). DAPI staining was used to visualize the nucleus (blue). **C)** Quantification of mAB13 antibody signal across the cellular membrane (mean ± s.d.; n=5). **D)** Quantification of the mAB13 signal taken as a ratio between the leading edge of the cell versus the trailing rear (n=50). **E)** Migratory front size analysis of U2OS WT cells versus WDR11 and Fam91A1 KO cells (n=35).

In contrast, Fam91A1- and WDR11-deficient cells displayed a disorganized β1 integrin distribution, with mAb13 signal randomized across the plasma membrane and lacking front-rear asymmetry (Fig. 13C, D). This disruption strongly suggests that the FWC complex is crucial for guiding integrin recycling to the leading edge, a key requirement for sustained polarity and directional motility.

As a result of altered integrin distribution and the inability to establish an integrin gradient along the rear-front axis, cell morphology was also affected. WT cells elongated along the migration axis, displaying pronounced forward extension and higher aspect ratios. Fam91A1- and WDR11-deficient cells failed to elongate effectively, resulting in a lower aspect ratio and impaired directional extension (Fig. 13E).

Taken together, these results demonstrate that the FWC complex is essential for the polarized recycling of inactive β1 integrins to the leading edge during directional cell migration. Loss of Fam91A1 or WDR11 results in aberrant integrin distribution, abrogates migratory polarity, and leads to morphological defects under conditions that require spatially restricted, directed motility.

4.7 FWC Complex- and TBC1D23-mediated vesicle tethering to the TGN is essential for quantitative surface expression of α5β1 integrins

Building on surface proteome analyses, the cell surface expression of Itgα5 and Itgβ1 was found to be reduced in WDR11 and Fam91A1 KO cells. To precisely assess the extent of integrin reduction, I performed flow cytometry experiments with the U2OS FWC complex KO cell lines to quantify the degree of reduction.

Quantitative flow cytometry analysis confirmed a significant reduction in surface Itgα5 expression: levels decreased by 59% in WDR11 KO cells and 31% in Fam91A1 KO cells ($p<0.05$). In contrast, C17orf75 KO cells exhibited no significant difference compared to the WT ($p>0.05$) (Fig. 14A). For Itgβ1, similar reductions were observed: 43% in WDR11 KO and 31% in Fam91A1 KO cells ($p<0.05$), with no notable change in C17orf75 KO cells ($p>0.05$) (Fig. 14B).

To further dissect the mechanism by which the FWC complex regulates integrin trafficking, I aimed to clarify whether its function depends on direct interaction with the known bridging factor TBC1D23 (204) or if the complex can operate independently of this connection. Given that TBC1D23 mediates tethering of retrograde vesicles to the TGN, its role as an FWC complex interactor may be critical for efficient integrin delivery to the cell surface. To test this, I performed siRNA-mediated knock-down of TBC1D23 in U2OS cells. This resulted in a comparable reduction in surface levels of Itgα5 and Itgβ1, consistent with the phenotypes observed in WDR11 and Fam91A1 KOs ($p<0.05$) (Fig. 14C, D).

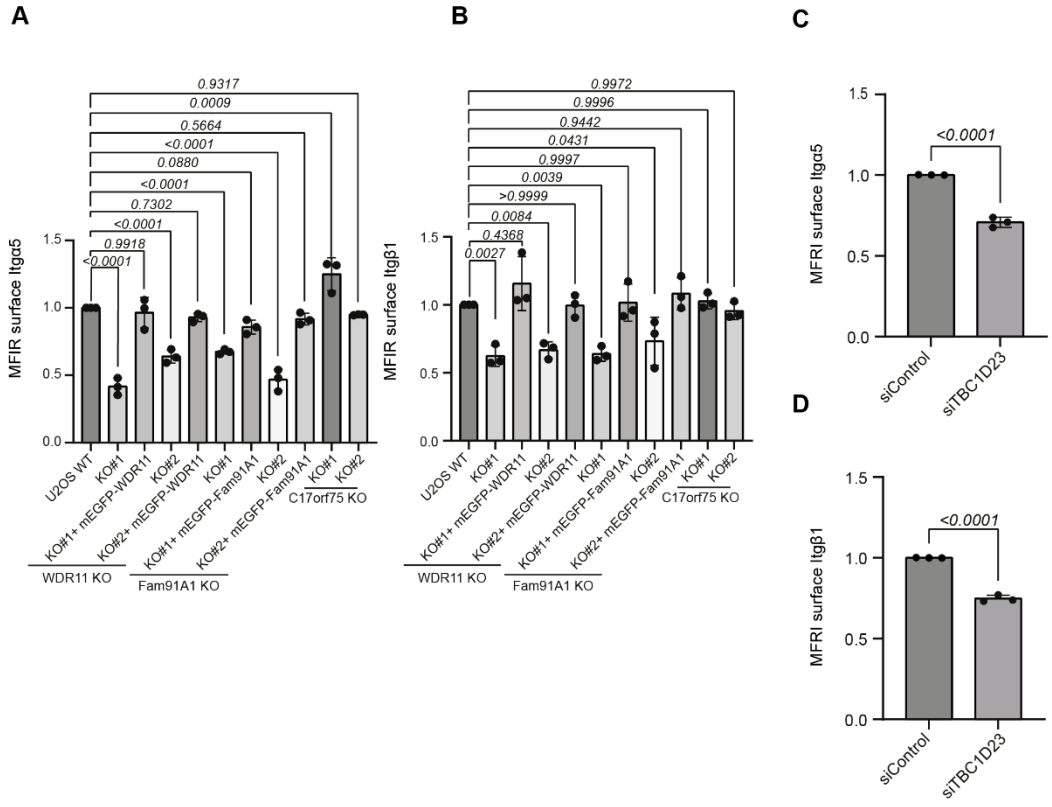

Figure 14. Reduced α5β1 integrin surface levels after WDR11 or Fam91A1 depletion in U2OS cells. A) Flow cytometry analysis of Itgα5 surface levels of U2OS WT, U2OS FWC complex KO cell lines, and their respective rescues. Y-axis shows mean fluorescence intensity ratio (MFIR) (mean ± s.d.; n=3). **B)** Flow cytometry analysis of Itgβ1 surface levels of U2OS WT, U2OS FWC complex KO cell lines, and their respective rescues (mean ± s.d.; n=3). **C, D)** Flow cytometry analysis of Itgα5 and Itgβ1 in U2OS TBC1D23 knock-down cells and siControl treated cells (mean ± s.d.; n=3).

These quantitative analyses reinforce the crucial function of the FWC complex and TBC1D23 in trafficking Itgα5 and Itgβ1 to the cell surface. The data strongly support the conclusion that impaired FWC complex assembly or its failure to engage with TGN tethers compromises integrin surface localization.

4.8 Fam91a1 mutant variants causing PCH affect integrin recycling

Genetic variants in *Fam91A1* and *WDR11* have been implicated in several neurodevelopmental disorders. Notably, mutations in *Fam91A1* are strongly associated with pontocerebellar hypoplasia (PCH), a severe neurological condition characterized by cerebellar atrophy and impaired motor coordination (211). To investigate whether PCH-associated *Fam91a1* mutations impair integrin surface expression, I examined the functional consequences of four disease-relevant *Fam91A1* variants, R61A, D198R, R569Q, and T589M, on integrin trafficking. The residues R61A and D198R have previously been identified as critical for TBC1D23 binding in zebrafish, whereas the variants R569Q and T589M were reported in a genetic disease repository (201).

Fam91A1 knock-out U2OS cells were transiently transfected with plasmids encoding mEGFP-tagged *Fam91A1* mutant variants (R61A, D198R, R569Q, and T589M) or wild-type *Fam91A1*. 48 hours post-transfection, the surface expression of α5 and β1 integrins was assessed by flow cytometry. As expected, wild-type mEGFP-Fam91A1 rescued the reduction of surface Itgα5 and Itgβ1 ($p>0.05$) (Fig. 15A, B). However, none of the four *Fam91A1* disease mutants restored integrin surface levels, behaving similarly to mEGFP-transfected negative controls, indicating a loss of function for these mutant constructs ($p<0.05$) (Fig. 15 A, B).

To further characterize the mutant proteins, I examined their subcellular localization by immunofluorescence. Whereas wild-type Fam91a1 localized to the TGN and recruited WDR11, all four Fam91A1 mutants displayed a diffuse cytoplasmic distribution and failed to recruit WDR11 to the TGN (Fig. 15C). This suggests that PCH-associated Fam91a1 mutations disrupt complex assembly or trafficking competence.

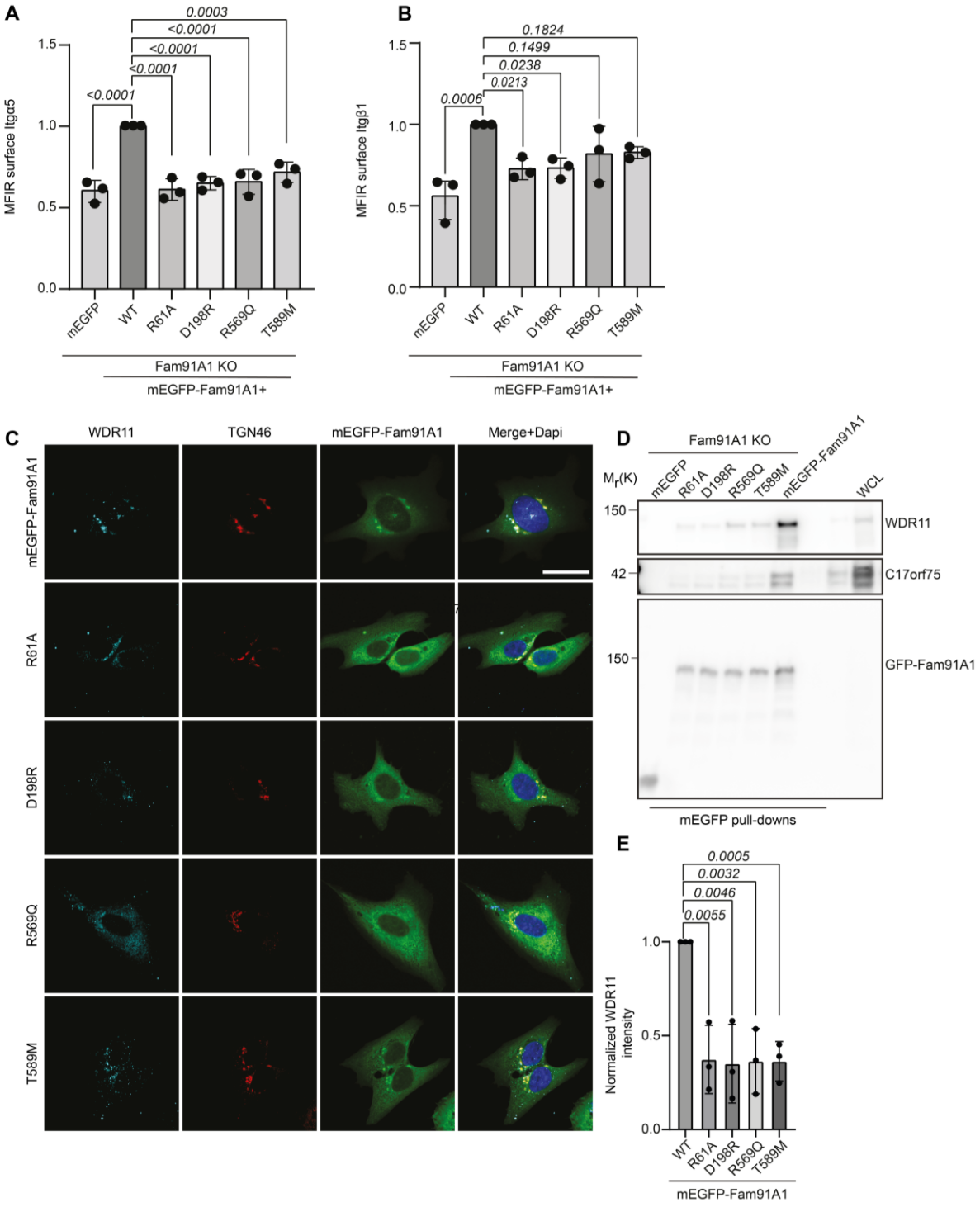

Figure 15. PCH-associated Fam91A1 point mutations reduce Itgα5 and Itgβ1 surface levels in U2OS cells. A-B) Flow cytometry analysis of surface Itgα5 (A) and Itgβ1 (B) levels in U2OS Fam91A1 KO cells transiently transfected with mEGFP or mEGFP-tagged Fam91A1 constructs (WT, R61A, D198R, R569Q, T589M) (mean ± s.d.; n=3). **C)** Immunofluorescence images of U2OS Fam91A1 KO cells transiently transfected with mEGFP-Fam91A1 constructs (WT, R61A, D198R, R569Q, T589M; green). The TGN was labeled with an antibody against TGN46 (red)

and WDR11 (cyan). Nuclei were stained with DAPI (blue). Scale bar: 20µm. **D)** Western blot analysis following GFP immunoprecipitation in U2OS Fam91A1 KO cells transiently transfected with mEGFP alone or mEGFP tagged Fam91A1 variants (WT, R61A, D198R, R569Q, T589M). Blots are probed with antibodies against FWC complex members. **E)** Quantification of Fam91A1 interaction with WDR11, normalized to mEGFP signal (mean ± s.d.; n=3).

To investigate whether the observed phenotypes were caused by impaired FWC complex assembly, I performed GFP pull-down assays using wild-type or mutant mEGFP-Fam91A1 transfected Fam91a1 KO U2OS cells. Consistent with the immunofluorescence results, none of the mutant *Fam91A1* variants efficiently co-precipitated WDR11 or C17orf75, in contrast to wild-type Fam91a1 (Fig. 15D, E).

Together, these results establish that PCH-associated Fam91A1 mutations abrogate its ability to (i) localize to the TGN, (ii) recruit and organize WDR11, and (iii) assemble the FWC complex. This leads to defective integrin trafficking and reduced integrin surface presentation. Given the essential roles of integrins in cell adhesion, migration, and polarization, impaired integrin recycling could contribute to the pathogenesis of PCH by disrupting neural development and tissue architecture.

4.9 Kallman Syndrome-associated mutations

The *WDR11* gene has been implicated in the etiology of Kallmann syndrome (KS) and idiopathic hypogonadotropic hypogonadism (IHH), two developmental disorders characterized by impaired sexual maturation and olfactory dysfunction (209, 226). Although multiple point mutations in *WDR11* have been identified in patients, the underlying molecular mechanisms by which these mutations contribute to pathogenesis remain incompletely understood.

To evaluate the functional impact of disease-associated *WDR11* mutations, mEGFP-tagged WDR11 variants (WT, A451G, T690A, R755H, I756H, as well as R395W, I435V, A436T, E448Q, and Δ966–969) were expressed in WDR11 KO U2OS cells, and integrin surface expression was measured by flow cytometry. Most point mutants failed to restore α5 and β1 integrin surface levels to those observed in wild-type controls ($p<0.05$), with some, including R395W, I435V, A436T, and E448Q variants, matching mEGFP-transfected

negative controls ($p<0.05$) (Fig. 16A, B). A subset of mutations (A451G, T690A, R755H, I756H and the deletion mutant Δ966–969) showed modest rescue of integrin surface levels but remained significantly below wild-type levels ($p<0.05$) (Fig. 16A, B).

To determine if impaired integrin surface trafficking was due to FWC mislocalization or complex formation, I analyzed the subcellular distribution of these mEGFP-tagged WDR11 variants by fluorescence microscopy. All tested mutants localized correctly to the TGN, similar to wild-type WDR11 (Fig. 16C), suggesting that the trafficking defects are not the result of FWC complex mislocalization but may arise from changes in binding affinity or specificity.

To test this hypothesis, I performed GFP pull-down assays coupled with Western blotting analysis to evaluate the integrity of the FWC complex in the context of Kallmann syndrome mutations. The most common KS-associated *WDR11* mutants (I435V, A436T, T690A, Δ966-969) were tested, and all variants retained the ability to co-precipitate Fam91A1, C17orf75, and TBC1D23, indicating that FWC complex assembly was not disrupted (Fig. 16D). These data indicate that WDR11 mutations causing KS and IHH impair integrin trafficking by disrupting interactions necessary for cargo binding and recycling, rather than by preventing TGN localization or complex formation. Indeed, the majority of KS-associated point mutations are localized within the WD40-2 domain of WDR11, which contains a positively charged groove that is hypothesized to mediate interactions with cargo molecules (200).

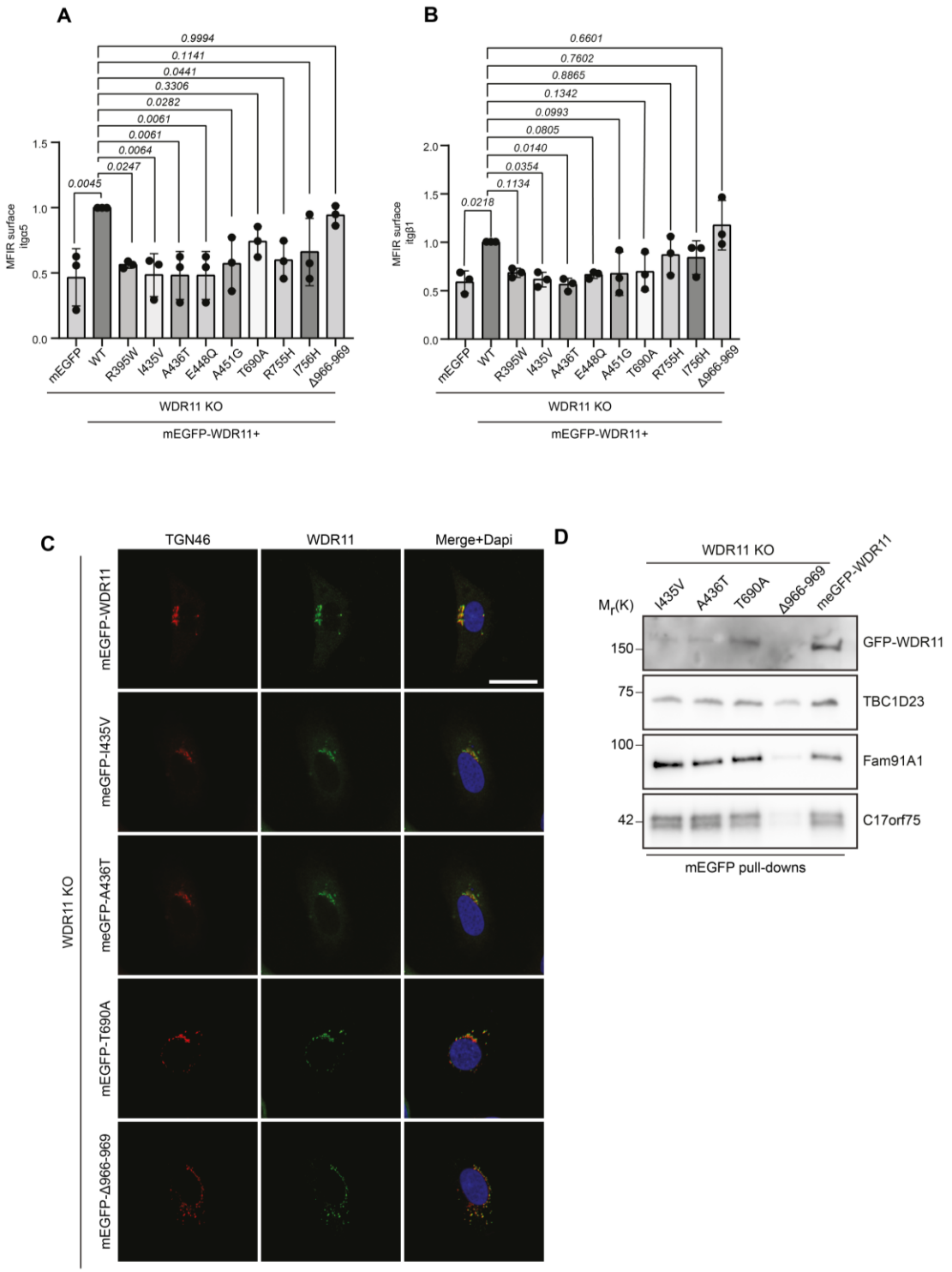

Figure 16. Kallmann syndrome-associated WDR11 point mutations reduce Itgα5 and Itgβ1 surface levels. A, B) Flow cytometry analysis of surface Itgα5 (A) and Itgβ1 (B) levels in U2OS WDR11 KO cells transiently transfected with mEGFP or mEGFP-tagged WDR11 constructs (WT, I435V, A436T, T690A, and Δ966-969) (mean ± s.d.; n=3). **C)** Immunofluorescence images of U2OS WDR11 KO cells transiently transfected with mEGFP-WDR11 constructs (WT, I435V,

A436T, T690A, and Δ966-969; green). TGN is visualized using the TGN specific marker TGN46 (red). Nuclei are counter stained with DAPI (blue). Scale bar: 20µm. **D)** Western blot analysis following GFP immunoprecipitation in U2OS WDR11 KO cells transiently transfected with mEGFP-tagged WDR11 variants (WT, I435V, A436T, T690A, and Δ966-969). Blots are probed for FWC complex members and TBC1D23.

Taken together, the presented results indicate that point mutations in *WDR11* associated with Kallmann syndrome and IHH impair integrin trafficking not by preventing FWC complex formation or localization, but likely by disrupting the functional interface necessary for retrograde trafficking of integrins. This provides a potential molecular link between *WDR11* dysfunction and the cellular phenotypes observed in KS and IHH, possibly through altered adhesion or migration during development.

4.10 The FWC complex and beyond: An interactome analysis

To further dissect the molecular dynamics of the FWC complex and to identify additional previously uncharacterized protein cargoes involved in FWC-mediated retrograde trafficking, I employed interaction proteomics. Using the WDR11, Fam91A1, and C17orf75 KO cell lines, I introduced mEGFP-tagged wild-type variants of each complex member, thus enabling the use of GFP-pulldown in combination with mass spectrometry-based proteomics.

In the mEGFP-WDR11 dataset, WDR11 and Fam91A1 (marked in red) were highly enriched as expected, but not C17orf75 (Fig. 17A). Out of 468 significant candidates in the WDR11 interactome, of particular interest is the finding of multiple members of the Adaptor protein complex 2 (AP2) family (AP2A1, AP2A2, AP2M1) marked in green (Fig. 17A). The AP2 complex is a principal player in clathrin-mediated endocytosis, particularly at the plasma membrane.

AP2A1 and AP2A2 recognize cargo proteins by binding to specific motifs within their cytoplasmic tails, and interact directly with clathrin to initiate coated pit formation (227). AP2M1 can also recognize the cytoplasmic NPXY motif present on integrin β-subunit cytoplasmic tails, thereby facilitating endocytosis of β1 and β3 integrins (228, 229). Until now, the FWC complex was implicated only in the trafficking of cargo proteins derived from

AP1-coated vesicles. The identification of AP2 components in the interactome, which do not typically traffic to the Golgi, suggests a broader role for FWC in vesicular trafficking.

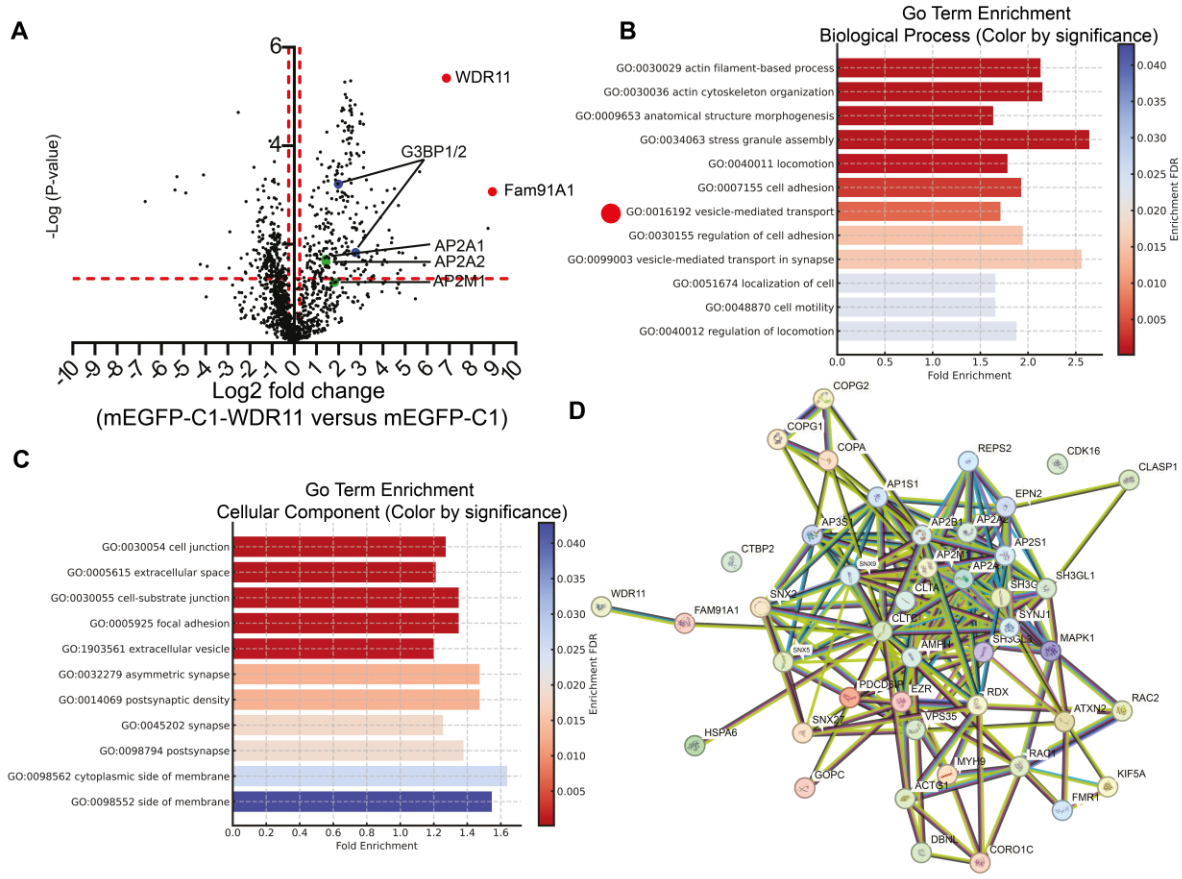

Figure 17. Proteomic analysis of the WDR11 interactome. A) Volcano plot depicting significant interaction partners of WDR11. Members of the FWC complex are annotated in red. Notable hits such as AP2 family proteins (green) and G3BP1 and G3BP2 (blue) are highlighted. **B-C)** GO term enrichment analysis of significantly enriched WDR11 interaction partners for biological process (B) and cellular component (C). Bar size represents fold enrichment; bar color denotes statistical significance. **D)** STRING network analysis of significantly enriched proteins associated with vesicle-mediated transport.

Additionally, the dataset revealed G3BP1 and G3BP2 (highlighted in blue) (Fig. 17A), which are crucial nucleators of stress granules (SGs), dynamic cytoplasmic assemblies of RNA and proteins that form in response to cellular stress (oxidative stress, heat shock, viral infection, etc.). While the link between SG formation and Golgi dynamics is not yet fully

mechanistically defined, evidence suggests that G3BP1/2-driven SG formation and Golgi dynamics are coordinated parts of the cellular stress response leading to Golgi fragmentation (230, 231). The FWC complex might work as an intermediary in the stress response cascade linking SGs with proteins associated with Golgi architecture.

GO analysis of the WDR11 interactome further uncovered a more than 2.5-fold enrichment for proteins governing stress granule assembly (Fig. 17B). The data indicate a previously unrecognized function of the FWC complex in regulating stress responses. This interpretation is supported by the interactome analysis of C17orf75, which reveals associations with multiple stress-related factors.

GO term enrichment analysis also revealed a significant overrepresentation of proteins involved in vesicle mediated transport, cell junctions, extracellular space, cell-substrate junction and focal adhesion (Fig. 17C). To further assess protein-protein interaction networks within these enriched categories, I performed a Search Tool for the Retrieval of Interacting Genes/Proteins (STRING) analysis to determine protein–protein interactions (PPIs) on the significant interactions for vesicle mediated trafficking (Fig. 17 D). The resulting network demonstrated interactions between WDR11 (and by extension, the FWC complex) and key vesicle trafficking proteins, including clathrin heavy chain 1 (CLTC), clathrin light chain A (CLTA), members of the AP2 family, REPS2, SNX9, SNX5, SNX27, ACTG1, and MAPK1. Collectively, these findings provide a robust interaction map for WDR11, highlighting its mechanistic integration into endocytosis and retrograde transport pathways.

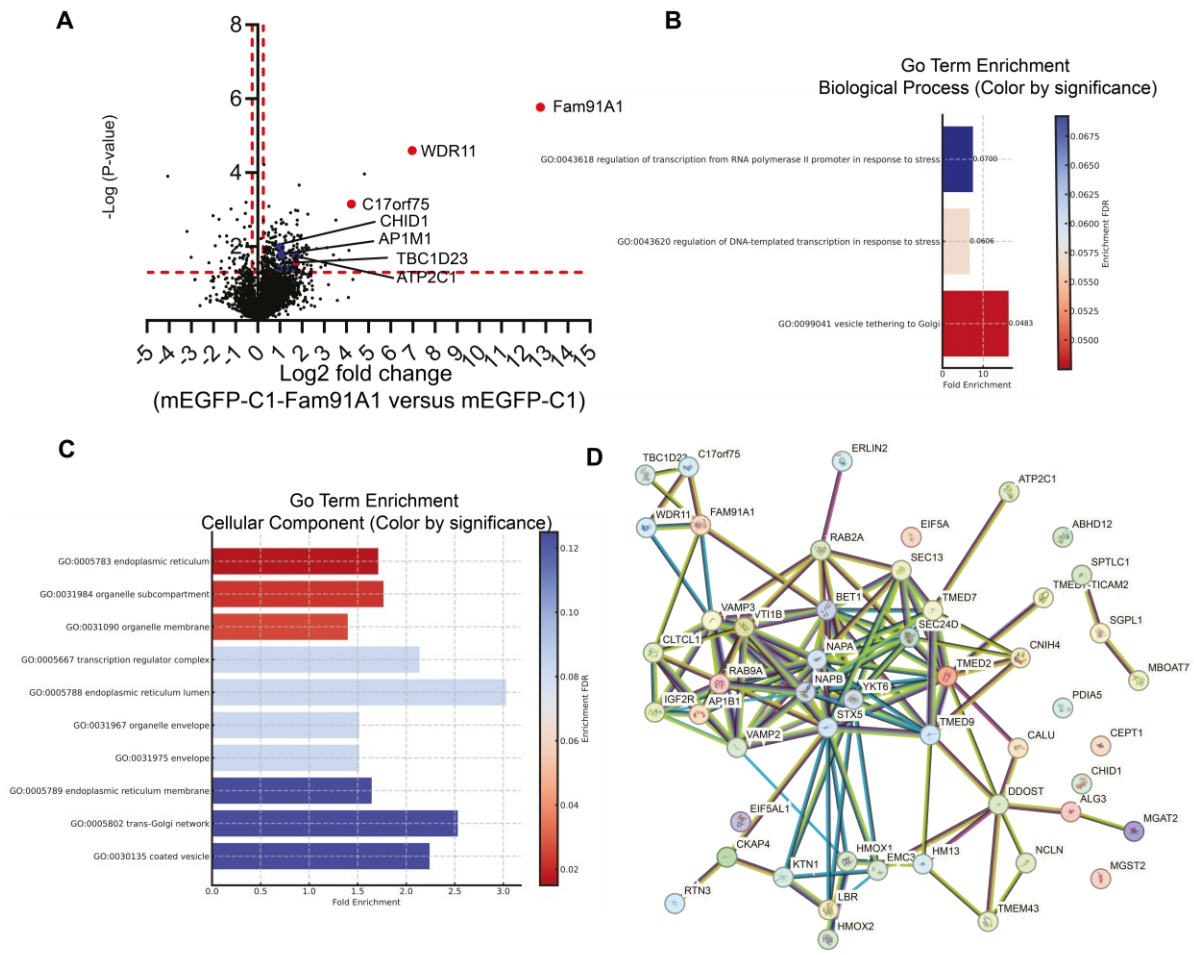

Figure 18. Proteomic analysis of the Fam91A1 interactome. A) Volcano plot depicting significant interaction partners of Fam91A1. Members of the FWC complex are annotated in red. Notable interactors, including members of the AP2 family, CHID1, and ATP2C1 are highlighted in blue. **B-C)** GO term enrichment analysis of significantly enriched interacting proteins for biological process (B) and cellular component (C). Bar size represents fold enrichment, and bar color indicates statistical significance. **D)** STRING network analysis of significantly enriched proteins associated with vesicle-mediated transport.

A parallel interactome analysis was performed for Fam91A1. Similar to the WDR11 interactome, the remaining members of the FWC complex are prominent hits. Additionally, TBC1D23, the bridging factor between the FWC complex and the TGN specific Golgins, also appears, uniquely found in the Fam91A1 interactome, as a prominent interactor (marked in red) (Fig. 18A). Notably, the Fam91A1 interactome is significantly smaller than that of WDR11, consistent with the current model that cargo recognition and vesicle coat interactions predominantly involve WDR11. In addition to FWC complex members, notable

Fam91A1 interactors include AP1M1 (a component of the AP-1 adaptor complex important for vesicle formation and cargo selection in the TGN and endosomes), CHID1 (a chitinase-like regulatory protein relevant for endocytosis and with suggested neuroimmune roles), and ATP1C1 (part of the Na+/K+-ATPase complex, with connections to neuronal function and polarity). The presence of these proteins, links Fam91A1 function to neurodegeneration and other pathologies associated with FWC mutations. Considering the abundance of evidence linking Fam91A1 to immune- and neurodegenerative disorders, CHID1 might be an important candidate for future research, especially regarding the development of therapies for PCH.

Finally, ATP1C1 is the regulatory subunit of the Na^+/K^+-ATPase complex, which maintains electrochemical gradients across the plasma membrane. ATPase components are trafficked dynamically, especially during cell polarization, neuronal differentiation, or synaptic remodeling. The Na^+/K^+-ATPase is highly enriched in neurons and testes. Its presence in the dataset and role in neuroplasticity and polarity maintenance in neurons and testes strongly correlates with disease development associated with mutations in the FWC complex, namely PCH and IHH or KS.

GO term analysis on biological processes enriched in the dataset further reinforced these connections, showing a 15-fold enrichment ($p < 0.05$) for proteins involved in “vesicle tethering to Golgi” (Fig. 18B). Subcellular localization analysis revealed significant enrichment for ER and organellar sub-compartments among these proteins (Fig. 18C), supporting the centrality of Fam91A1 in vesicle–Golgi interactions.

STRING network analysis of Fam91A1 interactors showed substantial connectivity to various SNX family members, Rab GTPases, members of the clathrin coat, and various SNARE proteins.

Among the top interactors in the STRING analysis were NAPA, NAPB, VTI1B, VAMP3, VAMP2, BET1, TMED7, and TMED9 (232). NAPA (α-SNAP) and its paralog NAPB (β-SNAP) are conserved regulators of membrane fusion, working with NSF and SNARE complexes to mediate ATP-dependent SNARE disassembly and recycling (233). Notably, NAPB is enriched in neuronal tissue, highlighting the relevance of Fam91A1 in neuronal disorders. VTI1B, VAMP3, VAMP2, and BET1 are v-SNAREs involved in Golgi–endosome

and endosome–Golgi trafficking (234, 235). TMED7 and TMED9, members of the p24 cargo receptor family, regulate ER–Golgi and intra-Golgi transport and are increasingly implicated in retrograde trafficking (232). These p24 proteins may facilitate cargo sorting for retrograde pathways mediated by the FWC complex (Fig. 18D).

Finally, interactome analysis was performed for C17orf75, the least characterized member of the FWC complex, using mEGFP-C17orf75 expressing U2OS C17orf75 KO cells. C17orf75 has not been linked functionally to FWC complex stability or localization and retrograde transport, but it might fulfill regulatory functions. Besides the expected FWC-complex members (Fig. 19A, red), interactors such as NSF, VCP, and COPG1 and COPG2 were identified (Fig. 19A, blue).

NSF and VCP are ATPases required for vesicle fusion and trafficking, with NAPA and NAPB (seen in the Fam91A1 interactome) linking NSF to SNARE complexes to drive disassembly and recycling (236, 237). The interactome data suggests new functions for C17orf75 and a broader role within the FWC complex (Fig. 19A). Moreover, COPG1 and COPG2, core COPI coat subunits, are essential for retrograde Golgi–ER trafficking, SNARE recycling, and Golgi integrity (238), further implicating C17orf75 in COPI-mediated trafficking and SNARE regulation (Fig. 19A).

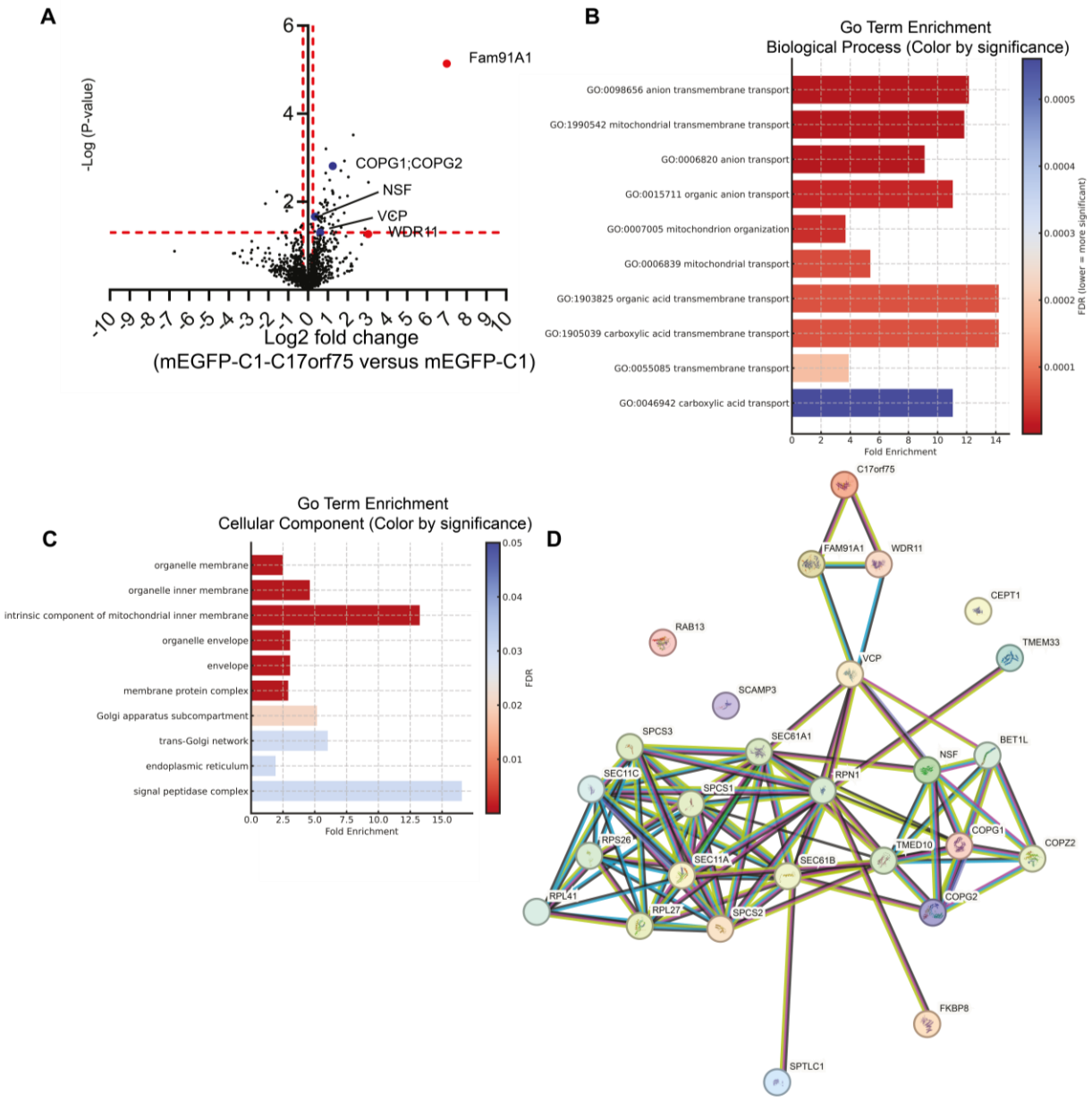

Figure 19. Interactome analysis of proteins associated with mEGFP-C17orf75. A) Volcano plot showing significant interaction partners of C17orf75. Members of the FWC complex are annotated in red. Notable hits - including members of the COP protein family, NSF, VCP - are highlighted in blue. **B-C)** GO term enrichment analysis of significantly enriched interacting proteins for biological process (B) and cellular component (C). Bar size represents fold enrichment, and bar color indicates statistical significance. **D)** STRING network analysis of significantly enriched hits linked to vesicle-mediated transport.

GO analysis revealed a significant enrichment for proteins related to anion transmembrane transport (Fig. 19B), with subcellular localization pointing to organelle membranes. This places C17orf75 at a nexus of membrane physiology, likely linked to Golgi function.

STRING analysis identified recurrent and unique interactors involved in ER protein processing and trafficking, including RPN1, SEC11A, SEC11C, SPCS1, SEC61A, SEC61B, and VCP. These proteins are central to co- and post-translational modifications, membrane protein folding, and trafficking, integral parts of both secretory and retrograde pathways. Taken together, these insights suggest that C17orf75 may coordinate SNARE disassembly and recycling as well as support ER-localized trafficking.

4.11 Structural determination of the FWC complex

At the beginning of this project, there was no structural data available on the FWC complex; therefore, I designed a strategy to express and purify the entire FWC complex to be used in biochemical experiments and for structural analysis.

To achieve this, I designed expression constructs with either GST, His, or Flag affinity tags, and tested three different tag configurations for efficient purification of the intact FWC complex (Fig. 20A).

Protein purification followed a sequential batch approach. His-tagged proteins were captured using His Mag Sepharose™ Ni magnetic beads (Cytiva, 11530894), followed by a GST pulldown using Glutathione-Sepharose™ 4B resin. Bound proteins were eluted in five steps using a suspension buffer supplemented with 300mM imidazole. Final separation and purification were accomplished by size exclusion chromatography on a Superose® 6 10/300 GL column, enabling high-resolution profiles of the eluted complexes.

A

Tag configuration #1	Tag configuration #2	Tag configuration #3
HIS-WDR11 (136 kDa)	GST-WDR11 (163 kDa)	Flag-WDR11 (136 kDa)
GST-Fam91A1 (120 kDa)	HIS-Fam91A1 (93 kDa)	HIS-Fam91A1 (93 kDa)
Flag-C17orf75 (44 kDa)	Flag-C17orf75 (44 kDa)	GST-C17orf75 (71 kDa)

B

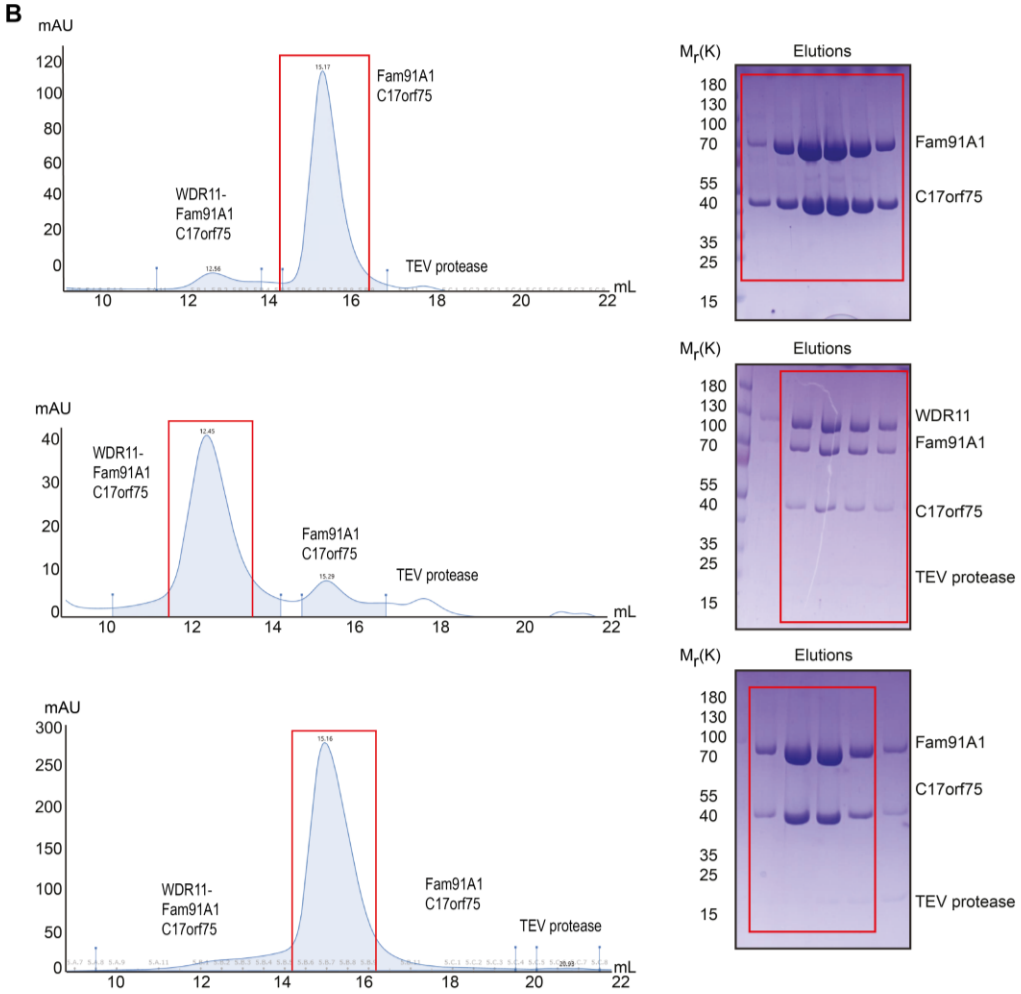

C

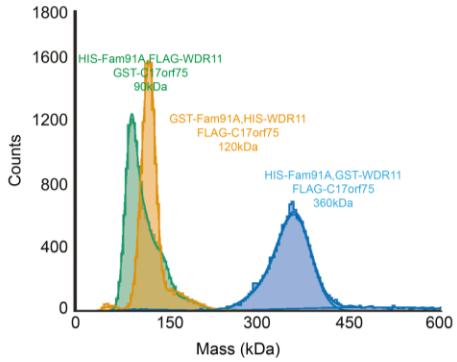

Figure 20. Purification of the FWC complex. A) Representation of the tag configurations tested for optimal FWC complex purification, alongside the molecular weights corresponding to

each tagged construct combination. **B)** High-performance liquid chromatography (HPLC) elution profiles of the FWC complex purification, with corresponding Coomassie-stained SDS-PAGE gels showing protein fractions and expected FWC component elution. **C)** Mass photometry analysis showing the molecular sizes of the Fam91a1/C17orf75 (FC) dimer and FWC trimer, reported in kDa.

Among the three tag configurations tested, configuration #2 yielded successful isolation of the trimeric FWC complex (Fig. 20B), whereas configurations #1 and #3 primarily generated Fam91A1–C17orf75 dimers. Coomassie-stained SDS-PAGE of the size exclusion chromatography fractions corroborated these results (Fig. 20B). Finally, I performed mass photometry to determine the molecular weight of the purified protein complexes, which further validated the composition and molecular weights of the purified species (Fig. 20C). Collectively, these results demonstrate that both Fam91A1-C17orf75 dimers and the complete FWC complex can be selectively purified by adjusting the tagging strategy.

To characterize the structure of the purified FWC complexes, I performed cryo-EM using a Thermo Fisher Glacios Cryo-Transmission Electron Microscope (Cryo-TEM). Image processing, including two-dimensional (2D) classification and three-dimensional (3D) reconstruction, was performed in CryoSPARC, in collaboration with Dr. Daniel Bollschweiler at the Cryo-EM facility of the Max-Planck Institute of Biochemistry.

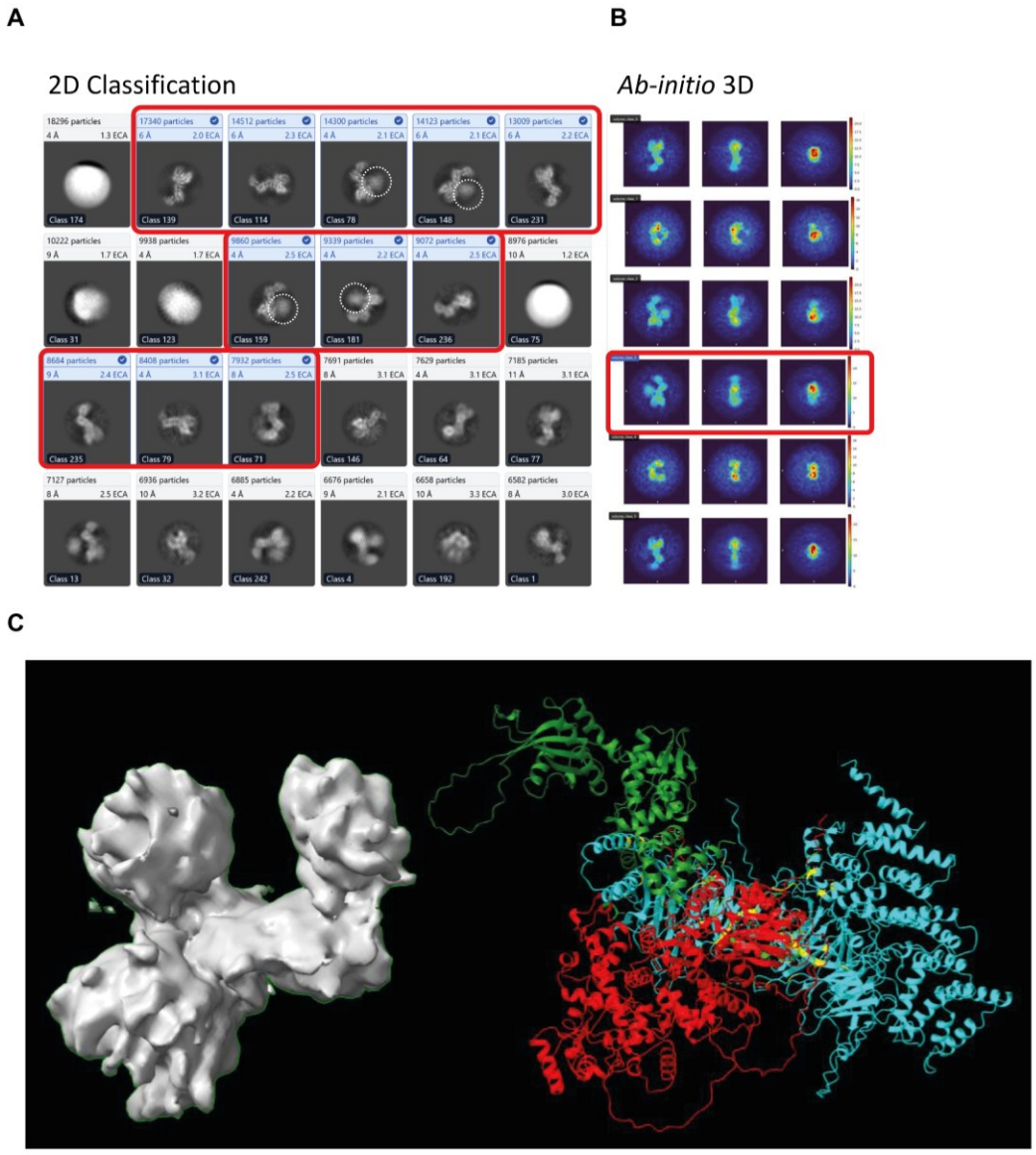

Figure 21. Cryo-EM and 3D reconstruction of the FWC complex. A, B) 2D classification and Ab-Initio 3D reconstruction of the purified FWC complex, performed in CryoSPARC. **C)** Comparison of the experimentally determined 3D CryoSPARC model (left) with the proposed AlphaFold2 model of the FWC complex (right). Color coding: WDR11 (cyan), Fam91A1 (red), C17orf75 (green).

Unfortunately, due to time limitations, I could only attempt the structural determination of the Fam91A1-C17orf75 dimer complex, which appeared to be more stable than the trimeric complex.

The 2D classification step yielded approximately 126,579 particle images, capturing the Fam91A1-C17orf75 dimer in multiple orientations (Fig. 21A,B). Structural interpretation was facilitated by AlphaFold2 modeling, which was superimposed onto the CryoSPARC-derived 3D reconstruction. This analysis revealed that the resolved particles corresponded to the Fam91A1–C17orf75 dimer, rather than the full trimeric complex. Notably, the 2D class averages indicated the presence of a highly flexible region within the Fam91A1 subunit that could not be resolved (Fig. 21).

These results underscore both the potential and the technical challenges in resolving the complete FWC complex at high resolution. Further optimization of sample preparation and imaging conditions will be necessary to obtain a high-resolution structure of the complete trimeric FWC complex. Only recently has the structural organization of the FWC complex been partially resolved. A study from the Jia laboratory revealed a tetrameric assembly composed of two WDR11–Fam91A1 heterodimers (200). However, this work did not account for C17orf75 in complex formation. The results presented in this thesis, together with the structural insights from the Jia laboratory, provide valuable guidance for future strategies aimed at purifying the complete complex.

5. Discussion

Retrograde protein transport is a fundamental cellular process essential for maintaining intracellular homeostasis, adaptation to environmental stimuli, and precise regulation of organelle organization and signaling. Its influence extends beyond classical protein "recycling" and includes the maintenance of cell polarity, adhesion, migration, immune surveillance, and neurodevelopment. Recent advances in cellular imaging, structural biology, and genetic manipulation have deepened our understanding of retrograde trafficking, revealing its key role not only as a salvage pathway but as an active regulatory mechanism.

This thesis contributes to our understanding of retrograde transport by elucidating the molecular function of the FWC complex, comprising Fam91A1, WDR11, and C17orf75, as a central player orchestrating retrograde integrin trafficking, cell polarity, and disease.

5.1 Retrograde integrin trafficking: mechanistic insights and pathway specificity

For the first time FWC complex binding to the NPXY motif in the cytoplasmic β1 integrin tail was observed, with a primary dependence on the membrane-proximal NPXY motif (Y783), a site previously implicated in integrin activation, endocytosis, and signaling. Notably, this interaction is specific but not exclusive to β1 integrins, with β2, β3, β5, and β6 integrins also showing FWC binding. Through proximity biotinylation, peptide pull-down assays, and immunostainings, I could demonstrate that the FWC complex establishes a direct molecular interface with inactive, bent β1 integrins, promoting their retrograde trafficking from endosomes to the TGN and subsequent polarized re-delivery to the plasma membrane. Importantly, the selective recognition of the bent/inactive conformation of β1 integrins by FWC suggests that integrin conformational state determines pathway entry, with inactive integrins exposing the NPXY motif for recognition and retrograde sorting.

Upon deletion of *Fam91A1* or *WDR11*, cells display intracellular accumulation of α5β1 integrin near the TGN, accompanied by reduced surface expression and losing the ability to define a polarized axis and maintain a leading front. These trafficking defects abolish leading-edge polarization and persistent migration, key cellular features underpinning

wound closure and directional movement on 1D or 2D substrates. The sorting decision likely occurs at the early endosome, where the FWC complex acts in parallel and in potential competition with Rab4/Rab11-driven recycling. Dynamic crosstalk between these pathways provides plasticity, allowing cells to prioritize adhesion molecule reallocation in response to environmental or metabolic cues.

A key question is how selectivity at endosomes is achieved for different integrin conformations and trafficking fates. One possibility is that conformational differences between inactive and active integrins dictate accessibility to endosomal sorting machinery. For example, in the bent, inactive conformation of α5β1, the NPXY motif in the β1 cytoplasmic tail is exposed, which could enable recognition by the FWC complex. By contrast, active integrins may retain Talin bound to the β-tail even at endosomes, as shown recently for internalized integrins (147). Post-translational modifications may provide an additional layer of regulation; for instance, integrin ubiquitination has been implicated in routing receptors towards lysosomal degradation (239, 240)

Evidence from this thesis supports a model wherein retrograde transport is crucial for recycling non-ligand-bound β1 integrin complexes to the leading edge through polarized secretion from the TGN. This mechanism becomes especially important during highly asymmetric tasks, e.g., persistent migration along fibronectin or effective wound repair. In contrast, ligand-bound β1 integrin is handled by Rab11-dependent long-loop recycling, which supports random movement but not persistent front–rear polarity.

Until recently, the αvβ3 integrin heterodimer was the only integrin species associated with persistent cell migration (241). Only in recent years have researchers found scarce evidence that β1 containing integrins are involved in establishing cellular polarization (155). The small GTPase Rab6 was implicated in facilitating retrograde trafficking of α5β1 from endosomes to the TGN, however, the exact pathway remained elusive and poorly characterized (155). Moreover, previous investigations into α3β1 integrin trafficking have elucidated the critical roles of syntaxin 6 (STX6) and vesicle-associated membrane protein 3 (VAMP3) in retrograde transport pathways. Riggs et al. (2012) demonstrated that STX6 and VAMP3 form a functional v-/t-SNARE complex that is essential for α3β1 integrin delivery to the cell surface. Their findings support a model wherein endocytosed integrins

undergo retrograde transport from VAMP3-positive recycling endosomes to STX6-containing TGN compartments before subsequent recycling to the plasma membrane, establishing a novel pathway that bypasses direct endosome-to-plasma membrane trafficking (147, 242).

Besides its purpose in establishing clear migratory fronts, an additional axis of selectivity may arise from retrograde detours to the Golgi that “reset” integrin glycans before onward sorting. Work from the Johannes lab has long argued that endocytic cargoes, including integrins, can be routed retrogradely from endosomes to the TGN/Golgi, where post-Golgi processing events fine-tune function and redeploy receptors, in some contexts for polarized secretion back to the membrane (177, 243, 244).

In summary, these findings suggest that in highly polarized cells, the non-ligand-bound β1 integrin conformation is preferentially routed through the retrograde pathway in a Rab6- and FWC complex-dependent manner. This model requires refinement to account for the dynamic nature of integrin activation states during trafficking and the potential role of mechanical forces in regulating pathway selection.

Supporting this hypothesis is the observation that the TGN position in highly polarized cells tends to face the leading edge, thereby providing an ideally positioned sorting hub to recycle focal adhesion components required for persistent migration (245).

5.2 Structure–function implications of the FWC complex

Fam91A1, WDR11, and C17orf75 have been shown to form a stable protein complex that orchestrates AP-1 derived vesicle tethering and cargo selection during transport from endosomes to the TGN. Within this complex, WDR11 functions as a scaffold that recognizes specific cargo proteins, while FAM91A1 is recruited via the bridging factor TBC1D23, thereby mediating the localization of the FWC complex to the TGN. The precise role of C17orf75 remains less defined; current evidence suggests it provides a supportive function within the complex.

Previous studies and data from this thesis show that Fam91A1 and WDR11 form the structural core essential for the complex's localization and stability, while C17orf75 serves

as a more dispensable subunit whose presence is necessary for complete complex assembly but not strictly for the stability of the other members. Each protein contributes distinct molecular functions to the complex.

Interestingly, recent biochemical assays and interactome analyses reveal dynamic stoichiometry and organizational plasticity within the FWC complex. While trimeric (Fam91A1–WDR11–C17orf75) and dimeric (Fam91A1–C17orf75) forms were consistently recovered during our purification protocol *in vitro* and in cell culture experiments (198, 200), recent cryo-EM data suggests a tetrameric WDR11–Fam91A1 arrangement mediated by the WDR11 C-terminal α-solenoid domain (200). This structural heterogeneity must be investigated in future experiments, but raises important questions about complex composition and regulation.

C17orf75 represents the least characterized FWC component, and its deletion produces surprisingly mild phenotypes. C17orf75 knock-out does not affect integrin surface expression or FWC complex localization, suggesting cell-type–specific or condition-dependent regulatory rather than essential functions. This mild phenotype implies: (1) functional redundancy, (2) cell-type-specific requirements, or (3) regulatory functions activated under specific conditions. To understand C17orf75's potential roles, the interactome was assessed. Unique interactome features include strong binding to proteins involved in SNARE disassembly (NSF, α-SNAP), anion transporter handling, and COPG1/G2 components, linking C17orf75 to vesicle fusion events. Supporting a specialized regulatory role. C17orf75 expression peaks in secretory tissues, suggesting importance during high trafficking flux. Its limited evolutionary conservation, with orthologs absent in lower vertebrates, indicates C17orf75 may represent a mammalian adaptation, possibly optimizing FWC function for increased trafficking complexity in specialized cell types (198).

Since the first discovery of the FWC complex’s involvement in retrograde trafficking, it has been shown to recognize acidic-cluster motifs on endocytosed cargo and to facilitate endosome-to-TGN transport (198). A recent publication by Deng et al. (2024) reported that WDR11 contains a positively charged groove on the upper surface of its WD40-2 domain that binds super acidic clusters (SACs) (200). The presented structural AlphaFold2 model

and biochemical data suggest that WDR11 interfaces not only with acidic-cluster but also NPXY motifs through residues G720, D721, L727, and K728. WDR11 may therefore possess multiple cargo-binding sites with distinct specificities, providing versatility in cargo selection. The performed interactome analysis corroborates WDR11s association with various SNARE proteins, proteins required for Golgi/ER maintenance, and cell surface receptors.

Finally, whole proteome analysis of *WDR11* and *Fam91A1* U2OS knock-out cells revealed distinct compensatory responses: WDR11 loss upregulated cell morphology regulators, while Fam91A1 loss increased vesicle-tethering factors. This differential compensation suggests non-redundant functions within the FWC complex, challenging assumptions that all components act as an obligate unit. Upregulation of tethering factors (COG and GARP complex subunits) in Fam91A1-KO cells indicates compensation for defective vesicle fusion, while cytoskeletal remodeling in WDR11-KO cells suggests direct roles in actin regulation.

Taken together, the presented structural and functional analyses reveal the FWC complex as a sophisticated trafficking regulator whose modular architecture and dynamic assembly enable precise cargo selection and context-dependent regulation. The complex's ability to recognize diverse cargo through multiple binding interfaces, while maintaining structural flexibility through dynamic assembly states, exemplifies how trafficking machinery integrates multiple cellular processes to maintain homeostasis and enable specialized functions.

5.3 FWC complex and disease: molecular defects, cellular phenotypes, and clinical implications

The performed Fam91A1 point mutation screening builds on previous studies linking Fam91A1 mutations to neurodevelopmental disorders such as PCH. Earlier work showed that Fam91A1 variants impair interaction with the tethering factor TBC1D23 and disrupt axonal outgrowth in zebrafish models, yet the cellular pathways connecting Fam91A1 to neuronal development remained unclear (201, 204). The presented results provide a mechanistic framework: Fam91A1 deficiency perturbs integrin recycling, resulting in

diminished lamellipodium formation and shortened migratory fronts, defects that parallel reduced axonal extension observed *in vivo*. Because neurons rely on integrin-mediated adhesion for growth cone navigation, they may be particularly susceptible to retrograde trafficking disruptions (246, 247). Notably, the high metabolic and trafficking demands of axonal transport could amplify the consequences of FWC dysfunction, helping to explain why mutations in ubiquitously expressed FWC components yield pronounced neural phenotypes.

Molecular characterization of disease-associated Fam91A1 point mutants (R61A, D198R, R569Q, T589M), all linked to PCH, revealed that these substitutions abolish the rescue of integrin surface expression in *Fam91A1* deficient cells and promote a diffuse cytoplasmic localization, impairing recruitment of WDR11 to the TGN. Structural modeling suggests these mutations cluster either within the TBC1D23-binding interface (R61A, D198R) or the WDR11-interaction region (R569Q, T589M), indicating that PCH may stem from disruption of FWC assembly or destabilization of vesicle tethering machinery (201, 204). Beyond integrin trafficking, it is important to recognize that the FWC complex regulates the sorting and delivery of a broader cohort of cargos, including multiple membrane, secretory, and signaling proteins, whose mislocalization might also contribute to the observed neurodevelopmental defects.

The relevance of Fam91A1 to neuropathies is underscored by recent biomarker studies, where Fam91A1 emerged among top candidates linked to epilepsy and was identified as a parthanatos-related gene (PRG) contributing to PARP-1–dependent cell death (248). This unexpected association with regulated cell death suggests that FWC complex dysfunction may trigger broader cellular stress pathways, such as the unfolded protein response, leading to maladaptive activation of parthanatos signaling. These findings highlight the importance of the FWC complex not just in retrograde trafficking but as a broader node of neuronal cell integrity, potentially impacting neuronal survival far beyond its role in cargo transport.

Similarly, WDR11 mutations (e.g., I435V, A436T, T690A, Δ966–969) implicated in Kallmann syndrome and idiopathic hypogonadotropic hypogonadism largely fail to restore integrin surface presentation, despite correct FWC assembly and TGN localization,

suggesting that the disease mechanism centers on defective cargo recognition, likely affecting a spectrum of essential proteins (211, 226). The neuroendocrine consequences are thought to result, at least in part, from impaired migration of GnRH neurons, whose journey from the nasal placode to the hypothalamus relies on regulated integrin-mediated adhesion and trafficking (210, 249).

Although earlier studies proposed a mechanistic role for WDR11 in transcriptional regulation via EMX1 interaction, neither the presented proteomic data nor immunofluorescence studies supplied supporting evidence for this link, pointing instead to vesicle trafficking defects as the primary driver of disease phenotype in KS and IHH (207, 213). However, given the diversity of FWC cargos, it remains possible that other affected proteins or pathways make significant contributions to disease pathology alongside integrins.

In summary, while integrin trafficking defects provide a compelling explanation for many phenotypic consequences of *Fam91A1* and *WDR11* mutations, it is essential to acknowledge that disruption of broader FWC-mediated cargo sorting likely underlies the full clinical manifestation of these neurodevelopmental disorders.

5.4 Conclusions and future directions

This thesis defines the FWC complex as a multifunctional regulator integrating intracellular trafficking and integrin recycling for persistent cell migration. Key advances include: (1) establishing direct molecular links between retrograde trafficking and cell migration, (2) revealing cargo recognition complexity with FWC recognizing both acidic clusters and NPXY motifs, (3) providing pathophysiological frameworks for understanding tissue-specific developmental disorders from ubiquitous trafficking protein mutations, and (4) identifying potential connections to endocytic machinery and stress responses.

These insights reveal how trafficking complexes integrate membrane dynamics with cytoskeletal regulation in health and disease. Future work should focus on understanding dynamic FWC assembly regulation, identifying tissue-specific modulators, and developing targeted therapeutic strategies for FWC-related diseases. The intersection of trafficking,

signaling, and cytoskeletal dynamics suggests similar integrated mechanisms may govern other cellular processes, warranting broader investigation of trafficking complex functions in cell biology.

In summary, this work positions the FWC complex as a master regulator in retrograde integrin trafficking, membrane organization, cell migration, and disease. The comprehensive mechanistic and structural insights presented here bridge molecular biology, cell physiology, and clinical pathology, and provide a robust platform for future research.

Key unresolved questions for future study include:

- How do FWC complex composition and NPXY motif engagement change in response to cell state or external signals?
- What are the detailed mechanisms of FWC dynamic assembly, post-translational regulation, and tissue-specific adaptation?
- How do FWC defects interface with immune responses, autophagy, or other forms of cell death?
- Can FWC complex components or their cargo interfaces serve as therapeutic targets for neurodevelopmental and migratory disorders?

Future work should focus on dissecting the dynamics of FWC complex assembly, mapping interactomes in different tissues, and exploring targeted strategies to correct FWC-linked trafficking defects in disease states. The integration of trafficking, cytoskeleton, and signaling mechanisms uncovered here exemplifies the complexity and physiological significance of retrograde transport and positions the FWC complex as a paradigm for multifunctional membrane trafficking regulators.

6. Acknowledgements

I would like to express my deepest gratitude to my supervisors, Prof. Dr. Veit Hornung and Dr. Ralph Böttcher, for their guidance, support, and invaluable advice throughout my PhD.

Along this journey, I was fortunate to meet many companions and receive help from unexpected places. I thank my colleagues Jacob Reber, for teaching me to remain calm in the face of adversity; Sebastian Grün, for giving me a reality check whenever I was whining too much; Andrea Seiwert, for befriending someone as unhinged as myself; and Kaikai Yu, for reminding me of the importance of pumping iron and for our many conversations at the gym.

I am also grateful to Dr. Moritz Weck for our many inspiring discussions accompanied by spectacular dinners, to Manar el Nagar for being a cheerful presence and Andreas Metousis for his help in the analysis of proteomic data and emotional support during the writing process. Special thanks go to Josephine Botsch, Eleftheria Papadopoulou, and Daniel Bollschweiler, whose support in my cryo-EM work was indispensable. I would also like to thank my “unofficial” students Riya, Lasse and Matus for their help and support.

Finally, I owe my deepest gratitude to my girlfriend, Anna Weber, for her patience, understanding, and love she showed me during all those years. My heartfelt thanks also go to my family, who stood by my side through the most difficult times of my PhD. I would especially like to thank, and apologize to, my grandparents, who always believed in me and supported me unconditionally, even with a grandson who was often absent, preoccupied, or buried in work.

6. References

1. Hynes RO, Zhao Q. The evolution of cell adhesion. J Cell Biol. 2000;150(2):F89-96. doi:10.1083/jcb.150.2.F89

2. Campbell ID, Humphries MJ. Integrin structure, activation, and interactions. Cold Spring Harb Perspect Biol. 2011;3(3):a004994. doi:10.1101/cshperspect.a004994

3. Tamkun JW, DeSimone DW, Fonda D, Patel RS, Buck C, Horwitz AF, Hynes RO. Structure of integrin, a glycoprotein involved in the transmembrane linkage between fibronectin and actin. Cell. 1986 Jul 18;46(2):271-82. doi:10.1016/0092-8674(86)90744-0

4. Johnson MS, Lu N, Denessiouk K, Heino J, Gullberg D. Integrins during evolution: evolutionary trees and model organisms. Biochim Biophys Acta. 2009 Apr;1788(4):779-89. doi:10.1016/j.bbamem.2008.12.013

5. Hynes RO. Integrins: bidirectional, allosteric signaling machines. Cell. 2002;110(6):673-87. doi:10.1016/S0092-8674(02)00971-6

6. Pang X, He X, Qiu Z, Zhang H, Xie R, Liu Z, et al. Targeting integrin pathways: mechanisms and advances in therapy. Signal Transduct Target Ther. 2023;8(1):1. doi:10.1038/s41392-022-01259-6

7. Longhurst CM, Jennings LK. Integrin-mediated signal transduction. Cell Mol Life Sci. 1998;54(6):514-26. doi:10.1007/s000180050180

8. Adair BD, Xiong J-P, Yeager M, Arnaout MA. Cryo-EM structures of full-length integrin αIIbβ3 in native lipids. Nat Commun. 2023;14(1):4168. doi:10.1038/s41467-023-39763-0

9. Larson RS, Corbi AL, Berman L, Springer T. Primary structure of the leukocyte function-associated molecule-1 alpha subunit: an integrin with an embedded domain defining a protein superfamily. J Cell Biol. 1989;108(2):703-12. doi:10.1083/jcb.108.2.703

10. Xiong J-P, Stehle T, Diefenbach B, Zhang R, Dunker R, Scott DL, et al. Crystal structure of the extracellular segment of integrin αVβ3. Science. 2001;294(5541):339-45. doi:10.1126/science.1064535

11. Xie C, Zhu J, Chen X, Mi L, Nishida N, Springer TA. Structure of an integrin with an αI domain, complement receptor type 4. EMBO J. 2010;29(3):666-79. doi:10.1038/emboj.2009.367

12. Oxvig C, Springer TA. Experimental support for a β-propeller domain in integrin α-subunits and a calcium binding site on its lower surface. Proc Natl Acad Sci U S A. 1998;95(9):4870-5. doi:10.1073/pnas.95.9.4870

13. Humphries MJ, Symonds EJ, Mould AP. Mapping functional residues onto integrin crystal structures. Curr Opin Struct Biol. 2003;13(2):236-43. doi:10.1016/S0959-440X(03)00035-6

14. Xiong J-P, Stehle T, Zhang R, Joachimiak A, Frech M, Goodman SL, et al. Crystal structure of the extracellular segment of integrin αVβ3 in complex with an Arg-Gly-Asp ligand. Science. 2002;296(5565):151-5. doi:10.1126/science.1069040

15. Temming K, Schiffelers RM, Molema G, Kok RJ. RGD-based strategies for selective delivery of therapeutics and imaging agents to the tumour vasculature. Drug Resist Updat. 2005;8(6):381-402. doi:10.1016/j.drup.2005.10.002

16. Hantgan RR, Paumi C, Rocco M, Weisel JW. Effects of ligand-mimetic peptides Arg-Gly-Asp-X (X= Phe, Trp, Ser) on αIIbβ3 integrin conformation and oligomerization. Biochemistry. 1999;38(44):14461-74. doi:10.1021/bi9907680

17. Nishiuchi R, Takagi J, Hayashi M, Ido H, Yagi Y, Sanzen N, et al. Ligand-binding specificities of laminin-binding integrins: a comprehensive survey of laminin-integrin interactions using recombinant α3β1, α6β1, α7β1 and α6β4 integrins. Matrix Biol. 2006;25(3):189-97. doi:10.1016/j.matbio.2005.12.001

18. Hernandez AM, Amenta P. The basement membrane in pathology. Lab Invest. 1983;48(6):656-77.

19. Jayadev R, Sherwood DR. Basement membranes. Curr Biol. 2017;27(6):R207-R11. doi:10.1016/j.cub.2017.02.006

20. Hohenester E, Yurchenco PD. Laminins in basement membrane assembly. Cell Adh Migr. 2013;7(1):56-63. doi:10.4161/cam.21831

21. Zeltz C, Gullberg D. The integrin-collagen connection - a glue for tissue repair? J Cell Sci. 2016;129:653-64. doi:10.1242/jcs.180992

22. White DJ, Puranen S, Johnson MS, Heino J. The collagen receptor subfamily of the integrins. Int J Biochem Cell Biol. 2004;36(8):1405-10. doi:10.1016/j.biocel.2003.08.016

23. Tuckwell D, Humphries M. Integrin-collagen binding. Semin Cell Dev Biol. 1996;7(5):649-57. doi:10.1006/scdb.1996.0079

24. Tan S-M. The leucocyte β2 (CD18) integrins: the structure, functional regulation and signalling properties. Biosci Rep. 2012;32(3):241-69. doi:10.1042/BSR20110101

25. Noti JD. Expression and function of the leukocyte integrins in medicine. Curr Genomics. 2003;4:527-42. doi:10.2174/1389202033490240

26. Bevilacqua MP. Endothelial-leukocyte adhesion molecules. Annu Rev Immunol. 1993;11:767-804. doi:10.1146/annurev.iy.11.040193.004003

27. Singh V, Kaur R, Kumari P, Pasricha C, Singh R. ICAM-1 and VCAM-1: gatekeepers in various inflammatory and cardiovascular disorders. Clin Chim Acta. 2023;546:117487. doi:10.1016/j.cca.2023.117487

28. Clements JM, Newham P, Shepherd M, Gilbert R, Dudgeon TJ, Needham LA, et al. Identification of a key integrin-binding sequence in VCAM-1 homologous to the LDV active site in fibronectin. J Cell Sci. 1994;107(Pt 8):2127-35. doi:10.1242/jcs.107.8.2127

29. Yang Z, Mu Z, Dabovic B, Jurukovski V, Yu D, Sung J, et al. Absence of integrin-mediated TGFβ1 activation in vivo recapitulates the phenotype of TGFβ1-null mice. J Cell Biol. 2007;176(6):787-93. doi: 10.1083/jcb.200611044

30. Munger JS, Sheppard D. Cross talk among TGF-β signaling pathways, integrins, and the extracellular matrix. Cold Spring Harb Perspect Biol. 2011;3(11):a005017. doi:10.1101/cshperspect.a005017

31. Lau TL, Dua V, Ulmer TS. Structure of the integrin alphaIIb transmembrane segment. J Biol Chem. 2008;283(23):16162-8. doi:10.1074/jbc.M801748200

32. Zhu J, Luo B-H, Barth P, Schonbrun J, Baker D, Springer TA. The structure of a receptor with two associating transmembrane domains on the cell surface: integrin αIIbβ3. Mol Cell. 2009;34(2):234-49. doi:10.1016/j.molcel.2009.02.022

33. Yang J, Ma Y-Q, Page RC, Misra S, Plow EF, Qin J. Structure of an integrin αIIbβ3 transmembrane-cytoplasmic heterocomplex provides insight into integrin activation. Proc Natl Acad Sci U S A. 2009;106(42):17729-34. doi:10.1073/pnas.0909589106

34. Hoefling M, Kessler H, Gottschalk K-E. The transmembrane structure of integrin αIIbβ3: significance for signal transduction. Angew Chem Int Ed Engl. 2009;48(36):6590-3. doi:10.1002/anie.200902016

35. Li R, Gorelik R, Nanda V, Law PB, Lear JD, DeGrado WF, et al. Dimerization of the transmembrane domain of integrin αIIb subunit in cell membranes. J Biol Chem. 2004;279(25):26666-73. doi:10.1074/jbc.M314168200

36. Hu P, Luo B-H. Integrin αIIbβ3 transmembrane domain separation mediates bi-directional signaling across the plasma membrane. PLoS One. 2015;10(1):e0116208. doi:10.1371/journal.pone.0116208

37. Liu S, Calderwood DA, Ginsberg MH. Integrin cytoplasmic domain-binding proteins. J Cell Sci. 2000;113(Pt 20):3563-71. doi:10.1242/jcs.113.20.3563

38. Pan L, Zhao Y, Yuan Z, Qin G. Research advances on structure and biological functions of integrins. Springerplus. 2016;5:1-11. doi:10.1186/s40064-016-2502-0

39. Vinogradova O, Velyvis A, Velyviene A, Hu B, Haas TA, Plow EF, et al. A structural mechanism of integrin alpha(IIb)beta(3) "inside-out" activation as regulated by its cytoplasmic face. Cell. 2002;110(5):587-97. doi:10.1016/S0092-8674(02)00906-6

40. Spinardi L, Ren Y, Sanders R, Giancotti F. The beta 4 subunit cytoplasmic domain mediates the interaction of alpha6beta4 integrin with the cytoskeleton of hemidesmosomes. Mol Biol Cell. 1993;4(9):871-84. doi:10.1091/mbc.4.9.871

41. Aylward K, Meade G, Ahrens IG, Devocelle M, Moran N. A novel functional role for the highly conserved alpha-subunit KVGFFKR motif distinct from integrin alphaIIbbeta3 activation processes. J Thromb Haemost. 2006;4(8):1804-12. doi:10.1111/j.1538-7836.2006.02041.x

42. Han J, Liu S, Rose DM, Schlaepfer DD, McDonald HW, Ginsberg MH. Phosphorylation of the integrin α4 cytoplasmic domain regulates paxillin binding. J Biol Chem. 2001;276:40903-9. doi:10.1074/jbc.M102665200

43. Hogervorst F, Kuikman I, Noteboom E, Sonnenberg A. The role of phosphorylation in activation of the alpha6A beta1 laminin receptor. J Biol Chem. 1993;268(25):18427-30. doi:10.1016/S0021-9258(17)46641-5

44. Takala H, Nurminen EM, Nurmi SM, Aatonen M, Strandin TM, Takatalo M, et al. Beta2 integrin phosphorylation on Thr758 acts as a molecular switch to regulate 14-3-3 and filamin binding. Blood. 2008;112(5):1853-62. doi:10.1182/blood-2007-12-127795

45. Bridgewater RE, Norman JC, Caswell PT. Integrin trafficking at a glance. J Cell Sci. 2012;125(Pt 16):3695-701. doi:10.1242/jcs.095810

46. Pellinen T, Tuomi S, Arjonen A, Wolf M, Edgren H, Meyer H, et al. Integrin trafficking regulated by Rab21 is necessary for cytokinesis. Dev Cell. 2008;15(3):371-85. doi: 10.1016/j.devcel.2008.08.001

47. Li J, Su Y, Xia W, Qin Y, Humphries MJ, Vestweber D, et al. Conformational equilibria and intrinsic affinities define integrin activation. EMBO J. 2017;36:629-45. doi:10.15252/embj.201695803

48. Van de Walle GR, Vanhoorelbeke K, Majer Z, Illyés E, Baert J, Pareyn I, et al. Two functional active conformations of the integrin α2β1, depending on activation condition and cell type. J Biol Chem. 2005;280:36873-82. doi:10.1074/jbc.M508148200

49. Li J, Jo MH, Yan J, Hall T, Lee J, López-Sánchez U, et al. Ligand binding initiates single-molecule integrin conformational activation. Cell. 2024;187(12):2990-3005.e17. doi:10.1016/j.cell.2024.04.049

50. Hu P, Luo B-H. Integrin bi-directional signaling across the plasma membrane. J Cell Physiol. 2013;228:306-12. doi:10.1002/jcp.24154

51. Shen B, Delaney MK, Du X. Inside-out, outside-in, and inside-outside-in: G protein signaling in integrin-mediated cell adhesion, spreading, and retraction. Curr Opin Cell Biol. 2012;24(5):600-6. doi:10.1016/j.ceb.2012.08.011

52. Guidetti GF, Canobbio I, Torti M. PI3K/Akt in platelet integrin signaling and implications in thrombosis. Adv Biol Regul. 2015;59:36-52. doi:10.1016/j.jbior.2015.06.001

53. Bos J, De Bruyn K, Enserink J, Kuiperij B, Rangarajan S, Rehmann H, et al. The role of Rap1 in integrin-mediated cell adhesion. Biochem Soc Trans. 2003;31(1):83-6. doi:10.1042/bst0310083

54. Calderwood D. Talin controls integrin activation. Biochem Soc Trans. 2004;32(3):434-7. doi:10.1042/bst0320434

55. Lu F, Zhu L, Bromberger T, Yang J, Yang Q, Liu J, et al. Mechanism of integrin activation by talin and its cooperation with kindlin. Nat Commun. 2022;13(1):2362. doi:10.1038/s41467-022-30117-w

56. Calderwood DA, Campbell ID, Critchley DR. Talins and kindlins: partners in integrin-mediated adhesion. Nat Rev Mol Cell Biol. 2013;14(8):503-17. doi:10.1038/nrm3624

57. Goult BT, Zacharchenko T, Bate N, Tsang R, Hey F, Gingras AR, et al. RIAM and vinculin binding to talin are mutually exclusive and regulate adhesion assembly and turnover. J Biol Chem. 2013;288(12):8238-49. doi:10.1074/jbc.M112.438119

58. Orłowski A, Kukkurainen S, Poyry A, Rissanen S, Vattulainen I, Hytönen VP, et al. PIP2 and talin join forces to activate integrin. J Phys Chem B. 2015;119(38):12381-9. doi:10.1021/acs.jpcb.5b06457

59. Calderwood DA. Integrin activation. J Cell Sci. 2004;117(5):657-66. doi:10.1242/jcs.01014

60. Meves A, Stremmel C, Böttcher RT, Fässler R. β1 integrins with individually disrupted cytoplasmic NPxY motifs are embryonic lethal but partially active in the epidermis. J Invest Dermatol. 2013;133(12):2722-31. doi:10.1038/jid.2013.232

61. Czuchra A, Meyer H, Legate KR, Brakebusch C, Fässler R. Genetic analysis of β1 integrin 'activation motifs' in mice. J Cell Biol. 2006;174:889-99. doi:10.1083/jcb.200604060

62. Zhang X, Jiang G, Cai Y, Monkley SJ, Critchley DR, Sheetz MP. Talin depletion reveals independence of initial cell spreading from integrin activation and traction. Nat Cell Biol. 2008;10(9):1062-8. doi:10.1038/ncb1765

63. Dedden D, Schumacher S, Kelley CF, Zacharias M, Biertümpfel C, Fässler R, et al. The architecture of Talin1 reveals an autoinhibition mechanism. Cell. 2019;179(1):120-31.e13. doi:10.1016/j.cell.2019.08.034

64. Margadant C, Kreft M, de Groot D-J, Norman JC, Sonnenberg A. Distinct roles of talin and kindlin in regulating integrin α5β1 function and trafficking. Curr Biol. 2012;22(17):1554-63. doi:10.1016/j.cub.2012.06.060

65. Schiller HB, Fässler R. Mechanosensitivity and compositional dynamics of cell-matrix adhesions. EMBO Rep. 2013;14. doi:10.1038/embor.2013.49

66. Bodescu MA, Aretz J, Grison M, Rief M, Fässler R. Kindlin stabilizes the talin·integrin bond under mechanical load by generating an ideal bond. Proc Natl Acad Sci U S A. 2023;120(26):e2218116120. doi:10.1073/pnas.2218116120

67. Müller M, Brunie L, Bächer A-S, Kessler H, Gottschalk K-E, Reuning U. Cytoplasmic salt bridge formation in integrin αvβ3 stabilizes its inactive state affecting integrin-mediated cell biological effects. Cell Signal. 2014;26(11):2493-503. doi:10.1016/j.cellsig.2014.07.013

68. Mehrbod M, Trisno SL, Mofrad MRK. On the activation of integrin αIIbβ3: outside-in and inside-out pathways. Biophys J. 2013;105(6):1304-15. doi:10.1016/j.bpj.2013.07.055

69. Zhu L, Plow EF, Qin J. Initiation of focal adhesion assembly by talin and kindlin: a dynamic view. Protein Sci. 2020;30:531-42. doi:10.1002/pro.4014

70. Winograd-Katz SE, Itzkovitz S, Kam Z, Geiger B. Multiparametric analysis of focal adhesion formation by RNAi-mediated gene knockdown. J Cell Biol. 2009;186:423-36. doi:10.1083/jcb.200901105

71. Schumacher S, Vazquez Nunez R, Biertümpfel C, Mizuno N. Bottom-up reconstitution of focal adhesion complexes. FEBS J. 2022;289(12):3360-73. doi:10.1111/febs.16023

72. Humphries JD, Wang P, Streuli CH, Geiger B, Humphries MJ, Ballestrem C. Vinculin controls focal adhesion formation by direct interactions with talin and actin. J Cell Biol. 2007;179:1043-57. doi:10.1083/jcb.200703036

73. Nikolopoulos SN, Turner CE. Integrin-linked kinase binding to paxillin LD1 motif regulates ILK localization to focal adhesions. J Biol Chem. 2001;276:23499-505. doi:10.1074/jbc.M102163200

74. Hildebrand JD, Schaller MD, Parsons JT. Paxillin, a tyrosine phosphorylated focal adhesion–associated protein binds to the carboxyl terminal domain of focal adhesion kinase. Mol Biol Cell. 1995;6(6):637-47. doi:10.1091/mbc.6.6.637

75. Hu Y-L, Lu S, Szeto KW, Sun J, Wang Y, Lasheras JC, et al. FAK and paxillin dynamics at focal adhesions in the protrusions of migrating cells. Sci Rep. 2014;4:6024. doi:10.1038/srep06024

76. Xing Z, Chen H-C, Nowlen JK, Taylor SJ, Shalloway D, Guan J-L. Direct interaction of v-Src with focal adhesion kinase mediated by the Src SH2 domain. Mol Biol Cell. 1994;5(4):413-21. doi:10.1091/mbc.5.4.413

77. Katoh K. Signal transduction mechanisms of focal adhesions: Src and FAK-mediated cell response. Front Biosci. 2024;29(11):392. doi:10.31083/j.fbl2911392

78. Burridge K, Chrzanowska-Wodnicka M. Focal adhesions, contractility, and signaling. Annu Rev Cell Dev Biol. 1996;12:463-518. doi:10.1146/annurev.cellbio.12.1.463

79. Renshaw MW, Price LS, Schwartz MA. Focal adhesion kinase mediates integrin signaling requirement for growth factor activation of MAP kinase. J Cell Biol. 1999;147:611-8. doi:10.1083/jcb.147.3.611

80. Huang D, Khoe M, Befekadu M, Chung S, Takata Y, Ilić D, et al. Focal adhesion kinase mediates cell survival via NF-κB and ERK signaling pathways. Am J Physiol Cell Physiol. 2007;292(4):C1339-52. doi:10.1152/ajpcell.00144.2006

81. Mavrakis M, Juanes MA. The compass to follow: focal adhesion turnover. Curr Opin Cell Biol. 2023;80:102152. doi:10.1016/j.ceb.2023.102152

82. Ballestrem C, Hinz B, Imhof BA, Wehrle-Haller B. Differential αvβ3-integrin turnover regulates focal adhesion behavior. J Cell Biol. 2001;155(7):1319-32. doi:10.1083/jcb.200107107

83. Chao W-T, Kunz J. Focal adhesion disassembly requires clathrin-dependent endocytosis of integrins. FEBS Lett. 2009;583:1337-43. doi:10.1016/j.febslet.2009.03.037

84. Hamadi A, Bouali M, Dontenwill M, Stoeckel H, Takeda K, Rondé P. Regulation of focal adhesion dynamics and disassembly by phosphorylation of FAK at tyrosine 397. J Cell Sci. 2005;118:4415-25. doi:10.1242/jcs.02565

85. Zaidel-Bar R, Milo R, Kam Z, Geiger B. A paxillin tyrosine phosphorylation switch regulates the assembly and form of cell–matrix adhesions. J Cell Sci. 2007;120:137-48. doi:10.1242/jcs.03314

86. Nagano M, Hoshino D, Koshikawa N, Akizawa T, Seiki M. Turnover of focal adhesions and cancer cell migration. Int J Cell Biol. 2012;2012:310616. doi:10.1155/2012/310616

87. Wolfenson H, Bershadsky A, Henis YI, Geiger B. Actomyosin-generated tension controls molecular kinetics of focal adhesions. J Cell Sci. 2011;124(9):1425-32. doi:10.1242/jcs.077388

88. O'Sullivan MJ, Lindsay AJ. The endosomal recycling pathway—at the crossroads of the cell. Int J Mol Sci. 2020;21(17):6074. doi:10.3390/ijms21176074

89. Huotari J, Helenius A. Endosome maturation. EMBO J. 2011;30(17):3481-500. doi:10.1038/emboj.2011.286

90. Podinovskaia M, Spang A. The endosomal network: mediators and regulators of endosome maturation. In: Lamaze C, Prior I, editors. Endocytosis and Signaling. Cham: Springer; 2018. p. 1-38. doi:10.1007/978-3-319-96704-2_1

91. Moreno-Layseca P, Icha J, Hamidi H, Ivaska J. Integrin trafficking in cells and tissues. Nat Cell Biol. 2019;21(2):122-32. doi:10.1038/s41556-018-0223-z

92. Scott CC, Vacca F, Gruenberg J. Endosome maturation, transport and functions. Semin Cell Dev Biol. 2014;31:2-10. doi:10.1016/j.semcdb.2014.03.034

93. Kamentseva R, Kosheverova V, Kharchenko M, et al. Functional cycle of EEA1-positive early endosome: evidence for pre-existing degradative compartment. PLoS One. 2020;15(5):e0232532. doi:10.1371/journal.pone.0232532

94. Kaur G, Lakkaraju A. Early endosome morphology in health and disease. In: Organelle Structure. Springer; 2018. doi:10.1007/978-3-319-75402-4_41

95. Gorvel J-P, Chavrier P, Zerial M, Gruenberg J. Rab5 controls early endosome fusion in vitro. Cell. 1991;64(5):915-25. doi:10.1016/0092-8674(91)90316-Q

96. Murray JT, Panaretou C, Stenmark H, Miaczynska M, Backer JM. Role of Rab5 in recruiting hVps34/p150 to early endosome. Traffic. 2002;3(6):416-27. doi:10.1034/j.1600-0854.2002.30605.x

97. Arumugam SK, Kaur A. The lipids of early endosomes: making multimodality work. ChemBioChem. 2017;18:184-90. doi:10.1002/cbic.201700046

98. Overduin M, Bhat R. Recognition and remodeling of endosomal zones by sorting nexins. Biochim Biophys Acta Biomembr. 2024:184305. doi:10.1016/j.bbamem.2024.184305

99. Antonin W, Holroyd C, Tikkanen R, Honing S, Jahn R. The R-SNARE endobrevin/VAMP-8 mediates homotypic fusion of early and late endosomes. Mol Biol Cell. 2000;11(10):3289-98. doi:10.1091/mbc.11.10.3289

100. Sun Q, Westphal W, Wong KN, Tan I, Zhong Q. Rubicon controls endosome maturation as a Rab7 effector. Proc Natl Acad Sci U S A. 2010;107(45):19338-43. doi: 10.1073/pnas.1010554107

101. Podinovskaia M, Spang A. The endosomal network: mediators and regulators of endosome maturation. Endocytosis and Signaling. 2018:1-38. doi:10.1007/978-3-319-96704-2_1

102. Seaman MN. Cargo-selective endosomal sorting for retrieval to the Golgi requires retromer. The Journal of cell biology. 2004;165(1):111-22. doi:10.1083/jcb.200312034

103. Hurley JH, Emr SD. The ESCRT complexes: structure and mechanism of a membrane-trafficking network. Annu Rev Biophys Biomol Struct. 2006;35(1):277-98. doi:10.1146/annurev.biophys.35.040405.102126

104. Stoorvogel W, Strous GJ, Geuze HJ, Oorschot V, Schwartzt AL. Late endosomes derive from early endosomes by maturation. Cell. 1991;65(3):417-27. doi:10.1016/0092-8674(91)90459-C

105. Rink J, Ghigo E, Kalaidzidis Y, Zerial M. Rab conversion as a mechanism of progression from early to late endosomes. Cell. 2005;122(5):735-49. doi:10.1016/j.cell.2005.06.043

106. Buser DP, Spang A. Protein sorting from endosomes to the TGN. Frontiers in Cell and Developmental Biology. 2023;11:1140605. doi:10.3389/fcell.2023.1140605

107. Popoff V, Mardones GA, Tenza DI, Rojas RI, Lamaze C, Bonifacino JS, et al. The retromer complex and clathrin define an early endosomal retrograde exit site. Journal of Cell Science. 2007;120(12):2022-31. doi:10.1242/jcs.003020

108. Vagnozzi AN, Praticò D. Endosomal sorting and trafficking, the retromer complex and neurodegeneration. Molecular psychiatry. 2019;24(6):857-68. doi:10.1038/s41380-018-0221-3

109. Lucas M, Hierro A. Retromer. Current Biology. 2017;27(14):R687-R9. doi:10.1016/j.cub.2017.05.072

110. Seaman MN, Michael McCaffery J, Emr SD. A membrane coat complex essential for endosome-to-Golgi retrograde transport in yeast. The Journal of cell biology. 1998;142(3):665-81. doi:10.1083/jcb.142.3.665

111. Haft CR, Sierra MdlL, Bafford R, Lesniak MA, Barr VA, Taylor SI. Human orthologs of yeast vacuolar protein sorting proteins Vps26, 29, and 35: assembly into multimeric complexes. Molecular biology of the cell. 2000;11(12):4105-16. doi:10.1091/mbc.11.12.4105

112. Damen E, Krieger E, Nielsen JE, Eygensteyn J, Van Leeuwen JE. The human Vps29 retromer component is a metallo-phosphoesterase for a cation-independent mannose 6-phosphate receptor substrate peptide. Biochemical journal. 2006;398(3):399-409. doi:10.1042/BJ20060033

113. Wang D, Guo M, Liang Z, Fan J, Zhu Z, Zang J, et al. Crystal structure of human vacuolar protein sorting protein 29 reveals a phosphodiesterase/nuclease-like fold and two protein-protein

interaction sites. Journal of biological chemistry. 2005;280(24):22962-7. doi:10.1074/jbc.M500464200

114. Collins BM, Skinner CF, Watson PJ, Seaman MN, Owen DJ. Vps29 has a phosphoesterase fold that acts as a protein interaction scaffold for retromer assembly. Nature structural & molecular biology. 2005;12(7):594-602. doi:10.1038/nsmb954

115. Shi H, Rojas R, Bonifacino JS, Hurley JH. The retromer subunit Vps26 has an arrestin fold and binds Vps35 through its C-terminal domain. Nature structural & molecular biology. 2006;13(6):540-8. doi:10.1038/nsmb1103

116. Wassmer T, Attar N, Bujny MV, Oakley J, Traer CJ, Cullen PJ. A loss-of-function screen reveals SNX5 and SNX6 as potential components of the mammalian retromer. Journal of cell science. 2007;120(1):45-54. doi:10.1242/jcs.03302

117. Rojas R, Kametaka S, Haft CR, Bonifacino JS. Interchangeable but essential functions of SNX1 and SNX2 in the association of retromer with endosomes and the trafficking of mannose 6-phosphate receptors. Molecular and cellular biology. 2007;27(3):1112-24. doi:10.1128/MCB.00156-06

118. Griffin CT, Trejo J, Magnuson T. Genetic evidence for a mammalian retromer complex containing sorting nexins 1 and 2. Proceedings of the National Academy of Sciences. 2005;102(42):15173-7. doi:10.1073/pnas.0409558102

119. Utskarpen A, Slagsvold HH, Dyve AB, Skånland SS, Sandvig K. SNX1 and SNX2 mediate retrograde transport of Shiga toxin. Biochemical and biophysical research communications. 2007;358(2):566-70. doi:10.1016/j.bbrc.2007.04.159

120. Carlton J, Bujny M, Peter BJ, Oorschot VM, Rutherford A, Mellor H, et al. Sorting nexin-1 mediates tubular endosome-to-TGN transport through coincidence sensing of high-curvature membranes and 3-phosphoinositides. Current biology. 2004;14(20):1791-800. doi:10.1016/j.cub.2004.09.077

121. Van Weering JR, Sessions RB, Traer CJ, Kloer DP, Bhatia VK, Stamou D, et al. Molecular basis for SNX-BAR-mediated assembly of distinct endosomal sorting tubules. The EMBO journal. 2012;31(23):4466-80. doi:10.1038/emboj.2012.283

122. van Weering JR, Verkade P, Cullen PJ. SNX-BAR-Mediated endosome tubulation is Co-ordinated with endosome maturation. Traffic. 2012;13(1):94-107. doi:10.1111/j.1600-0854.2011.01297.x

123. Simonetti B, Paul B, Chaudhari K, Weeratunga S, Steinberg F, Gorla M, et al. Molecular identification of a BAR domain-containing coat complex for endosomal recycling of transmembrane proteins. Nature cell biology. 2019;21(10):1219-33. doi:10.1038/s41556-019-0393-3

124. Gomez TS, Billadeau DD. A FAM21-containing WASH complex regulates retromer-dependent sorting. Developmental cell. 2009;17(5):699-711. doi:10.1016/j.devcel.2009.09.009

125. Romano-Moreno M, Astorga-Simón EN, Rojas AL, Hierro A. Retromer-mediated recruitment of the WASH complex involves discrete interactions between VPS35, VPS29, and FAM21. Protein Science. 2024;33(5):e4980. doi:10.1002/pro.4980

126. Reil LH. The role of WASH complex subunit Strumpellin in platelet function: Universität Würzburg; 2023.

127. Pácalt O. Analysis of WASH complex member strumpellin. 2019.: Univerzita Karlova

128. Dostál V, Humhalová T, Beránková P, Pácalt O, Libusová L. SWIP mediates retromer-independent membrane recruitment of the WASH complex. Traffic. 2023;24(5):216-30. doi:10.1111/tra.12884

129. Visweshwaran SP. The role of a trimeric coiled coil protein in WASH complex assembly: Université Paris Saclay (COmUE); 2017.

130. Carnell M, Zech T, Calaminus SD, Ura S, Hagedorn M, Johnston SA, et al. Actin polymerization driven by WASH causes V-ATPase retrieval and vesicle neutralization before exocytosis. Journal of cell biology. 2011;193(5):831-9. doi:10.1083/jcb.201009119

131. Hao Y-H, Doyle JM, Ramanathan S, Gomez TS, Jia D, Xu M, et al. Regulation of WASH-dependent actin polymerization and protein trafficking by ubiquitination. Cell. 2013;152(5):1051-64. doi:10.1016/j.cell.2013.01.051

132. Rottner K, Hänisch J, Campellone KG. WASH, WHAMM and JMY: regulation of Arp2/3 complex and beyond. Trends in cell biology. 2010;20(11):650-61. doi:10.1016/j.tcb.2010.08.014

133. Duleh SN, Welch MD. WASH and the Arp2/3 complex regulate endosome shape and trafficking. Cytoskeleton. 2010;67(3):193-206. doi:10.1002/cm.20437

134. Zavodszky E, Seaman MN, Moreau K, Jimenez-Sanchez M, Breusegem SY, Harbour ME, et al. Mutation in VPS35 associated with Parkinson's disease impairs WASH complex association and inhibits autophagy. Nature communications. 2014;5(1):3828. doi:10.1038/ncomms4828

135. Muhammad A, Flores I, Zhang H, Yu R, Staniszewski A, Planel E, et al. Retromer deficiency observed in Alzheimer's disease causes hippocampal dysfunction, neurodegeneration, and Aβ accumulation. Proceedings of the National Academy of Sciences. 2008;105(20):7327-32. doi:10.1073/pnas.0802545105

136. Metcalf D, Isaacs AM. The role of ESCRT proteins in fusion events involving lysosomes, endosomes and autophagosomes. Portland Press Ltd.; 2010. doi:10.1042/BST0381469

137. Votteler J, Sundquist WI. Virus budding and the ESCRT pathway. Cell host & microbe. 2013;14(3):232-41. doi:10.1016/j.chom.2013.08.012

138. Martin-Serrano J, Zang T, Bieniasz PD. Role of ESCRT-I in retroviral budding. Journal of virology. 2003;77(8):4794-804. doi:10.1128/JVI.77.8.4794-4804.2003

139. Hierro A, Sun J, Rusnak AS, Kim J, Prag G, Emr SD, et al. Structure of the ESCRT-II endosomal trafficking complex. Nature. 2004;431(7005):221-5. doi:10.1038/nature02914

140. Ren X, Kloer DP, Kim YC, Ghirlando R, Saidi LF, Hummer G, et al. Hybrid structural model of the complete human ESCRT-0 complex. Structure. 2009;17(3):406-16. doi:10.1016/j.str.2009.01.012

141. McCullough J, Frost A, Sundquist WI. Structures, functions, and dynamics of ESCRT-III/Vps4 membrane remodeling and fission complexes. Annual review of cell and developmental biology. 2018;34(1):85-109. doi:10.1146/annurev-cellbio-100616-060600

142. Szymanska E, Budick-Harmelin N, Miaczynska M. Endosomal "sort" of signaling control: The role of ESCRT machinery in regulation of receptor-mediated signaling pathways. Semin Cell Dev Biol. 2018;74:11-20. doi:10.1016/j.semcdb.2017.08.012

143. Oshima R, Hasegawa T, Tamai K, Sugeno N, Yoshida S, Kobayashi J, et al. ESCRT-0 dysfunction compromises autophagic degradation of protein aggregates and facilitates ER stress-mediated neurodegeneration via apoptotic and necroptotic pathways. Scientific Reports. 2016;6(1):24997. doi:10.1038/srep24997

144. Boesch DJ, Singla A, Han Y, Kramer DA, Liu Q, Suzuki K, et al. Structural Organization of the Retriever-CCC Endosomal Recycling Complex. bioRxiv. 2023. doi:10.21203/rs.3.rs-3026818/v1

145. Singla A, Boesch DJ, Fung HYJ, Ngoka C, Enriquez AS, Song R, et al. Structural basis for Retriever-SNX17 assembly and endosomal sorting. Nature Communications. 2024;15(1):10193. doi:10.1038/s41467-024-54583-6

146. Böttcher RT, Stremmel C, Meves A, Meyer H, Widmaier M, Tseng H-Y, et al. Sorting nexin 17 prevents lysosomal degradation of β1 integrins by binding to the β1-integrin tail. Nature Cell Biology. 2012;14(6):584-92. doi:10.1038/ncb2501

147. McNally KE, Faulkner R, Steinberg F, Gallon M, Ghai R, Pim D, et al. Retriever is a multiprotein complex for retromer-independent endosomal cargo recycling. Nature Cell Biology. 2017;19(10):1214-25. doi:10.1038/ncb3610

148. Stenmark H, Olkkonen VM. The rab gtpase family. Genome biology. 2001;2:1-7. doi:10.1186/gb-2001-2-5-reviews3007

149. Park HH. Structural basis of membrane trafficking by rab family small g protein. International journal of molecular sciences. 2013;14(5):8912-23. doi:10.3390/ijms14058912

150. Urbe S, Huber L, Zerial M, Tooze S, Parton R. Rab11, a small GTPase associated with both constitutive and regulated secretory pathways in PC12 cells. FEBS letters. 1993;334(2):175-82. doi:10.1016/0014-5793(93)81707-7

151. Subramani D, Alahari SK. Integrin-mediated function of Rab GTPases in cancer progression. Molecular cancer. 2010;9:1-9. doi:10.1186/1476-4598-9-312

152. Roberts MS, Barry ST, Woods AJ, van der Sluijs P, Norman JC. PDGF-regulated rab4-dependent recycling of alphavbeta3 integrin from early endosomes is necessary for cell adhesion and spreading. Current biology : CB. 2001;11 18:1392-402. doi:10.1016/S0960-9822(01)00442-0

153. Arjonen A, Alanko J, Veltel S, Ivaska J. Distinct recycling of active and inactive β1 integrins. Traffic. 2012;13(4):610-25. doi:10.1111/j.1600-0854.2012.01327.x

154. Eva R, Dassie E, Caswell PT, Dick G, ffrench-Constant C, Norman JC, et al. Rab11 and Its Effector Rab Coupling Protein Contribute to the Trafficking of β1 Integrins during Axon Growth in Adult Dorsal Root Ganglion Neurons and PC12 Cells. The Journal of Neuroscience. 2010;30:11654 - 69. doi:10.1523/JNEUROSCI.2425-10.2010

155. Shafaq-Zadah M, Gomes-Santos CS, Bardin S, Maiuri P, Maurin M, Iranzo J, et al. Persistent cell migration and adhesion rely on retrograde transport of β1 integrin. Nature cell biology. 2016;18(1):54-64. doi:10.1038/ncb3287

156. Spooner RA, Smith DC, Easton AJ, Roberts LM, Lord JM. Retrograde transport pathways utilised by viruses and protein toxins. Virol J. 2006;3:26. doi:10.1186/1743-422X-3-26

157. Spang A. Retrograde traffic from the Golgi to the endoplasmic reticulum. Cold Spring Harb Perspect Biol. 2013;5(6). doi:10.1101/cshperspect.a013391

158. Sannerud R, Saraste J, Goud B. Retrograde traffic in the biosynthetic-secretory route: pathways and machinery. Curr Opin Cell Biol. 2003;15(4):438-45. doi:10.1016/S0955-0674(03)00077-2

159. Cho JA, Chinnapen DJ, Aamar E, te Welscher YM, Lencer W, Massol R. Insights on the trafficking and retro-translocation of glycosphingolipid-binding bacterial toxins. Frontiers in Cellular and Infection Microbiology. 2012;2. doi:10.3389/fcimb.2012.00051

160. Lencer WI. Microbes and microbial toxins: paradigms for microbial-mucosal interactions. V. Cholera: invasion of the intestinal epithelial barrier by a stably folded protein toxin. AMERICAN JOURNAL OF PHYSIOLOGY. 2001;280(1):G781-G6. doi:10.1152/ajpgi.2001.280.5.G781

161. Cordeiro F, da Silva RIK, Vargas-Stampe TL, Cerqueira AM, Andrade JR. Cell invasion and survival of Shiga toxin-producing Escherichia coli within cultured human intestinal epithelial cells. Microbiology. 2013;159(Pt_8):1683-94. doi:10.1099/mic.0.064204-0

162. Michalska M, Wolf P. Pseudomonas Exotoxin A: optimized by evolution for effective killing. Front Microbiol. 2015;6:963. doi:10.3389/fmicb.2015.00963

163. Morlon-Guyot J, Méré J, Bonhoure A, Beaumelle B. Processing of Pseudomonas aeruginosa Exotoxin A Is Dispensable for Cell Intoxication. Infection and Immunity. 2009;77(7):3090-9. doi:10.1128/IAI.01390-08

164. Yamamoto K, Hamada H, Shinkai H, Kohno Y, Koseki H, Aoe T. The KDEL Receptor Modulates the Endoplasmic Reticulum Stress Response through Mitogen-activated Protein Kinase Signaling Cascades*. Journal of Biological Chemistry. 2003;278(36):34525-32. doi:10.1074/jbc.M304188200

165. Cela I, Dufrusine B, Rossi C, Luini A, De Laurenzi V, Federici L, et al. KDEL Receptors: Pathophysiological Functions, Therapeutic Options, and Biotechnological Opportunities. Biomedicines. 2022;10(6). doi:10.3390/biomedicines10061234

166. Tsai B, Gilbert JM, Stehle T, Lencer W, Benjamin TL, Rapoport TA. Gangliosides are receptors for murine polyoma virus and SV40. The EMBO Journal. 2003;22(17):4346-55. doi:10.1093/emboj/cdg439

167. Guo Y, Sirkis DW, Schekman R. Protein Sorting at the trans-Golgi Network. Annual Review of Cell and Developmental Biology. 2014;30(Volume 30, 2014):169-206. doi:10.1146/annurev-cellbio-100913-013012

168. Gleeson PA, Lock JG, Luke MR, Stow JL. Domains of the TGN: Coats, Tethers and G Proteins. Traffic. 2004;5(5):315-26. doi:10.1111/j.1398-9219.2004.00182.x

169. Ladinsky MS, Mastronarde DN, McIntosh JR, Howell KE, Staehelin LA. Golgi structure in three dimensions: functional insights from the normal rat kidney cell. The Journal of cell biology. 1999;144(6):1135-49. doi:10.1083/jcb.144.6.1135

170. Lippincott-Schwartz J, Cole N, Presley J. Unravelling Golgi membrane traffic with green fluorescent protein chimeras. Trends in Cell biology. 1998;8(1):16-20. doi:10.1016/S0962-8924(97)01199-9

171. Lippincott-Schwartz J, Roberts TH, Hirschberg K. Secretory protein trafficking and organelle dynamics in living cells. Annual review of cell and developmental biology. 2000;16(1):557-89. doi:10.1146/annurev.cellbio.16.1.557

172. Stanley P. Golgi glycosylation. Cold Spring Harbor perspectives in biology. 2011;3(4):a005199. doi:10.1101/cshperspect.a005199

173. Gu J. [Regulation of integrin functions by N-glycans]. Yakugaku Zasshi. 2007;127(4):571-8. doi:10.1248/yakushi.127.571

174. Janik ME, Lityńska A, Vereecken P. Cell migration-the role of integrin glycosylation. Biochim Biophys Acta. 2010;1800(6):545-55. doi:10.1016/j.bbagen.2010.03.013

175. Shimizu Y, Takagi J, Ito E, Ito Y, Ebine K, Komatsu Y, et al. Cargo sorting zones in the trans-Golgi network visualized by super-resolution confocal live imaging microscopy in plants. Nature Communications. 2021;12(1):1901. doi:10.1038/s41467-021-22267-0

176. Laufman O, Hong W, Lev S. The COG complex interacts directly with Syntaxin 6 and positively regulates endosome-to-TGN retrograde transport. Journal of Cell Biology. 2011;194(3):459-72. doi:10.1083/jcb.201102045

177. Mallard F, Tang BL, Galli T, Tenza D, Saint-Pol A, Yue X, et al. Early/recycling endosomes-to-TGN transport involves two SNARE complexes and a Rab6 isoform. The Journal of cell biology. 2002;156(4):653-64. doi:10.1083/jcb.200110081

178. Ganley IG, Espinosa E, Pfeffer SR. A syntaxin 10-SNARE complex distinguishes two distinct transport routes from endosomes to the trans-Golgi in human cells. The Journal of cell biology. 2008;180(1):159-72. doi:10.1083/jcb.200707136

179. Wang Y, Tai G, Lu L, Johannes L, Hong W, Tang BL. Trans-Golgi network syntaxin 10 functions distinctly from syntaxins 6 and 16. Mol Membr Biol. 2005;22(4):313-25. doi:10.1080/09687860500143829

180. Amessou M, Fradagrada A, Falguières T, Lord JM, Smith DC, Roberts LM, et al. Syntaxin 16 and syntaxin 5 are required for efficient retrograde transport of several exogenous and endogenous cargo proteins. Journal of cell science. 2007;120(8):1457-68. doi:10.1242/jcs.03436

181. Tai G, Lu L, Wang TL, Tang BL, Goud B, Johannes L, et al. Participation of the syntaxin 5/Ykt6/GS28/GS15 SNARE complex in transport from the early/recycling endosome to the trans-Golgi network. Molecular biology of the cell. 2004;15(9):4011-22. doi:10.1091/mbc.e03-12-0876

182. De Franceschi N, Hamidi H, Alanko J, Sahgal P, Ivaska J. Integrin traffic - the update. J Cell Sci. 2015;128(5):839-52. doi:10.1242/jcs.161653

183. Senga SS, Grose RP. Hallmarks of cancer-the new testament. Open Biol. 2021;11(1):200358. doi:10.1098/rsob.200358

184. Hapke S, Kessler H, Luber B, Benge A, Hutzler P, Höfler H, et al. Ovarian Cancer Cell Proliferation and Motility Is Induced by Engagement of Integrin αvβ3/Vitronectin Interaction. Biological Chemistry. 2003;384(7):1073-83. doi:10.1515/BC.2003.120

185. Vellon L, Menendez JA, Lupu R. A bidirectional "alpha(v)beta(3) integrin-ERK1/ERK2 MAPK" connection regulates the proliferation of breast cancer cells. Mol Carcinog. 2006;45(10):795-804. doi:10.1002/mc.20242

186. Bon G, Folgiero V, Di Carlo S, Sacchi A, Falcioni R. Involvement of alpha6beta4 integrin in the mechanisms that regulate breast cancer progression. Breast Cancer Res. 2007;9(1):203. doi:10.1186/bcr1651

187. Meloche S, Pouysségur J. The ERK1/2 mitogen-activated protein kinase pathway as a master regulator of the G1- to S-phase transition. Oncogene. 2007;26(22):3227-39. doi:10.1038/sj.onc.1210414

188. Alday-Parejo B, Stupp R, Rüegg C. Are Integrins Still Practicable Targets for Anti-Cancer Therapy? Cancers (Basel). 2019;11(7). doi:10.3390/cancers11070978

189. Nam EH, Lee Y, Park YK, Lee JW, Kim S. ZEB2 upregulates integrin α5 expression through cooperation with Sp1 to induce invasion during epithelial-mesenchymal transition of human cancer cells. Carcinogenesis. 2012;33(3):563-71. doi:10.1093/carcin/bgs005

190. Maschler S, Wirl G, Spring H, Bredow DV, Sordat I, Beug H, et al. Tumor cell invasiveness correlates with changes in integrin expression and localization. Oncogene. 2005;24(12):2032-41. doi:10.1038/sj.onc.1208423

191. Shah PP, Fong MY, Kakar SS. PTTG induces EMT through integrin αVβ3-focal adhesion kinase signaling in lung cancer cells. Oncogene. 2012;31(26):3124-35. doi:10.1038/onc.2011.488

192. Yamaguchi H, Lorenz M, Kempiak S, Sarmiento C, Coniglio S, Symons M, et al. Molecular mechanisms of invadopodium formation: the role of the N-WASP-Arp2/3 complex pathway and cofilin. J Cell Biol. 2005;168(3):441-52. doi:10.1083/jcb.200407076

193. Arjonen A, Kaukonen R, Ivaska J. Filopodia and adhesion in cancer cell motility. Cell Adh Migr. 2011;5(5):421-30. doi:10.4161/cam.5.5.17723

194. Bianchi A, Gervasi ME, Bakin A. Role of β5-integrin in epithelial-mesenchymal transition in response to TGF-β. Cell Cycle. 2010;9(8):1647-59. doi:10.4161/cc.9.8.11517

195. Davis FM, Stewart TA, Thompson EW, Monteith GR. Targeting EMT in cancer: opportunities for pharmacological intervention. Trends Pharmacol Sci. 2014;35(9):479-88. doi:10.1016/j.tips.2014.06.006

196. Kudo-Saito C, Shirako H, Takeuchi T, Kawakami Y. Cancer metastasis is accelerated through immunosuppression during Snail-induced EMT of cancer cells. Cancer cell. 2009;15(3):195-206. doi:10.1016/j.ccr.2009.01.023

197. Yuan J-W, Zhang Y-N, Liu Y-R, Li W, Dou S-X, Wei Y, et al. Diffusion Behaviors of Integrins in Single Cells Altered by Epithelial to Mesenchymal Transition. Small. 2022;18(5):2106498. doi:10.1002/smll.202106498

198. Navarro Negredo P, Edgar JR, Manna PT, Antrobus R, Robinson MS. The WDR11 complex facilitates the tethering of AP-1-derived vesicles. Nat Commun. 2018;9(1):596. doi:10.1038/s41467-018-02919-4

199. Shin JJ, Gillingham AK, Begum F, Chadwick J, Munro S. TBC1D23 is a bridging factor for endosomal vesicle capture by golgins at the trans-Golgi. Nature cell biology. 2017;19(12):1424-32. doi:10.1038/ncb3627

200. Deng H, Jia G, Li P, Tang Y, Zhao L, Yang Q, et al. The WDR11 complex is a receptor for acidic-cluster-containing cargo proteins. Cell. 2024;187(16):4272-88.e20. doi:10.1016/j.cell.2024.06.024

201. Zhao L, Deng H, Yang Q, Tang Y, Zhao J, Li P, et al. FAM91A1-TBC1D23 complex structure reveals human genetic variations susceptible for PCH. Proceedings of the National Academy of Sciences. 2023;120(45):e2309910120. doi:10.1073/pnas.2309910120

202. Ivanova EL, Mau-Them FT, Riazuddin S, Kahrizi K, Laugel V, Schaefer E, et al. Homozygous truncating variants in TBC1D23 cause pontocerebellar hypoplasia and alter cortical development. The American Journal of Human Genetics. 2017;101(3):428-40. doi:10.1016/j.ajhg.2017.07.010

203. Marin-Valencia I, Gerondopoulos A, Zaki MS, Ben-Omran T, Almureikhi M, Demir E, et al. Homozygous mutations in TBC1D23 lead to a non-degenerative form of pontocerebellar hypoplasia. The American Journal of Human Genetics. 2017;101(3):441-50. doi:10.1016/j.ajhg.2017.07.015

204. Huang W, Liu Z, Yang F, Zhou H, Yong X, Yang X, et al. Structural and functional studies of TBC1D23 C-terminal domain provide a link between endosomal trafficking and PCH. Proceedings of the National Academy of Sciences. 2019;116(45):22598-608. doi:10.1073/pnas.1909316116

205. Rudnik-Schöneborn S, Barth PG, Zerres K, editors. Pontocerebellar hypoplasia. American Journal of Medical Genetics Part C: Seminars in Medical Genetics; 2014: Wiley Online Library. doi:10.1002/ajmg.c.31403

206. van Dijk T, Baas F, Barth PG, Poll-The BT. What's new in pontocerebellar hypoplasia? An update on genes and subtypes. Orphanet Journal of Rare Diseases. 2018;13:1-16. doi:10.1186/s13023-018-0826-2

207. Kim YJ, Osborn DP, Lee JY, Araki M, Araki K, Mohun T, et al. WDR11-mediated Hedgehog signalling defects underlie a new ciliopathy related to Kallmann syndrome. EMBO reports. 2018;19(2):269-89. doi:10.15252/embr.201744632

208. Lee J, Kim Y, Ataliotis P, Kim H-G, Kim D-W, Bennett DC, et al. Loss of Kallmann syndrome-associated gene WDR11 disrupts primordial germ cell development by affecting canonical and non-canonical Hedgehog signalling. bioRxiv. 2020:2020.09. 06.284927. doi:10.1101/2020.09.06.284927

209. Haag N, Tan E-C, Begemann M, Buschmann L, Kraft F, Holschbach P, et al. Biallelic loss-of-function variants in WDR11 are associated with microcephaly and intellectual disability. European Journal of Human Genetics. 2021;29(11):1663-8. doi:10.1038/s41431-021-00943-5

210. Liu Y, Zhi X. Advances in Genetic Diagnosis of Kallmann Syndrome and Genetic Interruption. Reproductive Sciences. 2022;29(6):1697-709. doi:10.1007/s43032-021-00638-8

211. Kałużna M, Budny B, Rabijewski M, Kałużny J, Dubiel A, Trofimiuk-Müldner M, et al. Defects in GnRH neuron migration/development and hypothalamic-pituitary signaling impact clinical variability of Kallmann syndrome. Genes. 2021;12(6):868. doi:10.3390/genes12060868

212. Castro S, Brunello FG, Sansó G, Scaglia P, Esnaola Azcoiti M, Izquierdo A, et al. Delayed puberty due to a WDR11 truncation at its N-terminal domain leading to a mild form of ciliopathy presenting with dissociated central hypogonadism: case report. Frontiers in Pediatrics. 2022;10:887658. doi:10.3389/fped.2022.887658

213. Kim HG, Ahn JW, Kurth I, Ullmann R, Kim HT, Kulharya A, et al. WDR11, a WD protein that interacts with transcription factor EMX1, is mutated in idiopathic hypogonadotropic hypogonadism and Kallmann syndrome. Am J Hum Genet. 2010;87(4):465-79. doi:10.1016/j.ajhg.2010.08.018

214. Goodman L, Zallocchi M. Integrin α8 and Pcdh15 act as a complex to regulate cilia biogenesis in sensory cells. Journal of cell science. 2017;130(21):3698-712. doi:10.1242/jcs.206201

215. Yoo M, Barisoni LM, Lee K, Gusella GL. Integrin-β1 is required for the renal cystogenesis caused by ciliary defects. American Journal of Physiology-Renal Physiology. 2020;318(5):F1306-F12. doi:10.1152/ajprenal.00070.2020

216. Yang JT, Rayburn H, Hynes RO. Embryonic mesodermal defects in α5 integrin-deficient mice. Development. 1993;119(4):1093-105. doi:10.1242/dev.119.4.1093

217. Francis SE, Goh KL, Hodivala-Dilke K, Bader BL, Stark M, Davidson D, et al. Central roles of α5β1 integrin and fibronectin in vascular development in mouse embryos and embryoid bodies.

Arteriosclerosis, thrombosis, and vascular biology. 2002;22(6):927-33. doi:10.1161/01.ATV.0000016045.93313.F2

218. Hu S, Li Z, Liu H, Cao W, Meng Y, Liu C, et al. Kcnh2 deletion is associated with rat embryonic development defects via destruction of KCNH2-integrin β1 complex. International Journal of Molecular Medicine. 2023;53(2):14. doi:10.3892/ijmm.2023.5338

219. Rashid M, Olson EC. Delayed cortical development in mice with a neural specific deletion of β1 integrin. Frontiers in Neuroscience. 2023;17:1158419. doi:10.3389/fnins.2023.1158419

220. Kim EJY, Sorokin L, Hiiragi T. ECM-integrin signalling instructs cellular position sensing to pattern the early mouse embryo. Development. 2022;149(1):dev200140. doi:10.1242/dev.200140

221. Ran F, Hsu PD, Wright J, Agarwala V, Scott DA, Zhang F. Genome engineering using the CRISPR-Cas9 system. Nature protocols. 2013;8(11):2281-308. doi:10.1038/nprot.2013.143

222. Azioune A, Carpi N, Tseng Q, Théry M, Piel M. Chapter 8 - Protein Micropatterns: A Direct Printing Protocol Using Deep UVs. In: Cassimeris L, Tran P, editors. Methods in Cell Biology. 97: Academic Press; 2010. p. 133-46.

223. Branon TC, Bosch JA, Sanchez AD, Udeshi ND, Svinkina T, Carr SA, et al. Efficient proximity labeling in living cells and organisms with TurboID. Nat Biotechnol. 2018;36(9):880-7. doi:10.1038/nbt.4201

224. Hegedűs K, Takáts S, Kovács AL, Juhász G. Evolutionarily conserved role and physiological relevance of a STX17/Syx17 (syntaxin 17)-containing SNARE complex in autophagosome fusion with endosomes and lysosomes. Autophagy. 2013;9(10):1642-6. doi:10.4161/auto.25684

225. Bhattacharya K, Swaminathan K, Peche VS, Clemen CS, Knyphausen P, Lammers M, et al. Novel Coronin7 interactions with Cdc42 and N-WASP regulate actin organization and Golgi morphology. Scientific Reports. 2016;6(1):25411. doi:10.1038/srep25411

226. Kim H-G, Ahn J-W, Kurth I, Ullmann R, Kim H-T, Kulharya A, et al. WDR11, a WD protein that interacts with transcription factor EMX1, is mutated in idiopathic hypogonadotropic hypogonadism and Kallmann syndrome. The American Journal of Human Genetics. 2010;87(4):465-79. doi:10.1016/j.ajhg.2010.08.018

227. Kadlecova Z, Spielman SJ, Loerke D, Mohanakrishnan A, Reed DK, Schmid SL. Regulation of clathrin-mediated endocytosis by hierarchical allosteric activation of AP2. Journal of Cell Biology. 2017;216(1):167-79. doi:10.1083/jcb.201608071

228. Honda S, Honda Y, Bauer B, Ruan C, Kunicki TJ. The impact of three-dimensional structure on the expression of PlA alloantigens on human integrin beta 3. 1995. doi:10.1182/blood.V86.1.234.bloodjournal861234

229. Kunicki TJ, Orchekowski R, Annis D, Honda Y. Variability of integrin alpha 2 beta 1 activity on human platelets. 1993. doi:10.1182/blood.V82.9.2693.bloodjournal8292693

230. Shang Z, Zhang S, Wang J, Zhou L, Zhang X, Billadeau DD, et al. TRIM25 predominately associates with anti-viral stress granules. Nature Communications. 2024;15(1):4127. doi:10.1038/s41467-024-48596-4

231. Sanders DW, Kedersha N, Lee DSW, Strom AR, Drake V, Riback JA, et al. Competing Protein-RNA Interaction Networks Control Multiphase Intracellular Organization. Cell. 2020;181(2):306-24.e28. doi:10.1016/j.cell.2020.03.050

232. Zhou L, Li H, Yao H, Dai X, Gao P, Cheng H. TMED family genes and their roles in human diseases. International Journal of Medical Sciences. 2023;20(13):1732. doi:10.7150/ijms.87272

233. Conroy J, Allen N, Gorman K, Shahwan A, Ennis S, Lynch S, et al. NAPB-a novel SNARE-associated protein for early-onset epileptic encephalopathy. Clinical Genetics. 2016;89(2):E1-E3. doi:10.1111/cge.12648

234. Abou Jamra R, Gobina CM, Becker T, Georgi A, Schulze TG, Schmael C, et al. Association study between genetic variants at the VAMP2 and VAMP3 loci and bipolar affective disorder. Psychiatric Genetics. 2008;18(4):199-203. doi:10.1097/YPG.0b013e3283050a83

235. Eckardt A, Marble C, Fern B, Moritz H, Kotula C, Ke J, et al. Muscle-specific Bet1L knockdown induces neuromuscular denervation, motor neuron degeneration, and motor dysfunction in a rat model of familial ALS. Frontiers in Neuroscience. 2025;19:1527181. doi:10.3389/fnins.2025.1527181

236. Zhao C, Slevin JT, Whiteheart SW. Cellular functions of NSF: not just SNAPs and SNAREs. FEBS letters. 2007;581(11):2140-9. doi:10.1016/j.febslet.2007.03.032

237. Seguin S, Morelli FF, Vinet J, Amore D, De Biasi S, Poletti A, et al. Inhibition of autophagy, lysosome and VCP function impairs stress granule assembly. Cell Death & Differentiation. 2014;21(12):1838-51. doi:10.1038/cdd.2014.103

238. Goyal MJ, Zhao X, Bozhinova M, Andrade-López K, de Heus C, Schulze-Dramac S, et al. A paralog-specific role of COPI vesicles in the neuronal differentiation of mouse pluripotent cells. Life science alliance. 2020;3(9). doi:10.26508/lsa.202000714

239. Lobert VH, Stenmark H. Ubiquitination of α-integrin cytoplasmic tails. Commun Integr Biol. 2010;3(6):583-5. doi:10.4161/cib.3.6.13176

240. De Franceschi N, Peuhu E, Parsons M, Rissanen S, Vattulainen I, Salmi M, et al. Mutually Exclusive Roles of SHARPIN in Integrin Inactivation and NF-κB Signaling. PLoS One. 2015;10(11):e0143423. doi:10.1371/journal.pone.0143423

241. Danen EH, van Rheenen J, Franken W, Huveneers S, Sonneveld P, Jalink K, et al. Integrins control motile strategy through a Rho-cofilin pathway. The Journal of cell biology. 2005;169(3):515-26. doi:10.1083/jcb.200412081

242. Riggs KA, Hasan N, Humphrey D, Raleigh C, Nevitt C, Corbin D, et al. Regulation of integrin endocytic recycling and chemotactic cell migration by syntaxin 6 and VAMP3 interaction. J Cell Sci. 2012;125(Pt 16):3827-39. doi:10.1242/jcs.102566

243. Lakshminarayan R, Wunder C, Becken U, Howes MT, Benzing C, Arumugam S, et al. Galectin-3 drives glycosphingolipid-dependent biogenesis of clathrin-independent carriers. Nat Cell Biol. 2014;16(6):595-606. doi:10.1038/ncb2970

244. Mirgorodskaya E, Dransart E, Shafaq-Zadah M, Roderer D, Sihlbom C, Leffler H, et al. Site-specific N-glycan profiles of α(5) β(1) integrin from rat liver. Biol Cell. 2022;114(6):160-76. doi:10.1111/boc.202200017

245. Darido C, Jane SM. Golgi feels its own wound. Advances in wound care. 2013;2(3):87-92. doi:10.1089/wound.2011.0352

246. Yamashita M. Integrin-mediated electric axon guidance underlying optic nerve formation in the embryonic chick retina. Communications Biology. 2023;6(1):680. doi:10.1038/s42003-023-05056-x

247. Myers JP, Santiago-Medina M, Gomez TM. Regulation of axonal outgrowth and pathfinding by integrin-ECM interactions. Dev Neurobiol. 2011;71(11):901-23. doi:10.1002/dneu.20931

248. Zhao H, Guan C, Xu F, Li Q, Zhao K, Yang Y, et al. Unraveling Epilepsy Biomarkers through Single-Cell Sequencing and GEO Data Integration: A Focus on Parthanatos Pathway. 2025. doi:10.21203/rs.3.rs-7337638/v1

249. Kim H-G, Ahn J-W, Kurth I, Ullmann R, Kim H-T, Kulharya A, et al. WDR11, a WD Protein that Interacts with Transcription Factor EMX1, Is Mutated in Idiopathic Hypogonadotropic Hypogonadism and Kallmann Syndrome. The American Journal of Human Genetics. 2010;87(4):465-79. doi:10.1016/j.ajhg.2010.08.018

Disclaimer

The author incorporated Claude (Anthropic) into their manuscript preparation workflow to enhance writing quality and structural organization. This AI assistance focused on improving scientific communication clarity and suggesting editorial improvements. All AI contributions were subsequently reviewed, revised, and validated by the author, who maintains full responsibility for the published content.